LAND COVER MAPPING OF THE MEKONG DELTA WITH SENTINEL-1 SYNTHETIC APERTURE RADAR
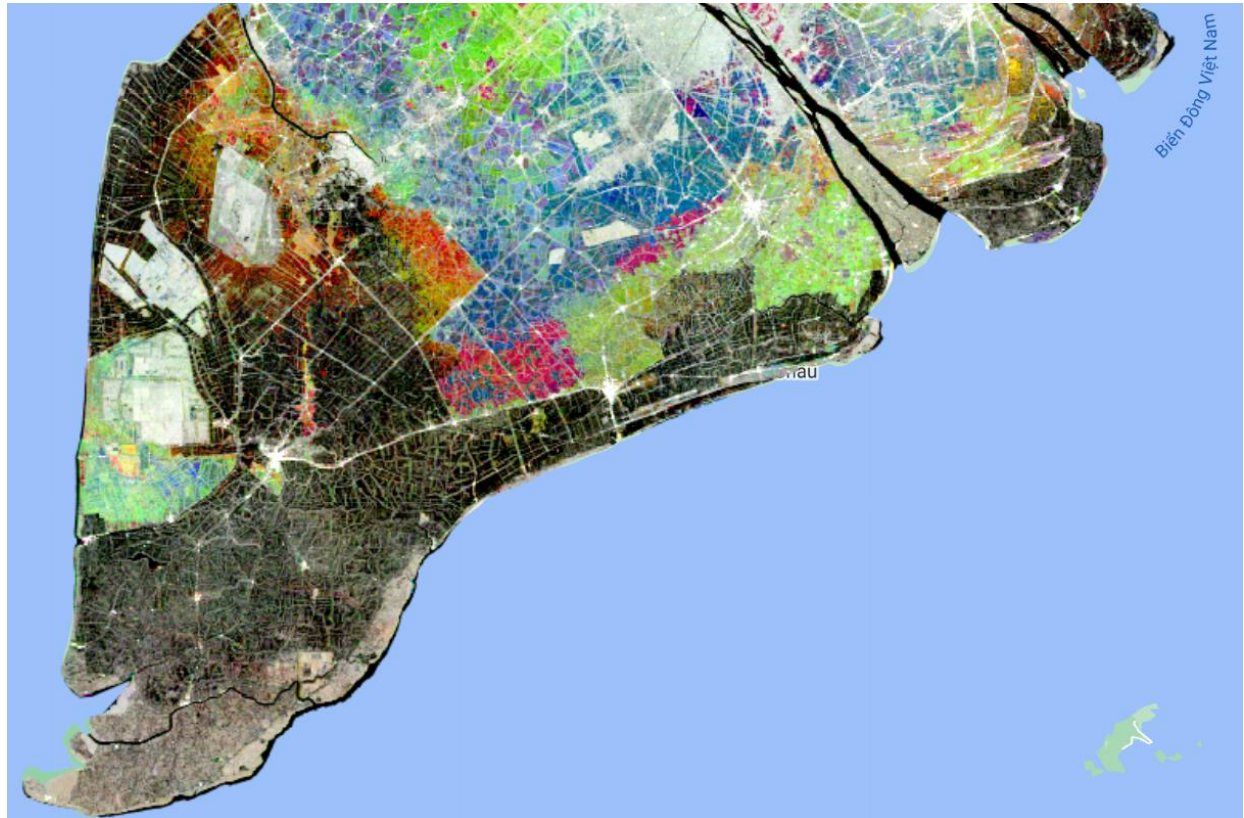
Khanh Duc Ngo

BSc, MSc
School of Environmental and Geographical Sciences
University of Nottingham Malaysia
Selangor, Malaysia
November 2022

A thesis submitted in fulfilment of the requirements
for the degree of Doctor of Philosophy

Cover photos:

- Top: a multi-temporal dual-polarization Sentinel-1 C-band synthetic aperture radar composite image in the Mekong Delta in 2017 (Photo: ESA, 2017)

- Bottom: from left to right, urban center in Bạc Liêu city; wind energy farm off the shore of Bạc Liêu; paddy field in Bạc Liêu; shrimp farm in Bạc Liêu; coastal mangrove forest in Cà Mau National Park (Photo: Khanh Ngo 2019)

Author's declaration

I hereby declare that this thesis is the result of my own work and any information or contribution used from others has been explicitly cited. It is being submitted for the degree of Doctor of Philosophy in Environmental and Geographical Sciences at University of Nottingham Malaysia and it has not been submitted to any other degree or examination in any other University or Institution.

Name: Ngo Duc Khanh

Date: November 2022

Abstract

Synthetic aperture radar (SAR) has great potential for land cover/land use (LCLU) mapping, especially in tropical regions, where frequent cloud cover obstructs optical remote sensing. The use of SAR data derived mapping results plays crucial role in urban and suburban extents characterizations, urban services, rice crop distribution delineation, and land use changes detection. As the Mekong Delta is a significant location ecologically, economically, and socially, food security, forest conservation, natural resource management, and urbanization are a matter of great concern. Urban expansion and conversion wetland areas to aquaculture have impacts on natural forest and coastal ecosystems in the Mekong Delta. Therefore, the use of latest Sentinel-1 C-band SAR data characterizing LCLU including urban expansion, aquaculture development, and productive land and unproductive lands is essential for natural resource management and land use planning.

This thesis demonstrated the use of Sentinel-1 SAR data and Google Earth Engine to map the LCLU of the Mekong Delta. The research in this thesis is divided into three parts: 1) the classification of multi-temporal Sentinel-1A C-band SAR imagery for characterizing the LCLU to support natural resource management; 2) identifying and mapping persistent building structures from coastal plains to high plateaus, as well as on the sea surface; 3) detecting and mapping persistent surface water and seasonal inundated LCLU.

Part 1 of the thesis investigated the classification of multi-temporal Sentinel-1A C-band SAR imagery for characterising LCLU to support natural resource management for land use planning and monitoring. Twenty-one SAR images acquired in 2016 over Bạc Liêu province, a rapidly developing province of the Mekong Delta, Vietnam were classified. To reduce the effects of rainfall variation confounding the classification, the images were divided into two categories: dry season (Jan–April) and wet season (May–December) and three input image sets were produced: 1) a single-date composite image, 2) a multi-temporal composite image and 3) a multi-temporal and textural composite image. Support Vector Machines (SVM) and Random Forest (RF) classifiers were then applied to

characterize urban, forest, aquaculture, and rice paddy field for the three input image sets. A combination of input images and classification algorithms was tested, and the mapping results showed that no matter the classification algorithms used, multi-temporal images had a higher overall classification accuracy than single-date images and that differences between classification algorithms were minimal. The results demonstrated the potential use of SAR as an up-to date complementary data source of land cover information for local authorities, to support their land use master plan and to monitor illegal land use changes.

Part 2 of the thesis developed novel and robust methods using time-series data acquired from Sentinel-1 C-band SAR to identify and map persistent building structures from coastal plains to high plateaus, as well as on the sea surface. Mapping building structures is crucial for environmental change and impact assessment and is especially important to accurately estimate fossil fuel CO_2 emissions from human settlements. From annual composites of SAR data in the two-dimensional VV-VH polarization space, the VV-VH domain was determined for detecting building structures, whose persistence was defined based on the number of times that a pixel was identified as a building in time-series data. Moreover, the algorithm accounted for misclassified buildings due to water-tree interactions in radar signatures and due to topography effects in complex mountainous landforms. The methods were tested in five cities (Bạc Liêu, Cà Mau, Sóc Trăng, Tân An, and Phan Thiết) in Vietnam located in different socio-environmental regions with a range of urban configurations. Using in-situ data and field observations, the methods were validated, and the results were found to be accurate, with an average false negative rate of 10.9% and average false positive rate of 6.4% for building detection. The new approach was developed to be robust against variations in SAR incidence and azimuth angles. The results demonstrated the potential use of satellite dual-polarization SAR to identify persistent building structures annually across rural–urban landscapes and on sea surfaces with different environmental conditions.

The final part of the thesis developed a novel method to map persistent surface water and seasonal inundated land cover and land use. The super-intensive shrimp culture in the

Mekong Delta region brings substantial profits to the local economy but it poses major challenges to soil and surface water in wetland areas. The use of geospatial data in monitoring the aquaculture areas is necessary but it has been inadequate in aquaculture areas in the Mekong Delta. In this study, a new algorithm was developed to address the problem of detecting LCLU that contains water such as persistent surface water (permanent lake, permanent rivers, persistently denuded unproductive land) and seasonal inundated land cover (rice paddy and aquaculture) in different environmental conditions. The three-dimensional (3-D) space of VV-VH polarization of the SAR data and Season space was introduced. This study found that the use of the three-dimensional polarization of the SAR and season space is successfully in detecting rice paddy, aquaculture, and persistent surface water. Therefore, the novel method can be utilized to monitor aquaculture in other wetland regions.

In conclusion, this thesis demonstrated the potential use of Sentinel-1 C-band SAR data to map LCLU across the urban suburban to rural-natural landscape on level terrains. The proposed methods can be used for urbanization monitoring, aquaculture development monitoring, and illegal land use change.

Preface

The work presented herein was completed as a body of work for this thesis and is substantially my own work. Publications from others are detailed below:

The work presented in Chapter 2 was published as:

Ngo, K. D., Lechner, A. M. and Vu, T. T. (2020). Land cover mapping of the Mekong Delta to support natural resource management with multi-temporal Sentinel-1A synthetic aperture radar imagery'. Remote Sensing Applications: Society and Environment. 17. 100272

The work presented in Chapter 3 was published as:

Ngo, K. D., Nghiem, S. V., Lechner, A. M., and Vu, T. T. (2021). Building structure mapping on level terrains and sea surfaces in Vietnam. Remote Sensing, 13(13):2439

The content in Chapter 4 is based on a paper in preparation:

Ngo, K. D., Nghiem, S. V., Lechner, A. M., and Vu, T. T. (in preparation). Surface cover classification.

Acknowledgements

Table of Contents

List of Publications

Jia, S., Nghiem, S.V., Kim, S.H., Krauser, L., Gaughan, A.E., Stevens, F.R., Kafatos, M.C. and **Ngo, K.D.**, 2022. Extreme Development of Dragon Fruit Agriculture with Nighttime Lighting in Southern Vietnam. In Remote Sensing of Agriculture and Land Cover/Land Use Changes in South and Southeast Asian Countries (pp. 553-571). Springer, Cham.

Danneck, J., Tiang, D.C.F., **Duc, K.N.**, Azhar, B., Sanusi, R., Campos-Arceiz, A. and Lechner, A.M., 2022. Green spaces are critical for connecting urban habitat in the tropics (Under review).

Ngo, K.D., Nghiem, S.V., Lechner, A.M. and Vu, T.T., 2021. Building Structure Mapping on Level Terrains and Sea Surfaces in Vietnam. Remote Sensing, 13(13), p.2439.

Ang, M.L.E., Arts, D., Crawford, D., Labatos Jr, B.V., **Ngo, K.D.**, Owen, J.R., Gibbins, C. and Lechner, A.M., 2021. Socio-environmental land cover time-series analysis of mining landscapes using Google Earth Engine and web-based mapping. Remote Sensing Applications: Society and Environment, 21, p.100458.

Ngo, K.D., Lechner, A.M. and Vu, T.T., 2020. Land cover mapping of the Mekong Delta to support natural resource management with multi-temporal Sentinel-1A synthetic aperture radar imagery. Remote Sensing Applications: Society and Environment, 17, p.100272.

Oon, A., **Ngo, K.D.**, Azhar, R., Ashton-Butt, A., Lechner, A.M. and Azhar, B., 2019. Assessment of ALOS-2 PALSAR-2L-band and Sentinel-1 C-band SAR backscatter for discriminating between large-scale oil palm plantations and smallholdings on tropical peatlands. Remote Sensing Applications: Society and Environment, 13, pp.183-190.

List of Figures

List of Tables

List of Equations

Chapter 1 Introduction

1.1 Introduction

The Vietnamese Mekong Delta region, often known as "Vietnam's rice bowl", is a significant location ecologically, economically, and socially. Tropical climate, fertile soil characteristics and the abundant availability of freshwater from the Mekong River facilitate agriculture and inland aquaculture production (Sakamoto *et al.*, 2009; Chapman and Darby, 2016; Dang *et al.*, 2018; Ha *et al.*, 2018). Coastal wetland areas in this region preserve rich biological and geological resources and support various ecosystems such as mangrove forests, peat wetlands, and marine ecosystems (Nguyen *et al.*, 2013; Tue *et al.*, 2014; Van *et al.*, 2015).

Over the past four decades, land cover and land use (LCLU) in the Mekong Delta has changed dramatically. At national and local scales, under industrialization and modernization, human activities supported by state policies which promote urbanization and agricultural transformation have led to dramatic land cover changes in the region (Li *et al.*, 2017; Son and Thanh, 2018). The Vietnamese government has introduced a wide range of policies on national-level economic reform and development. In 1986 the *Đổi Mới* (renovation or open door) policy was introduced by The Central Government of Vietnam which aimed to industrialize the country by maintaining the substantial control of the state's economic operations and involve the international market (Nguyen, 2013). Gradually, freshwater protection dykes, brackish sluice gate, and irrigation and transport system were built to improve fresh water supply for intensive rice production (Renaud *et al.*, 2015). Structural transformation in agriculture sector, for example, shifting from conventional rice cultivation to high-value shrimp farming, has led to a dramatic changes in the Mekong Delta landscape and its ecohydrology, from freshwater to saline ecosystems (Lan, 2011).

Rapid development and changes in LCLU have been driven by concerns around food security and economic development. These changes have impacts on important nature forest and coastal ecosystems which provide vital ecosystem. To ensure self-sufficiency

and optimize export earnings the Vietnamese State Government have restricted the shift from rice to other land use, commonly aquaculture, by forcing each local province keep certain areas for rice cultivation (Vietnamese State Government, 2018). While the state desires to make the Mekong Delta into an agricultural and aquaculture production area, combined with urban and industrial zones development, biodiversity and conservation must be guaranteed for future generation (Rutten *et al.*, 2014). With an awareness of the importance of coastal wetland forest in providing estuarine and coastal ecosystem services such as coastal protection from storms, local governments in the Mekong Delta have endeavoured to maintain and expand forest along the coast (Bac Lieu People Committee, 2017). LCLU mapping applications have an important role in this region for monitoring and mapping of LCLU change to support decision making.

Of the mapping technologies available, synthetic aperture radar (SAR) has a lot of potential for LCLU mapping applications in the tropical and sub-tropical areas, especially in the Mekong Delta where frequent cloud cover poses a challenge to the use of optical remote sensing. There are two key advantages in the application of SAR in this region: 1) their all-weather capacity and 2) specific responses from radar backscattering associated with inundated vegetation such as rice (Bouvet and Le Toan, 2011; Nguyen *et al.*, 2015; Phan *et al.*, 2018). Recent studies have demonstrated the usefulness of SAR data, at C and X band (ENVISAT ASAR, Sentinel-1, COSMO-SkyMed) for mapping rice. Bouvet and Le Toan (2011) proposed a novel approach to classify rice cultivation area for whole Mekong Delta by using all available Envisat ASAR WSM and showed that time-series SAR imagery can allow accurate mapping of spatial distribution of rice area even under adverse atmospheric condition. Nguyen, Gruber and Wagner (2016a) demonstrated the potential of Sentinel-1A C-band SAR data for mapping regional rice cropping extent and rice phenological stages and found that VH polarized backscatter is more sensitive to rice growth than VV polarized backscatter. While, Phan et al. (2018) found that the HH/VV ratio retrieved from COSMO-SkyMed X-band SAR data can be utilised for mapping of

actual rice cultivated area after three image acquisition and discriminating long-cycle and short-cycle rice.

The majority of previous studies using SAR in this region focused exclusively on rice crop mapping, however, there is an important role for its application to support LCLU. As land use change in the Mekong Delta is very dynamic, resource managers and land use planners are required to utilize out-of-date maps which fail to depict current land use trends. There are few examples of studies characterising LCLU including urbanization, shrimp farming and natural ecosystems especially using the latest freely available Sentinel-1 C-band SAR imagery. To address this gap in the literature this thesis will assess the application of the recently launched Sentinel-1 C-band SAR imagery, along with the Google Earth Engine (GEE) platform to map LCLU.

In the Mekong Delta and other regions across the world, LCLU maps are utilized as inputs in a wide range of applications including urban planning, natural resource management, and ecosystem services mapping (Sawaya *et al.*, 2003; Chan and Vu, 2017; Wang, Lechner and Baumgartl, 2018; Sorichetta *et al.*, 2020). Up-to-date land cover maps and land cover change analysis are useful for detecting long-term land use trends to assist agriculture policy making (Tran, Tran and Kervyn, 2015). LCLU mapping is utilised in the Mekong Delta to support a range of land use planning activities such as for food security, illegal land use monitoring and updating existing land use mapping information. In the Mekong Delta a land use master plan is developed in every 10 years and land use planning decisions may annually require land use maps be updated and modified by local authorities at the district level in accordance with current socio-economic development status (Vietnamese State Government, 2018). Supply of current land use information is critical for the land use master planning, but presently rely on self-reported data (Ngo, Lechner and Vu, 2020). The findings in this thesis will be expected to assist local officials in terms of natural resource management and land use planning and monitoring through the development of remote sensing LCLU mapping methods

1.2 Research objectives

The objectives of this thesis are: 1) to demonstrate the utility of multi-temporal Sentinel-1A C-band SAR images for LCLU mapping in coastal regions of the Mekong Delta, 2) to develop a new algorithm to address the problem of detecting persistent building structures on land in different environmental and geophysical conditions and on sea surfaces under various wind speeds and directions beyond the capability of current methods, 3) to develop a novel and robust method using Sentinel-1 SAR data to identify and map LCLU that contains persistent surface water and seasonal inundated land cover.

1.3 Research questions

The following key research questions are addressed in this thesis:

1. How can SAR imagery support in LCLU mapping for natural resource management in the Mekong Delta (Chapter 2)?
2. How can persistent building structures on land and on sea surfaces be detected using SAR data (Chapter 3)?
3. How can persistent surface water and seasonal inundated land cover be identified with the use of the 3-D dual-polarization VV-VH-Season space (Chapter 4)?

1.4 Thesis outline

The thesis includes five chapters, three of which are research chapters investigating various applications of SAR to mapping land cover features, as indicated in the research objectives. The thesis is written from the perspective of mapping current environmental and socioeconomic challenge in the Vietnamese Mekong Delta. Chapter 2 uses machine learning approach to create a general LCLU map. The next two chapters seek to develop novel methods to deal with the remaining LCLU misclassification issues, not addressed in the previous chapter, associated with mapping structures, and surface water and inundation associated with rice-paddies and aquaculture land covers. These research chapters have been accepted, submitted or are in preparation for peer-review publication.

Chapter 2 demonstrates the utility of Sentinel-1A C-band SAR imagery to characterize LCLU in Bạc Liêu, a coastal and rapidly developing province in the Mekong Delta.

Twenty-one SAR images acquired in 2016 were classified in a four-step process. The SAR images were pre-processed to produce texture images. To reduce the effects of rainfall variation confounding the classification, the SAR images were divided into two categories: dry season and wet season and three input image sets were produced: a single date composite image, a multi-temporal composite image, and a multi-temporal and textural composite image. Two classification algorithms were applied for the three input image sets to find the highest overall classification accuracy. This chapter investigates different LCLU supervised classification methods and compares single date versus multi-temporal SAR image datasets in terms of classification accuracy. While the approach successfully mapped LCLU in the study area, there were misclassification issues associated with mapping building structures vs trees, and aquaculture vs rice paddy classes, related to permanent water and inundation. In the following chapters (Chapter 3 and Chapter 4) novel LCLU classification methods were applied to address these two LCLU mapping issues separately.

Chapter 3 develops novel methods using time-series data acquired from Sentinel-1 synthetic aperture radar to identify and map persistent building structures from coastal plains to high plateaus, as well as on the sea surface. From annual composites of SAR data in the two-dimensional VV-VH polarization space, the VV-VH domain for detecting building structures was determined. The methods were tested in five cities (Bạc Liêu, Cà Mau, Sóc Trăng, Tân An, and Phan Thiết) in Vietnam located in different socio-environmental regions with a range of urban configurations. This chapter successfully detected persistent building structures and reduced the misclassification between building structures vs trees due to water-tree interaction.

Chapter 4 proposes a novel and robust method to map LCLU that contains persistent surface water and seasonal inundated land cover. This chapter used the three-dimensional VV-VH-Season space to identify four domains where each domain is either dominated by one of the four classes (urban, forest, shrimp farm, and bare surface). The results show that the use of the 3-D dual-polarization VV-VH-Season space allowed a robust algorithm to be developed to overcome the falsifying effects of variations in incidence and azimuth

angles of SAR data. The mapping method can be applied for detecting persistent surface water, which can be used to monitor aquaculture in other wetland regions. This chapter successfully mapped rice paddy and reduced the misclassification between rice paddy vs aquaculture.

The final chapter 5 summarizes the thesis findings and describes potential future directions for the application of SAR data and Google Earth Engine to LCLU mapping in the Mekong Delta and globally.

Chapter 2 Land cover mapping of the Mekong Delta with Sentinel-1A synthetic aperture radar to support natural resource management

Published as:

In previous chapter, an overview of this thesis is presented. In this chapter, to leverage the usefulness of GEE, an application of land cover mapping using Sentinel-1 SAR data is introduced to support natural resource management.

2.1 Introduction

During the past two decades, the Vietnamese Mekong Delta has undergone a range of dramatic changes primarily shaped by human interactions with the water flow regime of the Mekong river (Giri, Defourny and Shrestha, 2003; Käkönen, 2008; Minderhoud *et al.*, 2018). The availability of freshwater and riverine sediment from the Mekong river and a complex canal network have enabled wide-scale agriculture and fisheries to development (Dang *et al.*, 2018; Ha *et al.*, 2018). The region is also rich in biological and geological resources supporting seasonally inundated grasslands and coastal wetlands which preserve and support various ecosystems such as mangrove forests, and peat wetlands which are managed for conservation (Do and Bennett, 2009; Nguyen *et al.*, 2013; Tue *et al.*, 2014; Van *et al.*, 2015). As Vietnam, and the Mekong Delta in particular, industrializes and modernizes, wetland areas have been impacted by conversion to agriculture and urban expansion (Käkönen, 2008; Leinenkugel, Oppelt and Kuenzer, 2014). Consequently, conservation reserves in the Mekong Delta have declined (Campbell, 2012) and there are

only 68,000 ha remaining of the once widespread swamp forest ecosystem (Huu Nguyen *et al.*, 2016).

Besides the transformation of natural areas to agriculture, largely due to population growth and socio-economic development, cultivated lands have also been converted to built-up areas (Tran, Tran and Kervyn, 2015). These urban areas are continuing to expand following the building of road networks connecting rapidly growing settlements, cities and industrial areas (Minderhoud *et al.*, 2018). Uncontrolled urban expansion inevitably leads to increased runoff and subsequent flooding (Rizk and Rashed, 2015), and cities in the region frequently suffer inundation caused by ocean tides, river-based flooding and heavy rain in the wet season threatening local livelihoods and transportation (Van Long and Cheng, 2018).

Table 2.1 Land use area in 2015 surveying year and planned land use for the period 2016-2020 (hectares) (Vietnamese State Government, 2018). Note that the planning units can overlap spatially with the same location allocated to one or more land uses.

Land use type	Surveyed year	Planned year				
	2015	2016	2017	2018	2019	2020
Rice cultivation (agriculture category)	59,872	59,864	59,801	59,493	59,060	58,846
Protected forest (agriculture category)	3,556	3,556	3,539	6,048	8,149	11,249
Aquaculture (agriculture category)	116,011	116,010	115,072	115,656	116,262	115,452
Urban	26,302	26,302	26,302	26,302	28,604	48,174

In Bạc Liêu province - one of the thirteen provinces in the Mekong Delta and the focus of this study - food security and forest conservation are a matter of great concern. For instance, 22 % of the total land in the province must be kept for rice plantation to ensure self-sufficiency and optimize export earnings (Vietnamese State Government, 2018). In addition, natural forest should be maintained and expanded along the coast. The local government aims to triple its area of natural forest from 3,556 in 2015 ha to 11,249 ha in 2020. Natural forests, in particularly mangrove forests, provide estuarine and coastal

ecosystem services such as erosion prevention and coastal protection from storms (Bac Lieu People Committee, 2017).

Table 2.2 Summary of SAR and optical remote sensing land cover and land use (LCLU) studies conducted in Mekong Delta.

Locations	LCLU types	Classification methods	Remote sensing data	Multi-temporal images used (Yes/No)	Reference
An Giang province	Rice crops	Random forest and support vector machines	Sentinel-1A SAR	Yes	(Son *et al.*, 2017)
Mekong Delta (13 provinces)	Rice crops	Phenology-based classification	Sentinel-1A SAR	Yes	(Nguyen, Gruber and Wagner, 2016a)
Mekong Delta (13 provinces)	Rice crops	Phenology-based classification	Envisat ASAR	Yes	(Nguyen *et al.*, 2015)
Mekong Delta (13 provinces)	Rice crops	Vegetation trajectories, Random forest supervised classification	Landsat 5, 7, 8	Yes	(Kontgis, Schneider and Ozdogan, 2015)
Bến Tre and Trà Vinh provinces	Rice, aquaculture, settled areas, coconut, sugar cane and orchard	ISODATA (manual interpretation)	Envisat ASAR, SPOT1, SPOT4, Landsat 3, 7	Yes	(Karila *et al.*, 2014)
Cà Mau province	Mangrove ecosystems	Object-based decision tree approach	SPOT5	No	(Vo *et al.*, 2013)
Mekong Delta (13 provinces)	Rice crops	Phenology-based classification	MODIS	Yes	(Son *et al.*, 2013)
Mekong Delta (13 provinces)	Rice crops	ISODATA	SPOT	Yes	(Thu *et al.*, 2012)
Cần Thơ province	Impervious surface	Support vector regression	TerraSAR-X	No	(Leinenkugel, Esch and Kuenzer, 2011)
Bạc Liêu and Sóc Trăng province	Rice cropping and inland aquaculture.	Time-series analysis	MODIS	Yes	(Sakamoto *et al.*, 2009)

There are several existing maps such as cadastral maps, land inventory maps, and land use maps at different scales (1/2,000 to 1/50,000) that have been developed for the province, district, and village levels in the study area. Land inventory maps are annually made from

cadastral data by utilizing the landowner's annual registry data and land inventory data. While land use maps are made every five years through editing, aggregating, and generalizing land inventory maps. However, land cover in this region is much more dynamic (Table 2.1) and using out-of-date maps may fail to represent current land use. Annual surveying for whole province is costly and requires a lot of labor. In addition, if landowners illegally convert from one land cover type to another (rice cultivation land or forest land to aquaculture) and do not register and report to the Department of Natural Resources and Environment; this will affect the land use map accuracy. Remote sensing for land use and land cover mapping may address the drawbacks of the current manual and labor-intensive approach and can provide a method for dynamic land use monitoring and planning.

As the Mekong Delta is such a significant region ecologically, economically, and socially, there have been a number of studies over the years using earth observation data to characterize land cover. However, the majority of these studies focused on rice crop distribution delineation utilizing optical satellite images (Sakamoto *et al.*, 2006; Son *et al.*, 2013; Kontgis, Schneider and Ozdogan, 2015) and radar satellite images (Liew *et al.*, 1998; Karila *et al.*, 2014; Nguyen, Gruber and Wagner, 2016a; Kontgis *et al.*, 2017). While, several studies were conducted to detect shrimp farming expansion using optical remote sensing (Tong *et al.*, 2004; Sakamoto *et al.*, 2009; Vo *et al.*, 2013). There are few examples of studies characterizing land use and land cover including urbanization, farming and natural ecosystems, especially utilizing the latest Sentinel-1 C-band SAR sensor and characterizing shrimp farms (Table 2.2).

SAR plays a crucial role in remote sensing because of its observation capability regardless of cloud cover and darkness making it an all-weather sensor (Bouvet and Le Toan, 2011). Sentinel-1 SAR system developed by the European Space Agency (ESA) has a constellation of two satellites, aiming to respond to the Earth Observation requirements of the European Union's ESA Global Monitoring for Environment and Security program(Aschbacher and Milagro-Pérez, 2012) and providing frequent revisit times and

extensive coverage (Torres *et al.*, 2012). Testing the capability of Sentinel-1 SAR in the Mekong Delta is especially relevant to Vietnam and other countries in the tropics as SAR can address the frequent cloud cover rendering optical remote sensing difficult. Furthermore, thanks to the free and accessible data policy, Sentinel-1 SAR provides a valuable resource for lower- and middle-income countries in the tropics with limited budgets for buying satellite data.

Various classification and processing methods have been used with SAR to improve classification accuracies. One such pre-processing approach is the application of Grey Level Co-occurrence Matrices (GLCM) textures, proposed by Haralick et al. (1973). Multiple studies have utilized GLCM to incorporate texture information derived from both optical and radar satellite imagery with original images to improve classification accuracy (Su *et al.*, 2008; Zhang and Milanova, 2013; Mishra *et al.*, 2017; Zakeri, Yamazaki and Liu, 2017). Mishra et al. (Mishra *et al.*, 2017) demonstrated that single polarized images could not effectively distinguish different land cover/land use (LCLU) classes, but in combination with texture information derived from these polarized images LCLU classification accuracy could be significantly improved. While, two notable classifiers in remote sensing are Random Forest (RF) and Support Vector Machines (SVM). The RF classifier (Breiman, 2001) has received a lot of attention among the remote sensing community due to its processing robustness and good classification results (Belgiu and Dragut, 2016; Gómez, White and Wulder, 2016; Pelletier *et al.*, 2016), while, SVM (Burges, 1998; Vapnik, 1998) is a powerful machine learning approach for data classification and has been widely used for remote sensing (Wang et al. 2017).

The aim of this study is to characterize LCLU in the Bạc Liêu province, a rapidly developing province in the Mekong Delta, with Sentinel-1A SAR. The utility of Sentinel-1A SAR and multi-temporal imagery has yet to be tested in tropical regions for mapping coastal landscapes dominated by a combination of rice and aquaculture farming systems. Shrimp farming aquaculture is expected to be one of the most important sources of socio-economic development in Bạc Liêu province by 2025, while rice farming is considered

important for food security (Bac Lieu People Committee, 2018). However, the majority of previous applications of SAR and optical remote sensing in the Mekong Delta have focused exclusively on mapping rice crops (Table 2.2). The objective of this study is to demonstrate the utility of multi-temporal Sentinel-1A C-band SAR images for LCLU mapping in coastal regions of the Mekong Delta. In addition, the usefulness of the LCLU mapping for updating existing land cover maps and monitoring illegal land use activities for land use master planning is also reviewed. In the conclusions, the application of this approach for food security and coastal forest monitoring from the perspective of the local authorities is remarked.

2.2 Study area and data

2.2.1 Study area

The Vietnamese Mekong Delta region, popularly known by Vietnamese as "Cửu Long" ("Nine Dragons" in English), is in the tropics between $8^0 33^{'}$-$10^0 55^{'}$N and $104^0 30^{'}$-$106^0 50^{'}$E. It is a huge fertile flat plain covering an area of approximately 3.9 million hectares. It is the largest rice production region in Vietnam, providing livelihoods for a population of more than 20 million. The climate of the Mekong Delta region is characterized as monsoonal and mostly hot and humid. The two seasons, the wet season and the dry season, in the Mekong Delta region are well-defined. The mean annual rainfall in the Mekong Delta region is approximately 1,800 mm, and 90% of this falls in the wet season (from May to November) (Thu *et al.*, 2012).

The study area covers Bạc Liêu province, a southeastern part of the Mekong Delta region (shown in Figure 2.1), approximately 2,500 km^2. The area is dominated by rice production, shrimp farming inland aquaculture and also includes smaller remnant patches for biological conservation (Sakamoto *et al.*, 2009). The National Road 1-A main road divides the study region into two environmental sub-regions, a saline sub-region and a fresh water sub-region.

2.2.2 Datasets

Land cover was identified using Sentinel-1A SAR images covering the Mekong Delta in 2016 collected by the European Space Agency (ESA). Specifically, the Sentinel-1A C-band SAR images are Interferometric Wide (IW) swath Level-1 ground-range detected, high resolution (GRDH) products. The IW mode was operated in the dual polarization mode (VV and VH) with 250 km swath, 5 x 20 m spatial resolution (single look). To avoid the effects of rainfall variations confounding the classification by changing the characteristics of the land covers (i.e. dry versus shrimp ponds filled with water), the SAR images were divided into two categories: dry season (Jan-April) and wet season (May-December) (Thu *et al.*, 2012). Table 3.3 below presents the summary of Sentinel-1A C-band SAR IW Level 1 GRDH images used in this study.
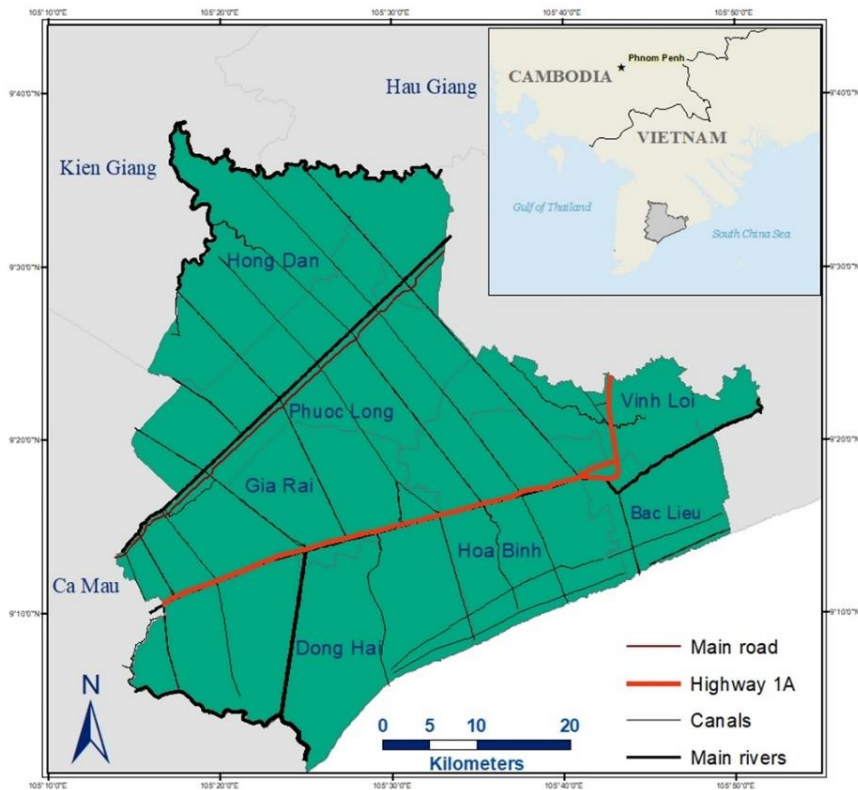
Figure 2.1 Study area location in the Mekong Delta (south-eastern of Vietnam).

Table 2.3 Sentinel-1A SAR images used in the study.

Product ID	Acquisition date
S1A_IW_GRDH_1SDV_20160117T224530_20160117T224558_009540_00DDCD_411A	17 Jan 2016
S1A_IW_GRDH_1SDV_20160210T224529_20160210T224557_009890_00E7FF_F199	10 Feb 2016
S1A_IW_GRDH_1SDV_20160305T224529_20160305T224557_010240_00F216_F126	05 Mar 2016
S1A_IW_GRDH_1SDV_20160410T224514_20160410T224539_010765_010140_2B69	10 Apr 2016
S1A_IW_GRDH_1SDV_20160410T224539_20160410T224604_010765_010140_B3F2	10 Apr 2016
S1A_IW_GRDH_1SDV_20160516T224518_20160516T224543_011290_0111B7_F5F5	16 May 2016
S1A_IW_GRDH_1SDV_20160516T224543_20160516T224608_011290_0111B7_E9A2	16 May 2016
S1A_IW_GRDH_1SDV_20160609T224520_20160609T224545_011640_011CF1_69C1	09 June 2016
S1A_IW_GRDH_1SDV_20160609T224545_20160609T224609_011640_011CF1_705A	09 June 2016
S1A_IW_GRDH_1SDV_20160703T224521_20160703T224546_011990_012808_2346	03 July 2016
S1A_IW_GRDH_1SDV_20160703T224546_20160703T224611_011990_012808_362D	03 July 2016
S1A_IW_GRDH_1SDV_20160808T224523_20160808T224548_012515_01394B_D4A2	08 Aug 2016
S1A_IW_GRDH_1SDV_20160808T224548_20160808T224613_012515_01394B_DD8B	08 Aug 2016
S1A_IW_GRDH_1SDV_20160901T224524_20160901T224549_012865_014504_1409	01 Sept 2016
S1A_IW_GRDH_1SDV_20160901T224549_20160901T224614_012865_014504_649C	01 Sept 2016
S1A_IW_GRDH_1SDV_20161007T224525_20161007T224550_013390_0155E8_55BD	07 Oct 2016
S1A_IW_GRDH_1SDV_20161007T224550_20161007T224615_013390_0155E8_325C	07 Oct 2016
S1A_IW_GRDH_1SDV_20161112T224525_20161112T224550_013915_016666_7CA2	12 Nov 2016
S1A_IW_GRDH_1SDV_20161112T224550_20161112T224615_013915_016666_7500	12 Nov 2016
S1A_IW_GRDH_1SDV_20161218T224524_20161218T224549_014440_0176B7_6929	18 Dec 2016
S1A_IW_GRDH_1SDV_20161218T224549_20161218T224614_014440_0176B7_22BA	18 Dec 2016

2.3 Methodology

2.3.1 Remote sensing method overview

A range of classification algorithms and input image datasets were systematically tested. The method can be divided into three steps: pre-processing, generation of texture images using GLCM measure, comparison of classification accuracy (single-date versus multi-temporal, single-date versus multi-temporal with texture, multi-temporal versus multi-

temporal with texture as in Table 2.4), and the calculation of the Z-test statistic. The flowchart shown in Figure 2.2 summarizes the methods.

Table 2.4 Input image sets.

Composite band image	Dry season	Wet season
Single date	VV and VH composite image.	VV and VH composite image.
Multi-temporal	Eight bands composite image of VV and VH for four image dates.	Sixteen bands composite image of VV and VH for eight image dates.
Multi-temporal with texture	Sixteen bands composite image made up of the multi-temporal 8-band composite plus texture versions for each.	Thirty-two bands composite image made up of the multi-temporal 16-band composite plus texture versions for each.
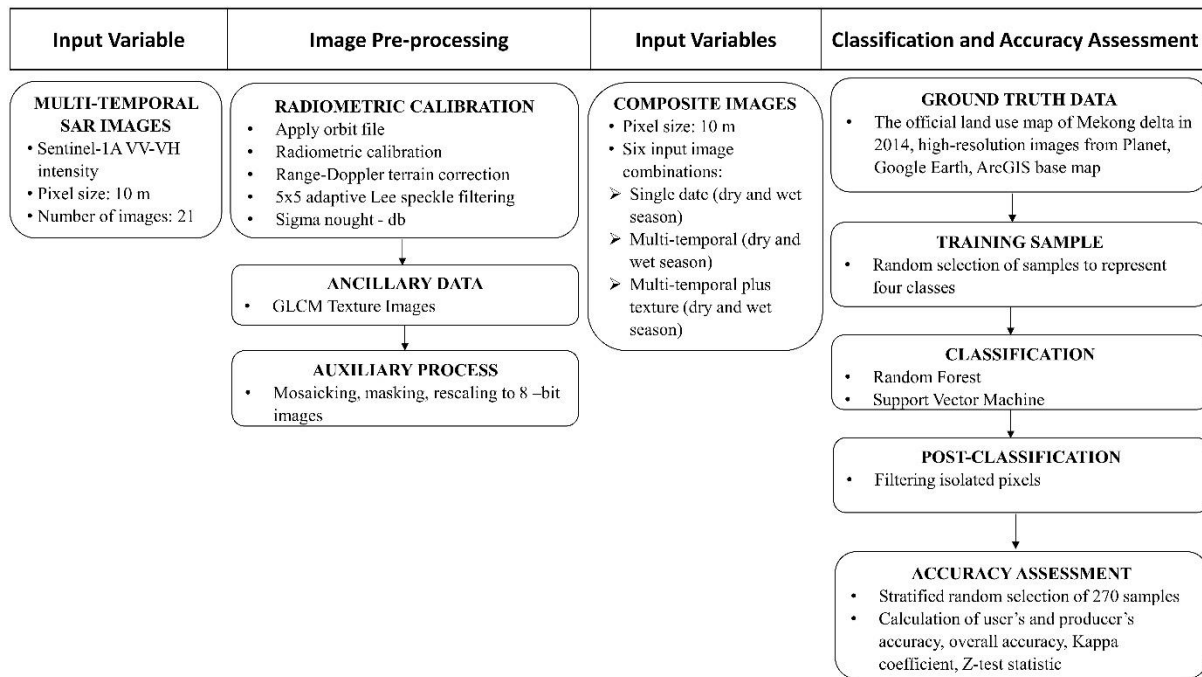
Figure 2.2 Processing and analysis workflow.

2.3.2 Land cover class description

The number of land cover classes chosen in this study was based on the official land management documents published by Vietnamese State Government and Bạc Liêu

Province People's Committee (Vietnamese National Assembly, 2013; Bac Lieu People Committee, 2017; Vietnamese State Government, 2018), and the practical limitations of Sentinel-1 SAR sensor. Coarse-scale resolution land use categories that correspond to the key land use classes used for land use management such as for the identification of the minimum area of rice cultivation for food security and forests for coastal protection are identified. At the coarsest scale, land cover and land use defined by the Vietnamese State Government are categorized as agriculture, non-agriculture, and unused land (Vietnamese National Assembly, 2013). Agricultural land use type includes rice cultivation, forest, aquaculture land while non-agriculture land use types include industrial land, and engineering infrastructure land (schools, medical centers, sport complex, cultural sites), settlement land (buildings and houses in rural and cities). For this study, four land cover classes, three of which - forest, shrimp farming, and rice paddy fields - correspond to government land use mapping were mapped. The fourth land cover, representing built up, was an aggregation of the engineering infrastructure land and settlement land classes. However, small features such as roads and canals are impossible to map due to the spatial resolution of Sentinel-1 SAR sensor. For example, linear-shaped features such as small irrigation canals and rural roads have widths smaller than 10 m and cannot be clearly captured and distinguished by the 10-m spatial resolution of Sentinel-1 SAR sensor (Figure 2.3).

In the study area, the landscape mostly consists of built-up, forest, shrimp farming, and rice paddy fields. Built-up areas included buildings in urban and in agricultural areas. The forest class comprised coastal mangrove trees, riparian trees along rivers, and mangrove trees in shrimp ponds, while roads and borders of paddy fields may be included due to their backscatter behaviors and the limitation of SAR resolution. The shrimp farming class included man-made canals and man-made ponds (typically with a rectangular shape filled with sea water) and natural/semi-natural shrimp ponds where mangrove trees are grown along the pond borders to produce habitat for shrimp. The paddy field class includes rice that may have double or triple rice cycles per year. The number of rice crop cycles and

planting time vary from place to place due to weather, economics, subjective decisions at a regional scale (Kontgis *et al.*, 2017).

(*a*)

(i) (ii) (iii) (iv)

(*b*)

(i) (ii) (iii) (iv)
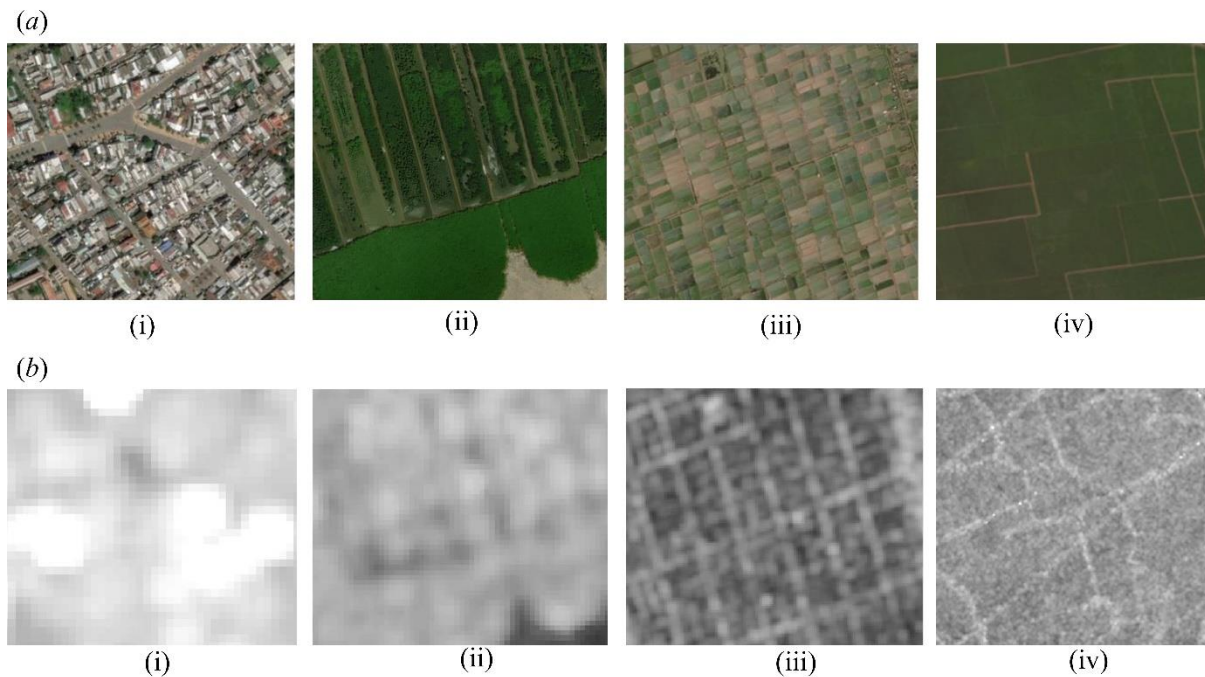
Figure 2.3 Land cover classes: (i) Built-up, (ii) Forest, (iii) Shrimp farming, (iv) Paddy field. (*a*) Optical images (DigitalGlobe's Vivid 50cm high-resolution imagery captured in 09 Nov 2014) extracted from ArcGIS basemap showing the same areas with Sentinel 1 subsets in (b). (*b*) SAR backscatter coefficient images extraction at VH polarization.

2.3.3 Data pre-processing

The Sentinel-1A images were radiometrically-calibrated, terrain-corrected, and speckle-filtered using the SNAP 5.0 Sentinel Application Platform toolbox (available at http://step.esa.int/main/toolboxes/snap/). The radiometric calibration was conducted to convert pixel values of VH and VV amplitude into sigma naught (σ^0) values representing the radar backscatter from the earth surface.

The calibrated multi-temporal images were then geometrically corrected using the Range-Doppler Terrain Correction algorithm with the 3-arc-sec Shuttle Radar Topography Mission (SRTM) elevation model. After applying geometric correction, the images were

resampled to a 10-m spatial resolution and re-projected to the Universal Transverse Mercator (UTM) coordinate system (zone 48N).

SAR images are effected by inherent speckles in backscatter data, which adversely impact image segmentation and classification accuracy (Lee *et al.*, 1999). In this study, a 5 x 5 adaptive Lee filter was applied to reduce speckle based on the methods described in Lee et al. (Lee *et al.* 1999), who demonstrated such approaches are important for preserving polarimetric properties, improve image quality, and boost the classification performance. The 5 x 5 kernel was used as it has been found to be suitable in many recent studies of similar environments (Son *et al.*, 2017; Oon *et al.*, 2019). Backscatter data in these images were in the decibel unit (dB), commonly used in radar remote sensing. Figure 3.4 presents a time series of backscatter values for the four classes in the study site for the whole of 2016.
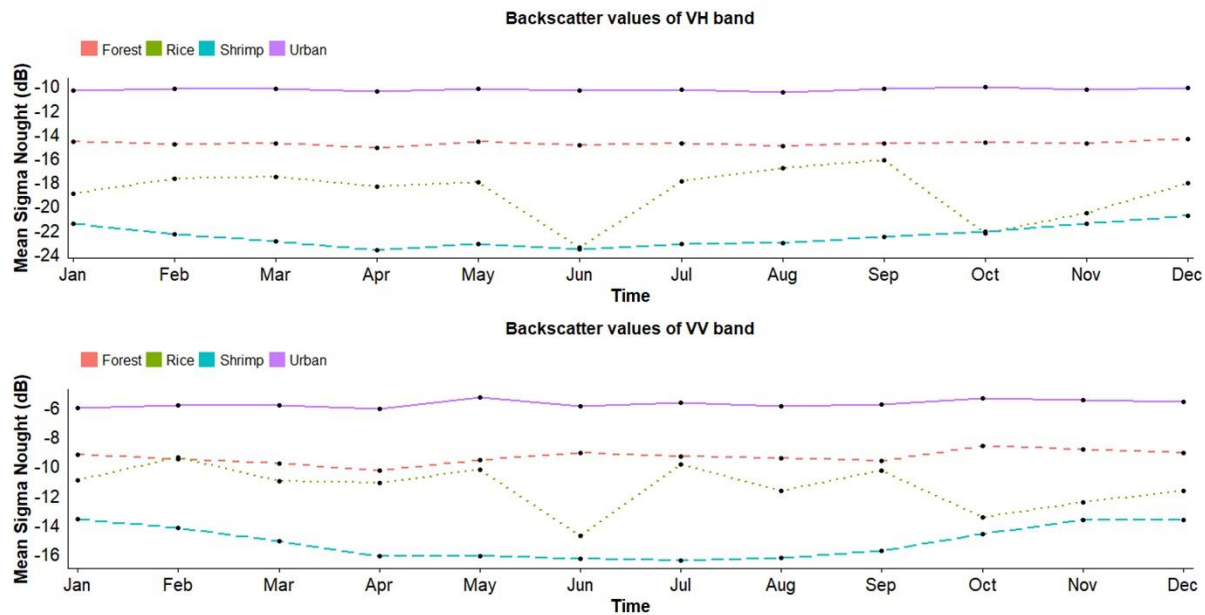
Figure 2.4 Mean multi-temporal backscatter values of Sentinel-1A VH and VV intensity images in 2016 based on 500 ground truth locations.

2.3.4 Grey level Co-occurrence matrices textures

To assist the classification, texture based images were computed from the original dataset based on Grey Level Co-occurrence Matrices (GLCM) textures, a procedure originally

proposed by Haralick et al. (Haralick, Shanmugam and Dinstein, 1973). GLCMs are a second order statistical texture measure considering the relationship between groups of two pixels and used widely in satellite image interpretation. The GLCM is a matrix of the frequencies of pixel pair values within a neighborhood of a given window size. The matrix is then normalized based on its co-occurrence probability which can be defined as (Clausi, 2002) :

Probability(x) = {$P_{i,j} | (\delta, \theta)$}

Equation 2.1 Normalization of GLCM co-occurrence probability

where δ is a pixel distance, θ is the direction, $P_{i,j}$ (the co-occurrence probability between grey level i and j) which is defined as:

$$P_{i,j} = V_{ij} / \sum_{i,j=0}^{N-1} V_{i,j}$$

Equation 2.2 GLCM co-occurrence probability

in which $V_{i,j}$ is the number of occurrences of grey level i and j within the given image window and N is the quantization level. The selection of the number of texture measures and their parameterization of the quantization level, window size, offset distance and orientation pose a challenge. However, Hall-Beyer (2017) indicated that texture measures within a specific group, for example, contrast group, orderliness group, and descriptive statistic groups are highly correlated in most cases and mean texture measure has been shown to be independent of other texture measures (r^2 <0.1). Therefore, in this study the mean texture measure for creating the texture images (Table 3.5) was chosen.

Table 2.5 GLCM mean texture measure equation.

Texture measure name	Calculation formula
Mean	$\mu_i = \sum_{i,j=0}^{N-1} i(P_{i,j}) \qquad \mu_j = \sum_{i,j=0}^{N-1} j(P_{i,j})$

$P_{i,j}$ is the probability of values i and j in adjacent pixels within the window specifying neighborhood. μ_i is the mean calculation based on the reference pixel and μ_j is the mean using the neighbor pixel.

For the GLCM texture measure parameterization of the quantization level, window size, offset distance and orientation, a range of values identified in the literature were selected. The value of 32 was selected for grey level quantization since a value of N under twenty-four or greater than sixty-four can cause unreliable classification outputs or not improve the accuracy (Clausi, 2002). The orientation was set to 0 as it has been demonstrated that it can improve the results in SAR image classification (Barber and LeDrew, 1991; Clausi, 2002). The window size was set to 9 x 9 and displacement value was set to 1. All GLCM texture images were performed by SNAP 5.0 Sentinel Application Platform toolbox.

2.3.5 Training samples

A total of 500 training samples in four classes were collected from the official land use map of the Mekong Delta in 2014 (Cantho University, 2017) in combination with the high-resolution images on Google Earth™, Planet (Google Earth Pro, 2017; Planet Labs Inc, 2017), the ArcGIS base map and knowledge of study site. All training samples were digitized as single points associated with a single pixel in SAR images and aligned at the center of 5 x 5 homogeneous pixels. The locations of the training samples were randomly spatially distributed across the study area (Figure 2.5).
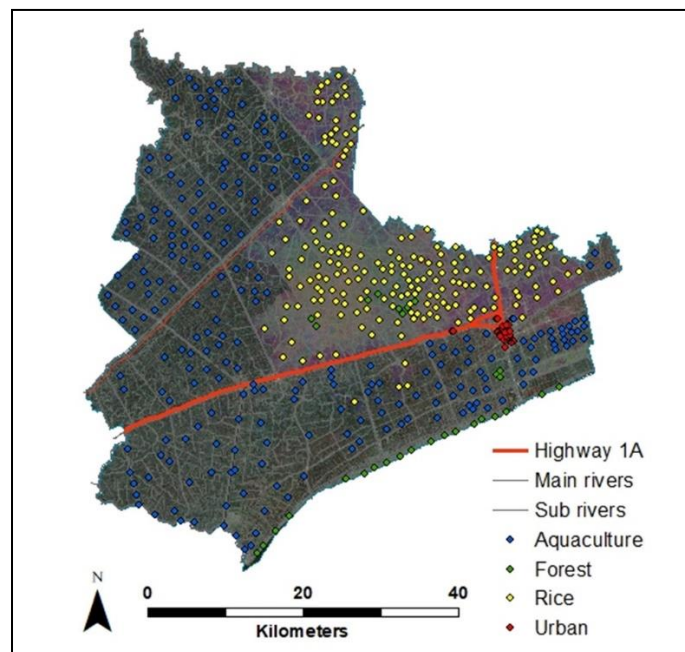
Figure 2.5 Training samples distribution map

2.3.6 Random forest and support vector machine classifier

The RF and SVM tools of EnMAP Box platform-independent software were used to classify SAR images. Two parameters need to be defined in RF classifier to construct a predictive model: the number of desired classification trees k and the number of prediction features m used in each split to grow the tree (Rodriguez-Galiano *et al.*, 2012). In this study, k was set to 100 and the number of prediction features m was set to square root of all features to generate the RF classification (Eisavi *et al.*, 2015).

The SVM algorithm separates the data training samples based on the optimal hyperplane into discrete predefined classes, with the decision boundary located to minimize misclassification between classes (Fukuda, Katagiri and Hirosawa, 2002). The SVM classification requires the selection of a kernel function. The Gaussian Radial Basic Function (RBF) kernel was selected (Lardeux *et al.*, 2009; Trisasongko *et al.*, 2017) in this study. To get the most appropriate parameter a grid search approach with default ranges that have been demonstrated to be successful was used (van der Linden *et al.*, 2015).

2.3.7 Post-classification

To filter out pixel noise and isolated pixels before generating the final classified images, an 8-neighbouring cells majority filter was used. Finally, the filtered images were post-processed further using the class boundary smoothing and region grouping algorithm in ArcMap 10.4.1 Spatial Analyst tools.

2.3.8 Accuracy assessment

In the final step the quality of the remote sensing products obtained through the combination of six datasets and two remote sensing classifiers was assessed. A stratified (by land cover) randomly spatial distributed set of 270 validation points were used to test accuracy. These points were positioned at the central of 5 x 5 homogeneous pixels. None of these points were from pixels used as training data. Like the training data, the validation points were informed by the official land use map of the Mekong Delta in 2014 (Cantho University, 2017), land use master planning map of Bạc Liêu province in 2013, high resolution images on Google Earth™, Planet (Google Earth Pro, 2017; Planet Labs Inc,

2017), and the ArcGIS base map and knowledge of study site. Accuracy was measured and described using an error matrix and a variety of measures such as the Z statistic, Kappa and producer and user accuracy. The error matrices, Z statistic and overall accuracy reports were generated from ArcMap 10.4.1 and calculated using Spyder platform (Scientific Python Development Environment).

In addition, the Z-test statistic was also used to verify whether the classification results generated by SVM or RF for the three sets of input data were significantly different. The Z statistic is based on the actual agreement in the error matrix between the classified image and the reference data from the major diagonal and chance agreement indicated by the row and column totals (Congalton and Green, 2009). The following equation was used to calculate the Z-statistic.

$$Z = |K_1 - K_2|/\sqrt{var(K_1) + var(K_2)}$$

Equation 2.3 Z-statistic calculation

where K_1 and K_2 are the Kappa coefficients calculated from two sets of input image (i.e. single-date vs multi-temporal, single-date vs multi-temporal with texture, multi-temporal vs multi-temporal with texture), and *var*(K_1) and *var*(K_2) are their associated variances respectively. If the test Z statistic absolute value is greater than 1.96 at 95% confident level, the result is significant and the difference between two error matrices are not random (Congalton and Green, 2009).

2.4 Results and discussion

2.4.1 Land cover mapping methods

The multi-temporal images had a higher overall classification accuracy than single-date images no matter which classification algorithms were used. The multi-temporal with texture 32 band composite image in wet season using SVM had the highest accuracy with an overall accuracy of 94.81% and Kappa coefficient of 0.92 (Figure 2.6). In contrast the single-date images in dry season, regardless of classification method had the lowest accuracies at 75.19 % and 73.33 % for SVM and RF respectively and a Kappa coefficient

of 0.62 and 0.59. Both the overall accuracy and Kappa statistic showed similar patterns with SVM performing better than RF and multi-temporal images with texture performing better than other input images (Figure 3.6).
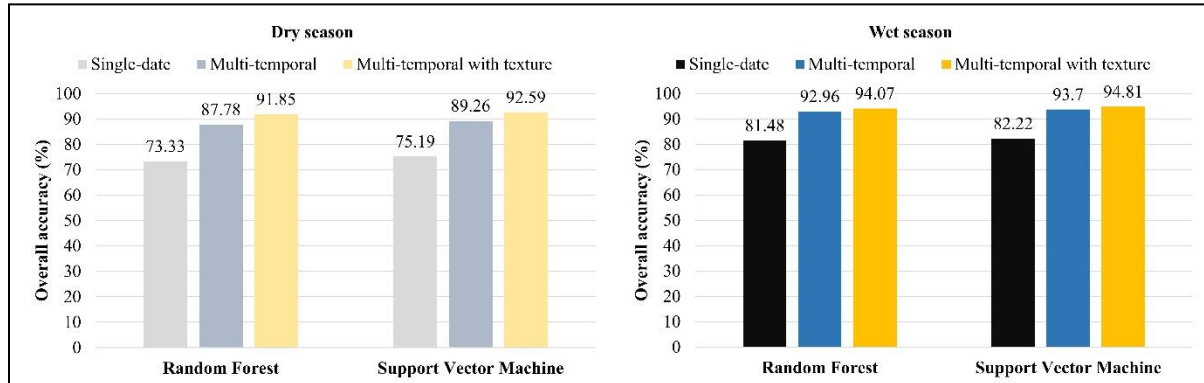
Figure 2.6 SVM and RF overall classification accuracy on six input image sets: single-date, multi-temporal, multi-temporal with texture in dry and wet seasons.

Table 2.6 shows the results of the Kappa analysis comparing the error matrices of single-date versus multi-temporal, single-date versus multi-temporal with texture, and multi-temporal versus multi-temporal with texture input image sets to determine if they are significant different. The results indicate that the classification results obtained from single-date versus multi-temporal, and single-date versus-multi-temporal with texture for both dry and wet seasons were significantly different since the Z statistic values were greater than the critical value of 1.96. However, this was not the case for multi-temporal versus multi-temporal with texture of both dry and wet season with a Z statistic value ranging from 0.6 to 1.54, smaller than the critical value of 1.96.

While the observed differences in accuracy between SVM and RF in Table 2.6 was small, the differences associated with using different image sets (i.e., multi-temporal versus single date) was far greater (Figure 2.7), though overall land cover patterns appeared similar regardless of input images and land cover classifiers used. For example, Figure 2.7 shows that both shrimp farming spatial patterns are correctly mapped as being distributed in the western part and the coastal regions of the Bạc Liêu province. In addition, the benefit of including texture were small in comparison to the difference between the single date versus

multi-temporal. While the results may be case-study specific, they suggest that the inclusion of multi-temporal images are the greatest driver for improving overall classification accuracies.

Table 2.6. Kappa analysis results for the pairwise comparison of the error matrices. A Z-statistic of greater than 1.96 indicate there is a significant difference between two error matrices.

	Pairwise comparison	Z Statistic	
		RF	**SVM**
Dry season	Single date versus multi-temporal	4.55	4.45
	Single date versus multi-temporal with texture	6.08	5.80
	Multi-temporal versus multi-temporal with texture	1.54	1.35
Wet season	Single date versus multi-temporal	3.77	4.37
	Single date versus multi-temporal with texture	4.37	5.00
	Multi-temporal versus multi-temporal with texture	0.60	0.67
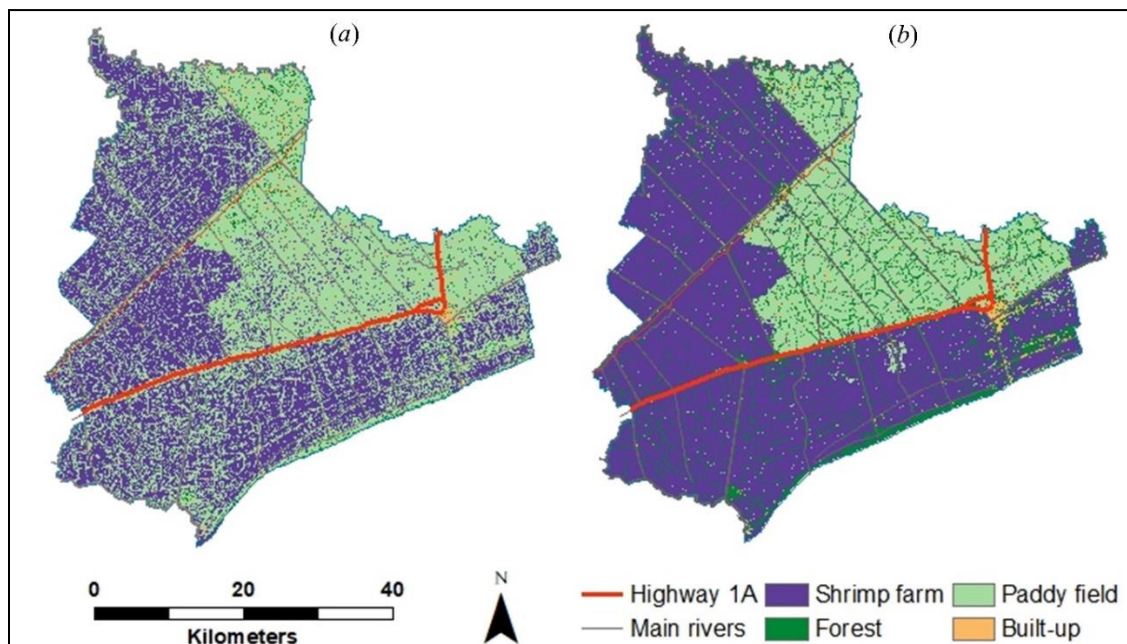
Figure 2.7 Land cover classification using SVM on a single-date (*a*) and a multi-temporal with texture (*b*) input image sets in wet season.

24

Out of four land cover classes mapped shrimp farming class tended to have higher accuracy than forest, paddy field, and built-up classes for both SVM and RF implemented with the same inputs. Table 2.7 summarizes the accuracy assessment results for error matrices using RF and SVM classification on a multi-temporal 16-band composite image, however, similar patterns in the error matrices were produced for all of the classification outputs regardless of classifiers or image sets. Shrimp farming had the highest accuracies as the backscatter intensity values and multi-temporal characteristics were unique compared to the other land cover classes. Due to the presence of surface water which results in specular reflection that directs the radar waves away from the backscatter direction, shrimp farming has low backscatter values in both VH and VV band throughout the year. In fact, shrimp-farm backscatter is far below and thus well distinguished from both the urban and forest classes (Figure 2.4). Whereas the rice backscatter may be close to that of the shrimp classes at some times in a year, the annual variability of shrimp-farm backscatter is low (~2 dB) and distinctively different from that of the very larger seasonal change of rice backscatter as much as 7 dB as seen in Figure 2.4, making it well distinguishable between shrimp and rice classes too. The forest class has a reasonable accuracy of ~76% given than it has the least number of ground-truth points for classification training and for verification accuracy. Figure 2.8 shows an example of four field trip photos at four different locations for the four land cover classes (shrimp farm, paddy field, forest, built-up) on land cover map derived from multi-temporal images.
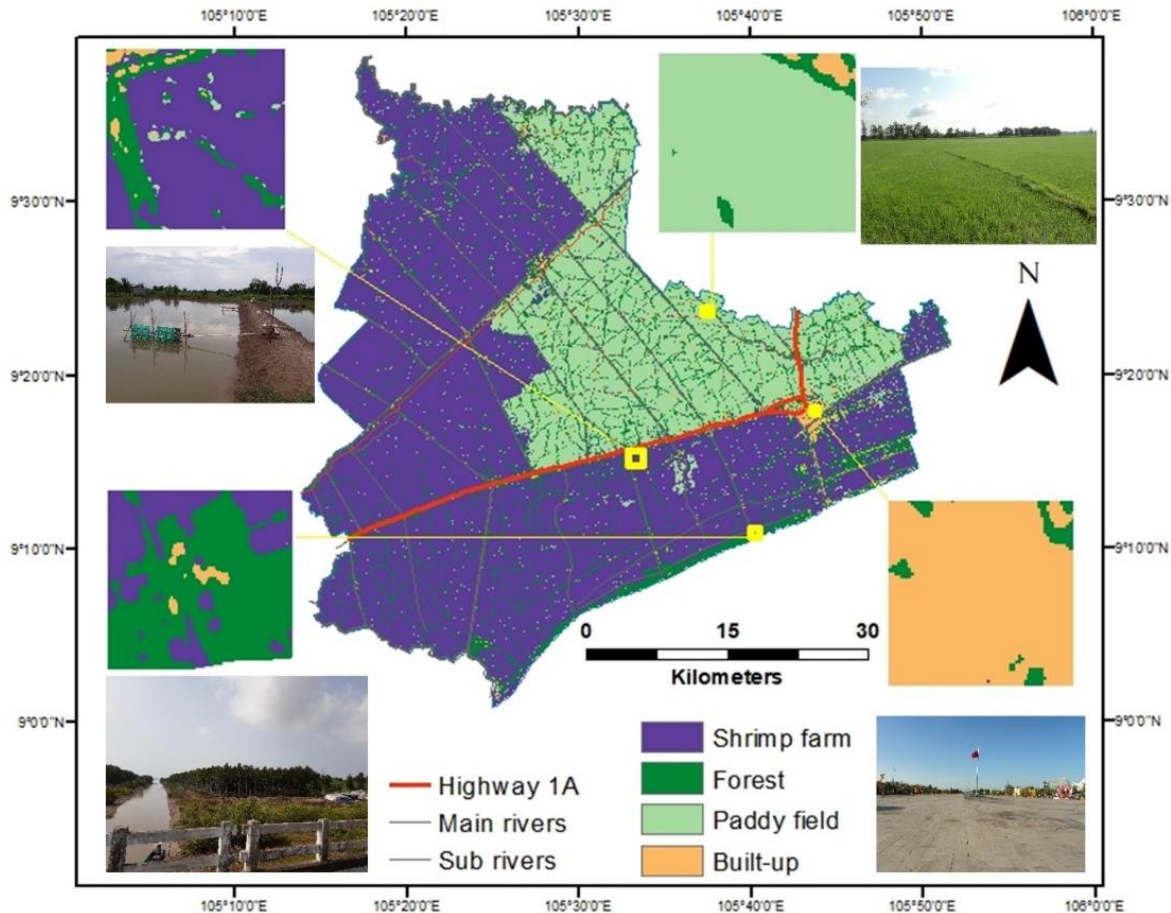
Figure 2.8 Field trip photos (taken on 15 Feb 2019) and land cover classification using SVM on a multi-temporal with texture input image set in wet season.

2.4.2 Characteristics of land cover in the study area

Table 2.8 presents information on the area and proportion of each land cover class in the Bạc Liêu province. The built-up area is 6.7 thousand hectares constituting the smallest proportion of land cover. As in other cities in the Mekong Delta, Bạc Liêu city experiences frequent flooding in wet season. Urban flooding is driven by uncontrolled urban expansion into unsuitable areas (e.g. low land susceptible to subsidence) in combination with heavy rainfall and high tide and negatively impacts on local transportation and livelihoods (Chi, 2018). Forests, covering an area of around 32 thousand hectares, play a crucial role in flood mitigation and in coastal erosion reduction. However, the recent growth of intensive shrimp farming has endangered the protective function of these coastal forests (Wölcke *et al.*, 2016). Because of the importance of these coastal wetland ecosystems for conservation and

coastal protection, there are several projects focusing on rehabilitation and enhancing ecological functionality; e.g., *GIZ* project supported by German and Australian government (GIZ, 2020).

Table 2.7 Accuracy assessment results for error matrices using RF and SVM classification on a multi-temporal 16-band composite image.

Ground reference data (pixels)	Classification results (points)				
	Shrimp	Forest	Rice	Built-up	Total
RF					
Shrimp farming	117	1	1	0	119
Forest	3	26	0	1	30
Paddy fields	10	2	79	0	91
Built-up	0	1	0	29	30
Total	130	30	80	30	270
Producer accuracy (%)	90.0	86.67	98.75	96.67	
User accuracy (%)	98.32	86.67	86.81	96.67	
Overall accuracy (%)	92.96				
Kappa coefficient	0.89				
SVM					
Shrimp farming	120	2	0	1	123
Forest	7	25	0	1	33
Paddy fields	3	1	80	0	84
Built-up	0	2	0	28	30
Total	130	30	80	30	270
Producer accuracy (%)	92.31	83.33	100	93.33	
User accuracy (%)	97.56	75.76	95.24	93.33	
Overall accuracy (%)	93.7				
Kappa coefficient	0.9				

Table 2.8 Area and proportion of land cover classes.

Land cover classes	Total area (ha)	Area proportions (%)
Built-up	6,711	2.7
Forest	32,242	13.0
Paddy fields	58,487	23.6
Shrimp farming	150,043	60.6

Within the Bạc Liêu province shrimp farming accounts for the greatest proportion of the landscape at approximately 150,000 ha. The second greatest proportion is rice paddy fields

at around 58,000 ha. During the 1990s a number of salinity protection systems such as irrigation canals, dykes and sluice gates were built to protect freshwater systems for rice farming and transform former brackish ecological zones into freshwater zones. Shrimp farming has also been supported through development schemes such as the well-known *Quan Lo Phung Hiep* canal project (Hoanh *et al.*, 2012) constructed in Bạc Liêu and its two neighboring provinces (Soc Trang and Ca Mau). The large expansion in shrimp farming area in Bạc Liêu mainly resulted from the state's policy of infrastructure investment in the construction of a dense network of dikes and embankments and favorable loans (Sakamoto *et al.*, 2009). More recently, as a consequence of a policy toward land use diversification extensive areas have been converted from freshwater back to brackish farming (i.e. shrimp farming) (Käkönen, 2008).

Shrimp exports in Vietnam have increased from two million dollars in 2010 (Lan, 2013) to 3.5 million dollars in 2017 (Thu, 2018). However, the ecological and social impacts are of great concern. These changes in land cover by intense engineered anthropogenic land uses in the Mekong Delta can be readily seen in the results of land cover mapping.

2.4.3 Challenges of applying SAR and Sentinel-1 for mapping in the Mekong Delta

One of the greatest challenges in the study area was distinguishing between paddy fields and shrimp farming in a given spatial snapshot. SAR backscatter is sensitive to surface roughness, soil moisture, and vegetation (Nguyen *et al.*, 2015), and backscattering characteristics of these two land cover classes could be quite similar at certain times of the year. During the early rice growing season, the images intensities between the two classes are similar as the rice paddies are filled with water, similar to the aquaculture ponds (as showed in Figure 2.4) resulting in misclassification between those two classes. Hence, the inclusion of multi-temporal images results in a large improvement in classification accuracies. Studies specifically characterizing rice growing land cover nearly always include multi-temporal images (Bouvet and Le Toan, 2011; Karila *et al.*, 2014; Kontgis *et al.*, 2017).

Another source of error which resulted in misclassification was between shrimp farms and paddy fields, as they all include different combinations of vegetation, water, and bare soil (Figure 2.9). For example, the shrimp farming class is made up of many shrimp ponds with mangroves grown to provide habitat for shrimp. These trees are commonly smaller than the pixel size making this class a combination of very different land cover features with different backscatter characteristics that are present at below the spatial resolution of the sensor. The study found some isolated pixels of shrimp pond class located inside paddy field and similarly paddy field class located inside shrimp pond class. As a result, the mixed-pixel and boundary effects contributed to mapping errors even though post-classification smoothing techniques were applied. Despite being an effective classifier for LCLU classification, decision tree classifier that are pixel-based and cannot fully suppress the influence of mixed pixels during classification process (Yang *et al.*, 2017).
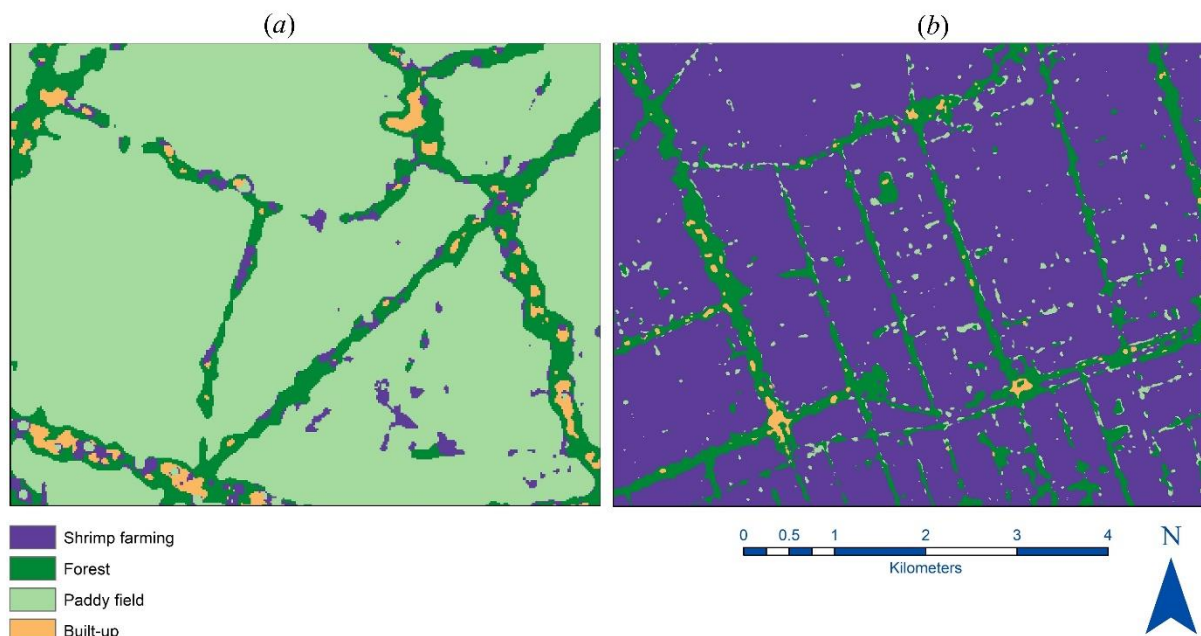
Figure 2.9 SVM (16 bands) misclassification between shrimp farming class and paddy field class: (*a*) isolated pixels of shrimp farming class located inside rice crop, and (*b*) paddy field class located inside shrimp farming class.

Other sources of error common to SAR classification in general are due to variations of the incidence angle of Sentinel-1A satellite and ground truth errors contributed the mapping

results. The incidence angle ranged from 30.84^0 to 45.99^0 over the study area and may influence the variation in backscatter values of land cover classes, leading to errors. Son et al. (2017) indicated that the variation of incidence angle could result in slight shifts in rice crop patterns. Additional sources of error in this study are due to changes of land cover and the difficulty of obtaining ground truth data that coincides with current land cover conditions. However, such issues are common to most remote sensing applications (Lunetta *et al.*, 1991; Wang and Gertner, 2013), calling for more satellite data coverage with more field validations.

The most problematic issue in the study area for classification was the confusion between rice crop and shrimp farming. To eliminate this, potentially additional extraction methods based on phenological characteristics of rice crop could be used to distinguish rice crop from shrimp-farming class. However, this is likely to not be such an issue in less dynamic environments than the Mekong Delta.

2.4.4 Land use planning with SAR in the Mekong Delta

This study demonstrated the potential for SAR to provide an up-to-date complementary source of information for updating existing land cover maps and for monitoring illegal land use activities in land use master planning at the provincial level. This information is required for a range of land use planning activities. For example, for food security, provinces need to have 22% of the total area as rice plantation. As in other regions of Vietnam, a land use master plan in Bạc Liêu province is made every 10 years and the local authority at district level may annually update, modify and make land use planning decisions in accordance with current socio-economic development conditions (Vietnamese State Government, 2018). The issue is that the provision of land use information currently depends on self-reported data that are disparate in time and in space. Remote sensing, in synergistic combination with existing surveying results from local authorities can provide valuable land cover information to local authorities. Up-to-date land cover maps are necessary to detect long-term land use trends as well as aid agriculture policy making

(Tran, Tran and Kervyn, 2015). This is especially the case in the Mekong Delta where land use is very dynamic.

The Department of Natural Resources and Environment can use remote sensing to annually examine and monitor whether actual land use (on the ground) corresponds to planned land use. The state government, under regulation 101/NQ-CP (Vietnamese State Government, 2018) requires that the committee of Bạc Liêu province takes responsibility for specifying and publicizing the border and size of rice cultivation and protected forests areas. In addition, the local government must investigate and monitor the status of coastal protection forests. A comparison of the current state government land use maps and this remote sensing maps was undertaken, and the percentage agreement was 85% (Figure 2.10). The difference between state government land use map and SAR data primarily occurred between parcels of aquaculture and rice. Some parcels were incorrectly labelled as aquaculture; although this may be because the land holder has a shrimp-rice rotational cropping system. Areas of disagreement can be used to a trigger an effective ground assessment of the potential reasons for discrepancy. In some cases, this could be from unplanned land use activities, in other cases it could be errors in the land use inventory and in some cases, it could be due to remote sensing mapping error so that satellite mapping can be further improved.

Sentinel-1A C-band SAR has a 12-days revisit and 6-day when combined with Sentinel-1B. The advent of the NASA-ISRO NISAR L- and S-band SAR Mission (NISAR, 2018) and the Vietnam National Space Center (VNSC) LOTUSat-1 X-band SAR Mission (Vietnam National Space Center, 2019) will bring not only more coverage but also the multi-frequency capability. SAR can provide the latest information on land use where frequent cloud cover obstructs optical remote sensing. For example, in 2016 there was only 2 scenes of Landsat-8 with cloud cover less than 10%. While existing optical remote sensing land cover studies in the region can provide useful information, that information may not be timely as scenes chosen may be determined and thereby biased by periods with low cloud cover rather than to coincide with monitoring dates. In addition, the quality of

optical remote sensing for mapping aquaculture will depend very much of the date of the image as in dry season when the ponds are empty it may be difficult to detect aquaculture from rice paddies. On the other hand, optical/multi-spectral data can offer independence data for cross-validation of remote sensing results, and thus the synergy among the difference satellite data sources should be utilized.

The conversion of agriculture land to aquaculture or urban development needs further attention in Bạc Liêu province. Converting agricultural to urban land exerts negative effects on agriculture-based people (ABP) groups. Research conducted in Cai Rang district, Can Tho city, a rapidly urbanizing district of the Mekong Delta, showed that socio-economic transformation including urbanization have negative impacts on ABP groups in the peri-urban areas (Garschagen, Renaud and Birkmann, 2011). While aquaculture is more profitable than rice cultivation, the transformation of long-term aquaculture lands to rice cultivation is problematic as salinity intrusion become more pervasive and less suitable for rice cultivation. Hence for the long-term future of the region, monitoring of land use is essentially to ensure the sustainability and food security in this Mekong Delta region.

2.5 Conclusion

This study quantified the distribution and area of key land covers in the Bạc Liêu province of the Mekong Delta and demonstrated the utility of multi-temporal Sentinel-1A SAR for land cover mapping. Overall, the results indicated that multi-temporal Sentinel-1 images along with the use of machine learning algorithms especially RF classifier can be used as an effective tool for land cover mapping. The results indicated that the overall accuracy and Kappa coefficient achieved from multi-temporal images are higher than single date regardless of the classification algorithm.

This study showed that classified Sentinel-1A SAR images can be used as a reference source to assess the accuracy of existing cadastral maps and monitor land conversion activities in Bạc Liêu province. Discussions with local experts confirmed that in the "existing cadastral maps and inventory documents, land use could be recorded as rice farming but in reality, the land was converted to aquaculture. The revisit time of 12 days

of SAR satellite help[s] track locals' land use activities and monitor land use conversion of the locals" (personal communication, Department of Natural Resources and Environment, Bạc Liêu province, Vietnam). They also confirmed that the mapping outputs could be used for land use master planning, for example, to monitor increase or decrease of aquaculture area.

The study shows that multi-temporal Sentinel-1A SAR is effective for land cover mapping and contributing to a better understanding of spatial-temporal changes in the coastal landscapes. This is particularly important, in tropical countries where frequent cloud cover hinders optical remote sensing. "To ensure national food security Bạc Liêu province was requested to maintain about 60,000 ha of rice by Vietnamese State Government. The land use map output derived from SAR imagery could support local land managers to determine [the agreement in] increase or decrease of annual rice cultivation areas to allocated rice areas by State Government. … Impacts of climate change and sea level rise have caused the erosion and loss of coastal forest land and due to socio-economic development, illegal forest activities and rural livelihoods have reduced forest land. The mapping outputs could help local officials monitor annual and local variation in forest land" (personal communication, Department of Natural Resources and Environment, Bạc Liêu province, Vietnam).

This chapter demonstrates the utility of Sentinel-1 SAR time series data in support of the activities of natural resources management and detection of illegal land use changes. To minimize the LCLU misclassification due to running supervised classification algorithm on images all together at once, the next chapters will develop a novel method to detect land cover/land use classes on by one separately.
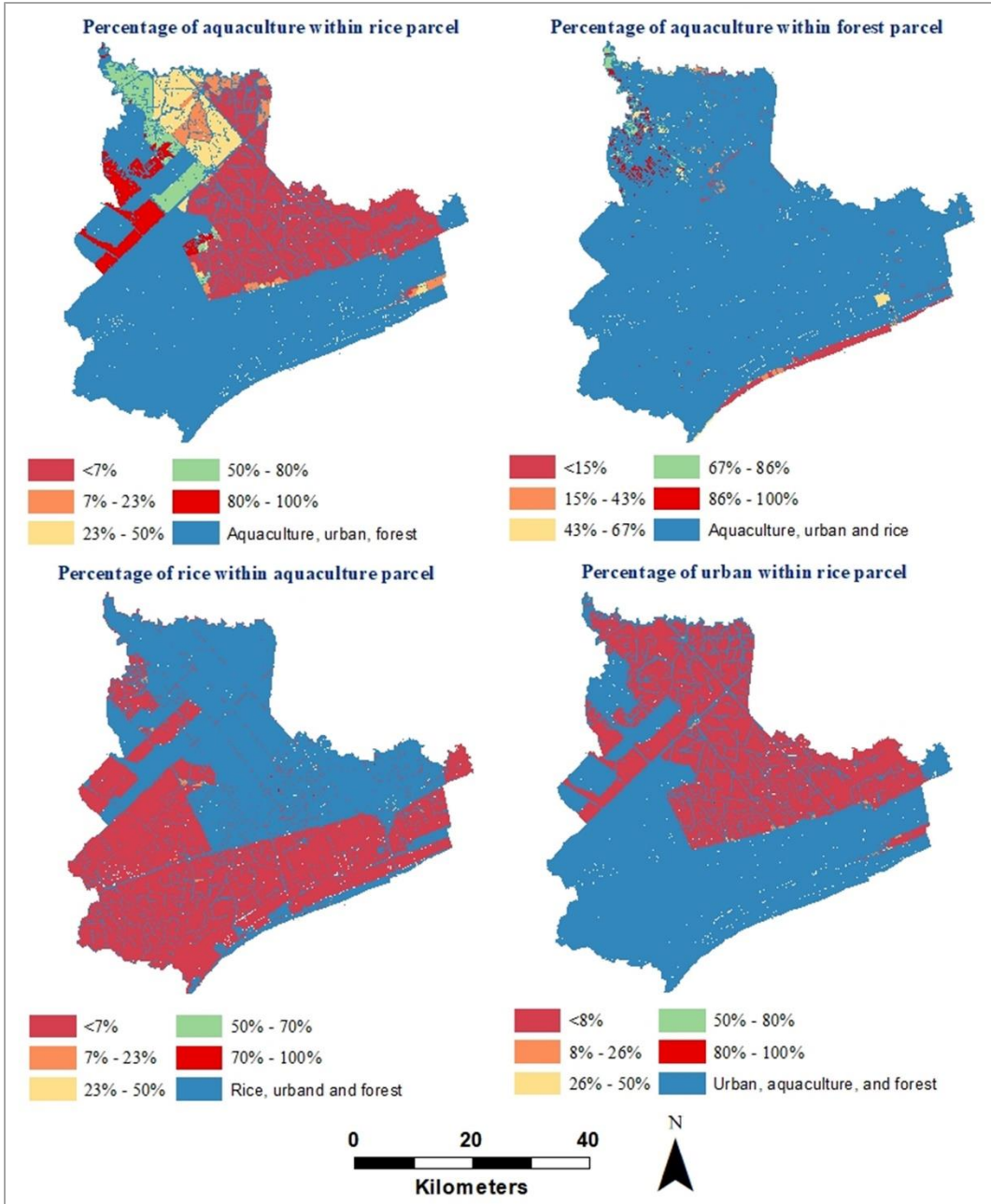
Figure 2.10 Disagreement map between state government land use map and SAR data Land cover mapping in Bạc Liêu in 2016.

Chapter 3 Building Structure Mapping on Level Terrains and Sea Surfaces in Vietnam

Published as:

In previous chapter, the usefulness of GEE to classify the LCLU using Sentinel-1 SAR data to support natural resource management is presented. In this chapter, an innovative method to detect and map building structures on land and sea using Sentinel-1 SAR time-series data is developed. The mapping outcomes are validated with in-situ and field truth observations obtained in southern and central regions of Vietnam.

3.1 Introduction

Accurately mapping urban infrastructure is considered a high priority, not only for resource and service allocation and administration, but also for addressing environmental, socioeconomic, and geopolitical issues (Lwin and Murayama, 2009; Mathews *et al.*, 2019). Extensive information on urban land use, including urban construction and green coverage, helps planners prepare and arrange the structure of the urban transportation, water and green system, and determine the scale and directions of future urban development in urban master planning processes (Xiao and Zhan, 2009). Moreover, crucial to the successful implementation of the Paris Agreement within the United Nations Framework Convention on Climate Change (UNFCCC) are accurate mapping and monitoring of greenhouse gases such as CO_2 (Gaughan *et al.*, 2019). Currently, fossil fuel CO_2 (FFCO2) emission is estimated with night-time light (NTL) data as a proxy for human settlements, which can be improved by maps of physically defined building structures (Sorichetta *et al.*, 2020). SAR data have a high spatial resolution ranging from 10 to 100 m, and are collected piecewise at different times over different areas of the world regardless of darkness and cloud cover conditions (Nghiem *et al.*, 2009). SAR data have been utilized to characterize urban and suburban extents with reliable results (Gamba and Lisini, 2013; Ban *et al.*, 2017; Lisini *et al.*, 2018). For example, geospatial datasets such as the Global Urban Footprint (GUF) and World Settlement Footprint (WSF) products (Esch *et al.*, 2013, 2018) have been successfully derived from TerraSAR-X and TanDEM-X SAR data. Ban et al. (Ban *et al.*, 2017) investigated the use of multi-temporal Sentinel-1A SAR and Sentinel-2A Multispectral Instrument (MSI) data for developing pilot global urban services. They found

that Sentinel-1A SAR data in association with historical SAR data produced good results for new built-up area characterization.

Here, the objective of this study is to develop novel and robust methods using Sentinel-1 SAR to identify and map persistent building structures that represent sustained human settlement and circumvent the limitations of NTL to improve estimation of FFCO2 emission. Temporary buildings such as pavilions in festivals or exhibition events exist temporarily for a short time (days to weeks) and therefore do not persistently represent true human settlements. This particular objective requires the detection of structures that are persistently built rather than being temporarily constructed. Such an approach necessitates a new development of an innovative method utilizing time-series SAR data to determine the building persistency, rather than past methods using data at a given time or at various disparate points in time. The new method demands that each pixel in a study area is consistently treated with a persistent time-series data record over a time duration (e.g., semi-annual, annual, or interannual), instead of using usual change detection methods from multi-temporal images acquired on different days in different years (Corbane *et al.*, 2018; Holobâcă, Ivan and Alexe, 2019; Manzoni, Monti-Guarnieri and Molinari, 2021; Zhang *et al.*, 2021).

The method developed in this study considers building structures on complex landscapes and sea surfaces. In both cases, SAR signatures of the background geophysical media on land and sea can widely vary as functions of incidence and azimuth angles (Kong, 1990; Nghiem, S.V.; Borgeaud, M.; Kong, J.A.; Shin, 1990; Carswell *et al.*, 1994; Nghiem *et al.*, 1995; Phung *et al.*, 2020), which need to be accounted for in the development of a robust algorithm. On land, complex topography can change the local incidence angle at different azimuth looks and cause polarization mixing of transverse electric and transverse magnetic fields at the medium interface (Kong, 1990), which alters backscatter signatures and leads to false building identification. Another complicated challenge is that strong reflections of radar signals from water surfaces of rivers, lakes, reservoirs, or wetlands cause intensive scattering from nearby trees that appear similar to building structures. Sea surfaces may have a wide range of radar return under different wind speeds and wind directions (Carswell *et al.*, 1994; Nghiem *et al.*, 1995), introducing sea clutter and confounding the capacity of SAR to detect building structures in the marine environment.

In view of the above challenges and complexities, a new algorithm was developed to address the problem of detecting persistent building structures on land in different environmental and geophysical conditions and on sea surfaces under various wind speeds and directions beyond the capability of current methods. The algorithm was tested across urban, suburban, rural, and natural areas on land and over sea surfaces in Vietnam using

Sentinel-1 SAR time series data. First, a novel method to identify building structures using the two-dimensional (2-D) space of VV-VH polarization of the SAR data is introduced. Next, a method for accuracy assessment is described and the case studies for five cities with different developmental and environmental conditions are presented. Moreover, maps of man-made structures from small shacks to large oil rigs on sea surfaces are shown.

Regarding the advances in the new method, (1) the advantage of utilizing the two-dimensional (2-D) space of VV-VH for building structure mapping is highlighted to robustly resolve the issue of radar backscatter incidence and azimuth angle dependence; (2) the ability of consistent time-series Sentinel-1 SAR to identify persistent buildings in a multitude of environmental conditions across the rural-urban continuum; (3) the utilization of multiple SAR signature interactions between trees and water surface to correct for building misclassification; (4) the use of the geomorphon concept and its applications (Jasiewicz and Stepinski, 2013; Veselský *et al.*, 2015; Silveira *et al.*, 2018; Gawrysiak and Kociuba, 2020) to account for effects of complex topography; and (5) the SAR ability to detect stationary structures or installations that are maintained on sea surfaces. Finally, in the discussion and conclusion, future research extensions with multiple international SAR datasets to support the Paris Agreement on climate change are noted, through the potential improvement in the estimation of FFCO2 emission using data products of persistent building structures to represent true settlements.

3.2 Methods

A new robust approach is presented to identify persistent building structures, paying particular attention to the effects of the terrain and water-tree radar signal interactions. The analysis, including image processing, mapping, and accuracy assessment, was carried out using the Google Earth Engine (GEE) platform, Geographic Resources Analysis Support System (GRASS), and ArcGIS software. The flow chart in Figure 3.1 summarizes the overall methods in which each component is described in further detail below.

REMOTE SENSING IMAGERY
- Sentinel-1A SAR: 35 time series images, VV-VH polarization, 10 m resolution.
- Sentinel-2 MSI: 20–27 images (cloudiness < 20%), 10 m resolution.
- Shuttle Radar Topography Mission (SRTM): 30 m resolution.

IMAGE CALIBRATION
- Apply orbit file.
- Radiometric calibration.
- Terrain correction.
- Speckle filtering (using a multi-temporal 3-point mean filter).
- Cloud masking (Sentinel-2 MSI).

BUILDING DOMAIN CLASSIFICATION
- Extract pixel values for all land cover types (both VV and VH polarization, all incidence angle bins and azimuth looks).
- Plot 2-D space of VV-VH.
- Determine threshold to classify building domain.
- Count the number of times that each pixel identified as building.
- Determine the optimal building count threshold.
- Calculate NDVI to account for effects of water-tree interactions.
- Calculate geomorphons to account for effects of topography.

ACCURACY CALCULATION
- Collect in-situ ground truth data.
- Calculate mapping accuracy based on ground truth data, Google Earth Image, ArcGIS base map.

Figure 3.1 Processing and mapping workflow.

3.2.1 Image Processing

All Sentinel-1 SAR images were pre-processed using the GEE platform to derive the backscatter coefficient in decibel (dB) for each pixel through the following steps: applying orbit file, thermal noise removal, radiometric calibration and terrain correction using the Shuttle Radar Topography Mission (SRTM) 30-m topographic data, and then spatial co-registration of temporal data based on a referenced image so that the time series has the same coordinate system.

To reduce speckle noise in SAR images, a multi-temporal 3-point mean filter (a moving average over a given time window) that would be computationally effective for noise reduction was used. The calculation was made as follows:

$$p_{mean(ij\ at\ t)} = \text{average}(p_{ij\ at\ t-1} : p_{ij\ at\ t+1}) \tag{1}$$

Equation 3.1 Calculation of multi-temporal 3-point mean

In (1), $p_{mean(ij\ at\ t)}$ is the output pixel value at location i,j (i: numbers of image rows, j: numbers of image columns) at time t; $p_{ij\ at\ t-1}$ is the input pixel value at location i,j at time t − 1; and $p_{ij\ at\ t+1}$ is the input pixel value at location i,j at time t + 1.

In this study, the values of t had a range of 1 to 35 (35 being the total number of SAR images in the time period under consideration). After the mean calculation, the first and last images in the time-series were then removed and only 33 images were used for further analysis. This time series spans approximately 1.3 years within which building structures need to persistently exist to be detected.

The calculation was applied to obtain the geometric mean in dB and the arithmetic mean in the linear unit (including conversion from dB to linear values). As an example, Figure 3.2 shows the raw backscatters, geometric mean, and arithmetic mean. The multi-temporal 3-point mean filter provided sufficient noise reduction and preserved temporal fidelity. The study found that results from the geometric mean in dB and the arithmetic mean (converted back to dB) were similar, so the geometric mean was used for effective computations without the conversions back and forth between dB and linear units.

3.2.2 Mapping

The 2-D space of VV-VH was used to characterize the building domain (Figure 3.3). The incidence angle in SAR images may have significant effects on backscatter values across the radar swath. To determine how backscatter changes as a function of incidence angle for various types of land cover, the VV and VH data were separated for each incidence angle bin at 35, 38, and 42 degrees. Then, for each incidence angle bin and azimuth direction (ascending versus descending), a scatter plot was made with VV polarization for the x-axis and VH polarization for the y-axis using the 3-point mean backscatter filter for all types of land cover including buildings, trees, paddy fields (such as rice paddies), and aquaculture areas (such as shrimp farms) as shown in Figure 3.2. From the scatter plot, the study found that the VV-VH domain for the building type stands out clearly and distinctively, independent of the effects of incidence and azimuth angles. However, there is a minor overlap between the building and tree domains due to high backscatter from water-tree radar signal interactions (to be addressed later in this section). Next, the thresholds in the 2-D VV-VH space were determined to define the domain specifically pertaining to building structures on land and on the sea surface. A pixel was assigned to a building class on land if it satisfied the following conditions: VH backscatter greater than −12 dB (VH > −12 dB) or VV backscatter greater than −5 dB (VV > −5 dB).

While on the sea, building pixels were assigned where VH backscatter greater than −20 dB (VH > −20 dB) or VV backscatter greater than −5 dB (VV > −5 dB). If a pixel did not satisfy that condition, it would be assigned to a non-building class.

(a)

(b)
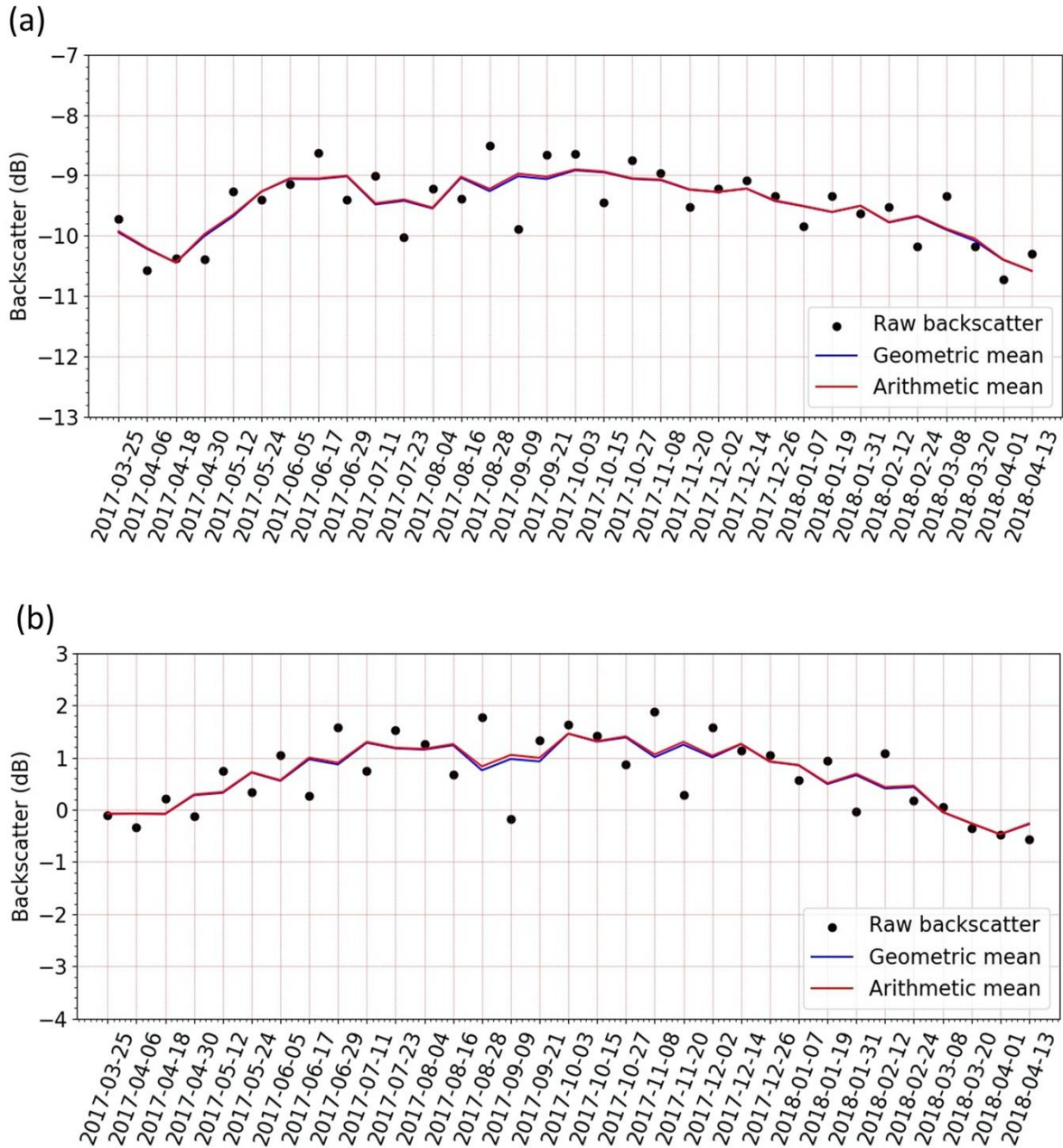
Figure 3.2 Example of filtering of raw Sentinel-1A SAR time series for (a) VH and (b) VV polarizations over Bạc Liêu city.
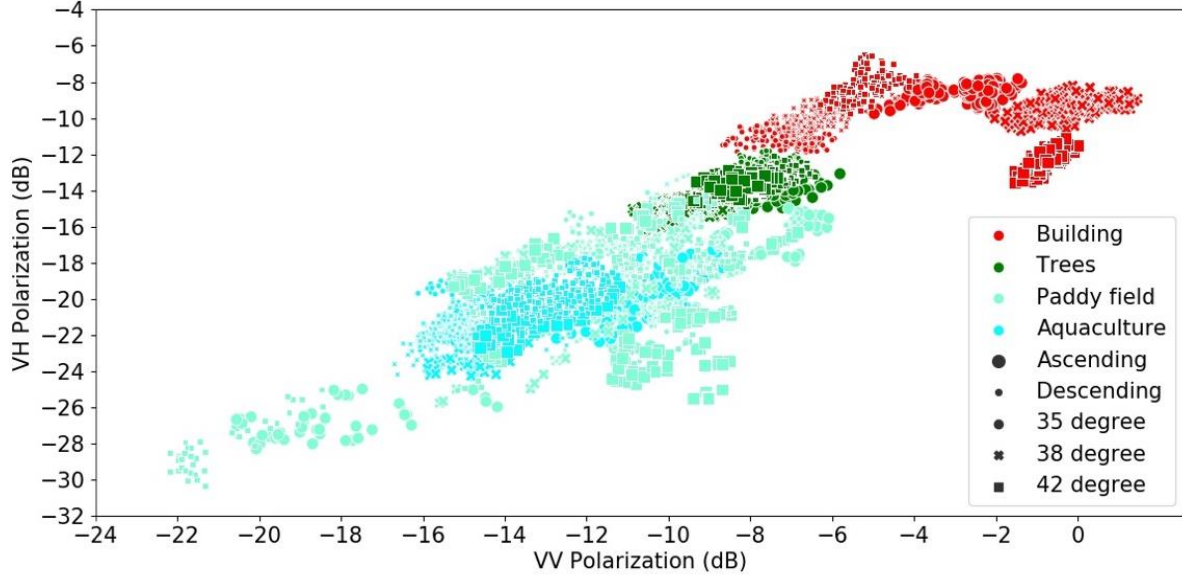
Figure 3.3 Multi-temporal backscatters of building structures and other land cover classes in the 2-D space for VV on the horizontal axis and VH on the vertical axis in dB.

To account for missing building pixels, the VV and VH thresholds were applied to all Sentinel-1A images in the time series (33 images). All output images (with value 1 for building pixels, and with value 0 for non-building pixels) were combined to count the number of times that each pixel was identified as building. If pixel_ij was detected as a building T times out of the 33 images, then the count of pixel_ij was set to T. Each pixel in the combined output image could have a value of T from a minimum of 0 (for pixels in which buildings were never identified) to 33 (for pixels identified as buildings at all the times). To minimize misclassifying building pixels from real non-building pixels, the optimal building count threshold (building_count_threshold) with the discrete derivative of building pixels (Δ_{m_n}) was determined depending on where the Δ_{m_n} curve became invariant or flattened. Pixel_ij was identified as a building if building_count_ij > building_count_threshold where the building_count_threshold could be from 1 to 33. The discrete derivative of building pixels was calculated as follows:

$$\Delta_{m\_n} = N_{threshold\_m} - N_{threshold\_n} \qquad (2)$$

Equation 3.2 Calculation of discrete derivative of building pixels

where the terms: Δ_{m_n} for the derivative between thresholds m and n, $N_{threshold\_m}$ for the number of building pixels at threshold m ($1 \leq m \leq 33$), and $N_{threshold\_n}$ for number of building pixels at threshold n ($1 \leq n \leq 33$). Based on the formulation given by Equation (2), discrete derivative curves were used to determine the optimal building count threshold

applicable to all study cases. This method requires a building structure to exist persistently for a minimum period of about 4 months (see Appendix A).

Due to strong radar reflection, such as from water surface (e.g., rivers, lakes, reservoirs, or wetlands, etc.), nearby trees can have intense radar returns. Figure 4 illustrates water-tree radar reflection interactions, where T represents the radar transmission direction and R represents the radar return direction. The terms A and B represent forward scattering mechanisms, and the terms C and D are backward scattering mechanisms. These account for multiple electromagnetic-wave interactions (Nghiem, S.V.; Borgeaud, M.; Kong, J.A.; Shin, 1990) involving scatterers (such as leaves, branches, and trunks of trees) and the interface between different media (such as the interface between water and air). The forward terms (A and B) give rise to strong scattering from water-tree interactions, causing backscatter enhancement (Nghiem, S.V.; Borgeaud, M.; Kong, J.A.; Shin, 1990) from trees to be similar to the backscatter from building structures. These effects result in a common range in the backscatter values of trees and building structures, contributing to the overlap of the building and tree backscatter signatures in the 2-D VV-VH space and thereby leading to some misclassification between these two land cover types.

To address the water-tree problem, the Normalized Different Vegetation Index (NDVI) (Zhang *et al.*, 2021) derived from the Multi-Spectral Instrument (MSI) aboard Sentinel-2 satellites was used. GEE was used to select Sentinel-2 MSI data on mostly-clear-sky days (cloudiness < 20%) to compute NDVI in the same time period of the Sentinel-1 SAR data acquisition. The NDVI in each 10-m pixel was then calculated and the average of N largest values of NDVI (NDVI_avg_Nmax) in each pixel obtained over the time period under consideration was computed. For each pixel that was classified as building, the building pixels were reclassified as non-building if NDVI_avg _Nmax > NDVI_threshold. Multiple cases for N = 3, 5, 10, and 15 were examined and NDVI_threshold was found to range from 0.25 to 0.5 in each case. Based on this assessment, the parameters to N = 3 and NDVI_threshold = 0.35 were set as these values yielded optimal results in reducing most of the misclassified buildings, as seen in Figure 3.4b before the correction and Figure 3.4c after the correction. This was necessary as many human settlements including small towns and big cities may have trees along rivers, lakes, and other water bodies.
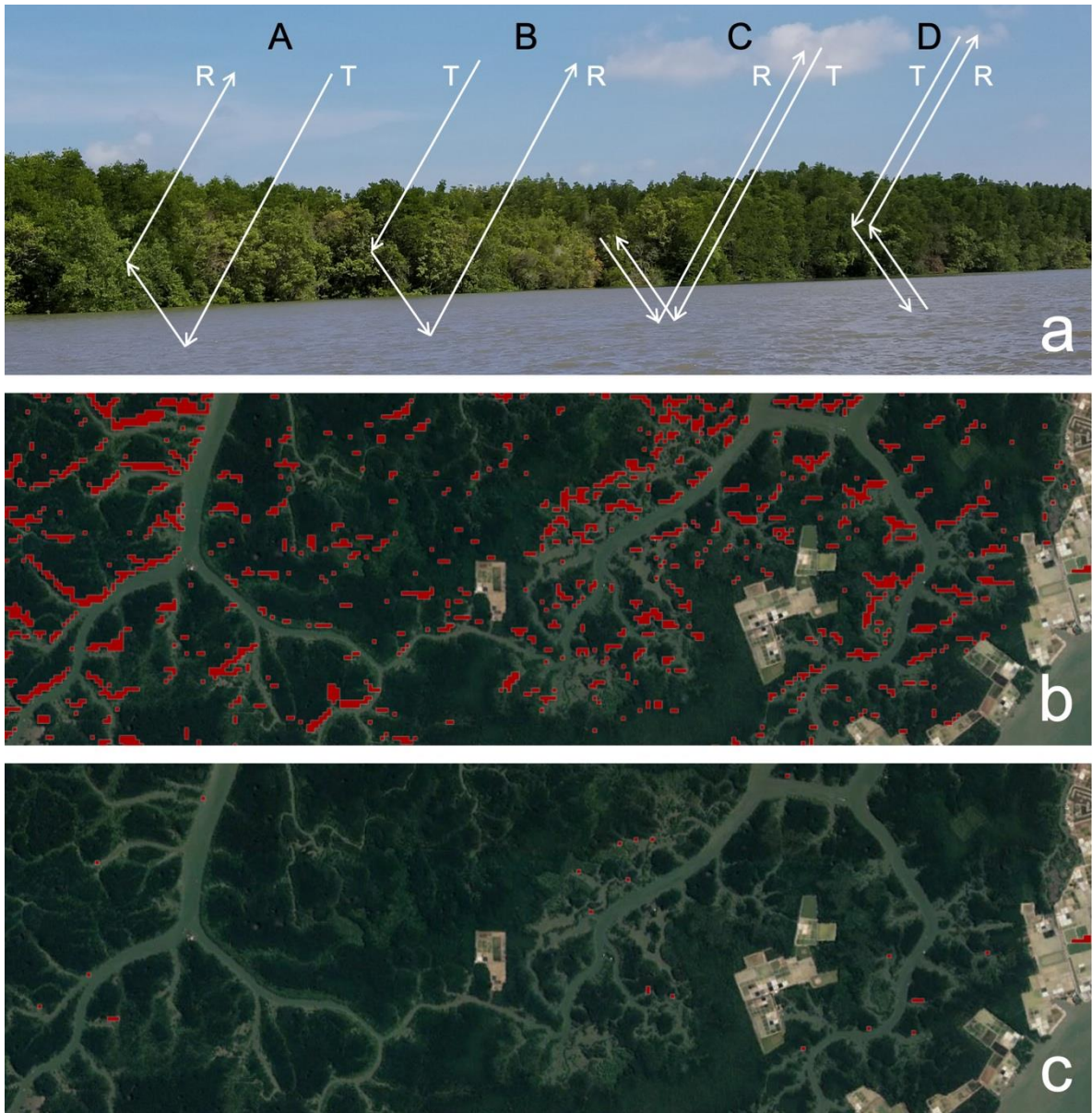
Figure 3.4 Effects of water-tree interactions on radar scattering mechanisms. Panel (a) illustrates water-tree radar interactions using a photograph taken on 20 May 2018 at 10°29′17.37" N and 106°49′41.76" E in the Cần Giờ Biosphere Reserve, a UNESCO wetland about 40 km southeast of Hồ Chí Minh City. Panel (b) shows misclassified buildings (red pixels) that were mostly removed as seen in Panel (c) after the corrections using Sentinel-2 MSI NDVI. Cần Giờ was the worst place for water-tree effects to test the efficacy of the correction method, where misclassification occurred all over the place as in Panel (b).

On sloped surfaces in mountainous areas with a complex topography, the local incidence angle of radar transmission is not the nominal incidence angle with respect to a horizontal level surface. Moreover, a radar transmission signal at a given polarization (e.g.,

horizontal or vertical polarization) can excite both the transverse-electric (TE) and transverse-magnetic (TM) fields causing polarization mixing in the radar return signals (Kong, 1990). These effects alter backscatter signatures and cause false building identifications.

To address the misclassification problem due to topography effects, complex landforms in mountainous areas were accounted for based on the geomorphon concept (Jasiewicz and Stepinski, 2013; Veselský *et al.*, 2015; Silveira *et al.*, 2018; Gawrysiak and Kociuba, 2020) to circumvent the ill-posed calculus of taking spatial derivatives from noisy topography data. The SRTM digital elevation model (DEM) (JPL, 2020) derived from satellite SAR data was employed to calculate geomorphons. A geomorphon represents one of the multiple possible landforms in terms of a three-dimensional morphological feature in ten different landform classes: flat, peak, ridge, shoulder, spur, slope, pit, valley, foot-slope, and hollow. The geomorphon approach uses three input parameters: inner search radius, outer search radius, and flatness threshold to calculate height differences (Kramm *et al.*, 2017). The outer search radius was set to 10 pixels (300 m) and the inner search radius was set to 5 pixels (150 m), while the flatness threshold was set to 3 degrees. In the algorithm, a building pixel would be retained in the building type only when it was represented by a "flat" geomorphon.

This approach using geomorphons means that structures built on mountain slopes may not be detected, while buildings can be identified on flat terrains in the lowlands in coastal plains or in valleys, or level plateaus at high altitudes where structures are usually built and persistently maintained. To illustrate the ability of the geomorphon method to account for topographic effects, Figure 3.5 shows that most of the misclassified buildings on the slopes of Hàm Cần Mountains (~17 km northwest of Phan Thiết) were removed, while the true building area (a settlement in Lò To Village, Hàm Cần Commune, Hàm Thuận Nam District, Bình Thuận Province) was consistently detected on the relatively flat terrain near the foothill.
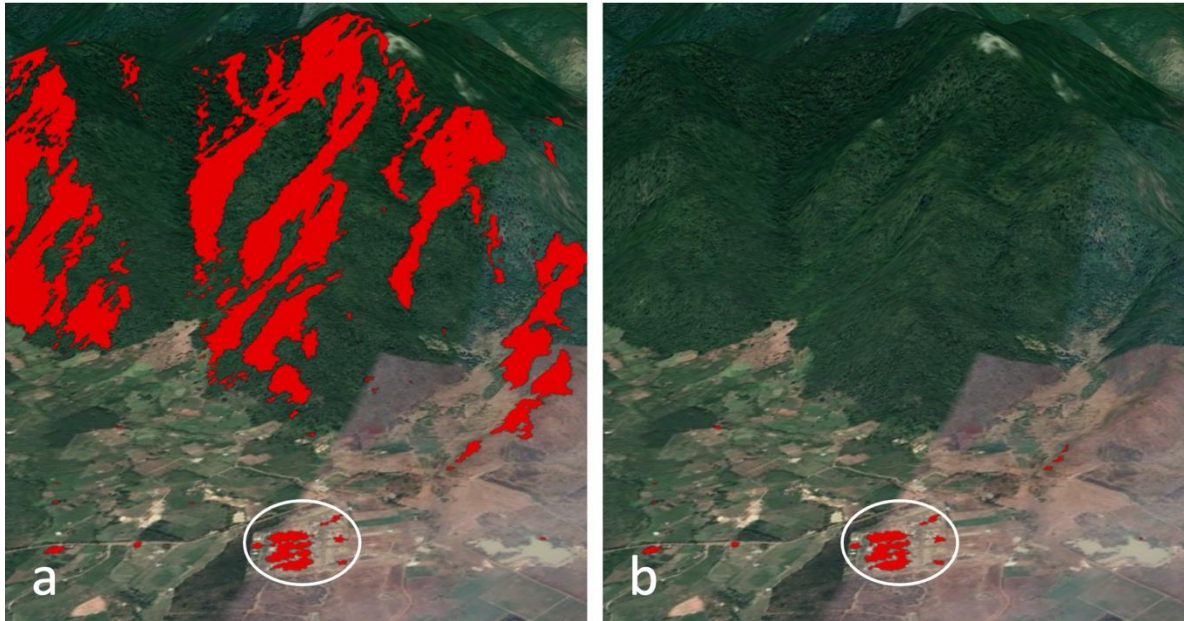
Figure 3.5. Detection of building structures (red areas) in an area around Hàm Cần Mountains without geomorphon correction (a), and with geomorphon correction (b). The ellipse marks a small settlement area (6.4 hectares) in Lò To Village where a built area was identified on the relatively flat terrain about 0.5 km from the foothill. The building structure map was overlayed on the topography using Google Earth Pro in a three-dimensional view.

3.2.3 Ground Truth Data Collection and Accuracy Assessment

In-situ ground truth data were collected in four cities (Bạc Liêu, Cà Mau, Sóc Trăng, and Tân An) in the Mekong Delta. Field work included traveling along main roads and waterways (e.g., rivers and canals) and taking field observations with geotagged photographs of different land cover types such as building structures (schools, hospitals, commercial centers, residential houses, etc.), trees (coastal forest, perennial trees, plantations), paddy fields (rice paddies), and aquaculture areas (shrimp farms). In addition, geotagged photographs were taken at different locations from rural to urban areas of Phan Thiết in the southern region of central Vietnam. The photographs were imported into ArcMap software and converted into points. These points were used as validation points in the accuracy assessment.

Based on in-situ ground truth data and field photographs together with high-resolution true color images in Google Earth™ and the ArcGIS base map, the quality of the mapping results was assessed. Since the algorithm identified a pixel as building or non-building rather than a range of fuzzy values, the accuracy assessment was carried out based on a set of four possible ensembles. Each ensemble population was represented by the number of counts of all pixel elements within each ensemble set. For these ensembles, the count parameters were assessed as: (1) the number of building pixels that were classified

45

correctly as building (N_building), (2) the number of pixels that were misclassified as building while they were actually other land cover types (n_um), (3) the number of pixels that were misclassified as other land cover types while they were actually buildings (n_om), and (4) the number of other land cover types pixels that were classified correctly as other land cover types (N_others). Using the results of N_building, n_um, n_om, and N_others, the false negative rate and false positive rate were calculated in percentage as (Barsi *et al.*, 2018):

$$\text{false negative rate} = [\text{n\_om}/(\text{n\_om} + \text{N\_building})] \times 100\% \tag{3}$$

Equation 3.3 False negative rate

$$\text{false positive rate} = [\text{n\_um}/(\text{n\_um} + \text{N\_others})] \times 100\% \tag{4}$$

Equation 3.4 False positive rate

3.2.4 Building Structures on Land

Multiple cases in different environments on land were examined. This study included four cities (Bạc Liêu, Cà Mau, Sóc Trăng, and Tân An) in the Mekong Delta on wet and level terrains with a tropical monsoon climate. In a stark contrast, one city (Phan Thiết) in dry land extending from mountainous terrain in the west to the coast in the east in Bình Thuận was also studied, one of the most arid provinces in Vietnam at risk of desertification, making Phan Thiết vulnerable to moving sand dunes.

As in other cities in the Mekong Delta, due to socioeconomic developments, new settlements as well as other public infrastructures have been constructed in Bạc Liêu, Cà Mau, Sóc Trăng, and Tân An to meet housing and industrial demand. In recent years, these cities have suffered flooding from heavy rain, compounded by high tides in the rainy season. Bạc Liêu is a coastal city surrounded by rice farming and shrimp farming areas. This city is on a track to be a Class I urban (a regional central city) by 2025 and is likely to expand to 4950 ha by 2030 (T. Linh, 2020). Being on a relatively flat terrain, in a landscape with a high density of rivers and canals, Cà Mau is planned to expand in all directions to adapt to climate change (MoC, 2020a). Sóc Trăng will be a Class II city (a provincial city) in 2025 and is expanding toward the east and west (P. Linh, 2020). Located in Long An

Province, Tân An is currently a central city and in Class II, and will be a Class I city by 2025 (MoC, 2020b).

Famous as a coastal resort city in Bình Thuận Province in the south-central coast of Vietnam, Phan Thiết has received substantial investments in building large hotels and resorts. As mountains in the west of Phan Thiết can induce orographic effects resulting in intensive rains, this city suffers flash flooding compounded by the impacts of sea level rise on Cà Ty river, and beach erosion has also become a major issue. Despite transient intense rains in the mountains, Phan Thiết is actually located in an arid land region of Bình Thuận in a magnificent coastal setting. Surrounded by extensive plantations of dragon fruit (*Hylocereus undatus* in the cactus family Cactaceae) and a beautiful shoreline, authorities have attempted to develop Phan Thiết into an environmentally sustainable and friendly city (Hai, 2019). This region has been undergoing an intensive agriculture transformation by the development of extensive dragon fruit plantations, considered the "Dragon Fruit Kingdom" (or the "Dragon Kingdom" in short). The rural areas together with rapid urbanization due to the tourism boom in the city are creating the conditions for a dual rural-urban hotspot where both city areas and farmlands have been intensively and contemporaneously developed.

Generally, in Vietnam, each province has its own urban development strategies, depending on its geographical location and certain socioeconomic conditions pertaining to different urban classes. Table 3.1 and Table 3.2 below summarize the population and infrastructure development standards for each urban class in Vietnam, which are applicable to the different cities in different provinces noted above. The study sites were chosen to represent a range of urban patterns along the rural–urban continuum, consisting of different urban classes listed in Table 3.1 and Table 3.2.

Table 3.1 Population scale standard.

No.	Standard	Unit	Special	I State	I Province	II	III	IV	V
1	Population in urban and suburban	1000 people	≥6000 5000	≥5000 1000	≥1000 500	≥500 200	≥200 100	≥100 50	4–50
2	Population in urban	1000 people	≥4000 3000	≥3000 500	≥500 200	≥200 100	≥100 50	≥50 20	

Table 3.2. Infrastructure development standard.

No.	Standard	Unit	Special	I	II	III	IV	V
I	Infrastructure standard							
I.1	Housing							
1	Average floor area	m² floor/person	≥29 26.5	≥29 26.5	≥29 26.5	≥29 26.5	≥29 26.5	≥29 26.5
2	House rate	%	100 90	≥95 90	≥95 90	≥95 90	≥90 85	≥90 85
I.2	Public infrastructure							
1	Settlement land, open-green land, parks, traffic land	m²/person	61 54	61 54	61 54	78 61	78 61	78 61
2	Education	buildings	≥40 30	≥30 20	≥20 10	≥10 4	≥4 2	≥2 1
3	Culture	buildings	≥20 14	≥14 10	≥10 6	≥6 4	≥4 2	≥2 1
4	Sports	buildings	≥15 10	≥10 7	≥7 5	≥5 3	≥3 2	≥2 1

3.2.5 Building Structures on Sea Surface

Vietnam has an extensive coastline (>3400 km^2) with rich natural resources for aquaculture, fisheries, and offshore fossil and renewable energy. In the marine environment, this study included two offshore fossil oil fields (Bạch Hổ oil field and Sư Tử Đen oil field), a renewable wind power farm off the shore of Bạc Liêu, two islands (Hòn Tre and Hòn Sơn in Kiên Giang Province), and a marine aquaculture area for blood clam (*Tegillarca granosa*) farming also in Kiên Giang Province. These cases encompassed various types of stationary and persistent building structures on the sea surfaces including very large oil platforms, tall wind power towers, smaller power poles, and even very small individual guard shacks in the marine farm. On the sea surface, winds and waves can generate a large range of radar backscatter signatures that confound the detection of marine structures. The algorithm developed in this study accounts for the problem of sea surface radar clutter to achieve a robust method for accurately identifying persistent marine structures using time-series Sentinel-1 SAR data.

3.3 Results

3.3.1 Results for Building Structures on Land

Figure 3.6 shows the results of the building classification and Figure 3.7 presents the building classification maps at a posting grid size of 10 m for the five cities (Bạc Liêu, Cà Mau, Sóc Trăng, Tân An, and Phan Thiết) overlayed on the true-color ArcGIS base map. These maps show that most building pixels cluster around cities and disperse along roads and waterways emanating outward from urban to rural areas. The results from the building classification for each city reveal distinctive spatial patterns associated with their unique development history, socio-environmental constraints, population distribution drivers (Table 3.1) and infrastructure development standards (Table 3.2). The maps also highlight that these spatial patterns were captured by the classification method at a high spatial resolution, even identifying the footprint of individual buildings.

The Bạc Liêu Province Public Administration Center and Bạc Liêu Market in Ward 3 are found at the center. Built in the 1920s, Bạc Liêu Market was initially a busy trading place among Chinese and Vietnamese. Many old houses and shopping stores are present. In the 2010s, a wide range of public and private infrastructures such as Bạc Liêu university, Coopmart supermarket, Vincom shopping center, and Thanh Vũ hospital were newly built and expanded to meet population growth, labor demands, and economic development in Bạc Liêu. To comply with the Nation Urban Development Programme 2012–2020 and to meet housing demands, four new residential areas (Phường 2, Phường 5, Hoàng Phát, Tràng An) have been constructed. Along Trần Phú street and Quốc Lộ 1A street—two

main roads to city center—more houses, shopping stores, banks, and restaurants have also been constructed and are visible in the classified map. High building densities can also be seen at tourist places like Khu du lịch Nhà Mát on Hoàng Sa Street by the seashore and at religious places like Quán Âm Phật Đài pagodas. North of Bạc Liêu city are agricultural rice paddy fields while south of the city has aquacultural shrimp farms. In these rural areas, fewer buildings were found on the rice paddies while more guard shacks were detected in shrimp farms.
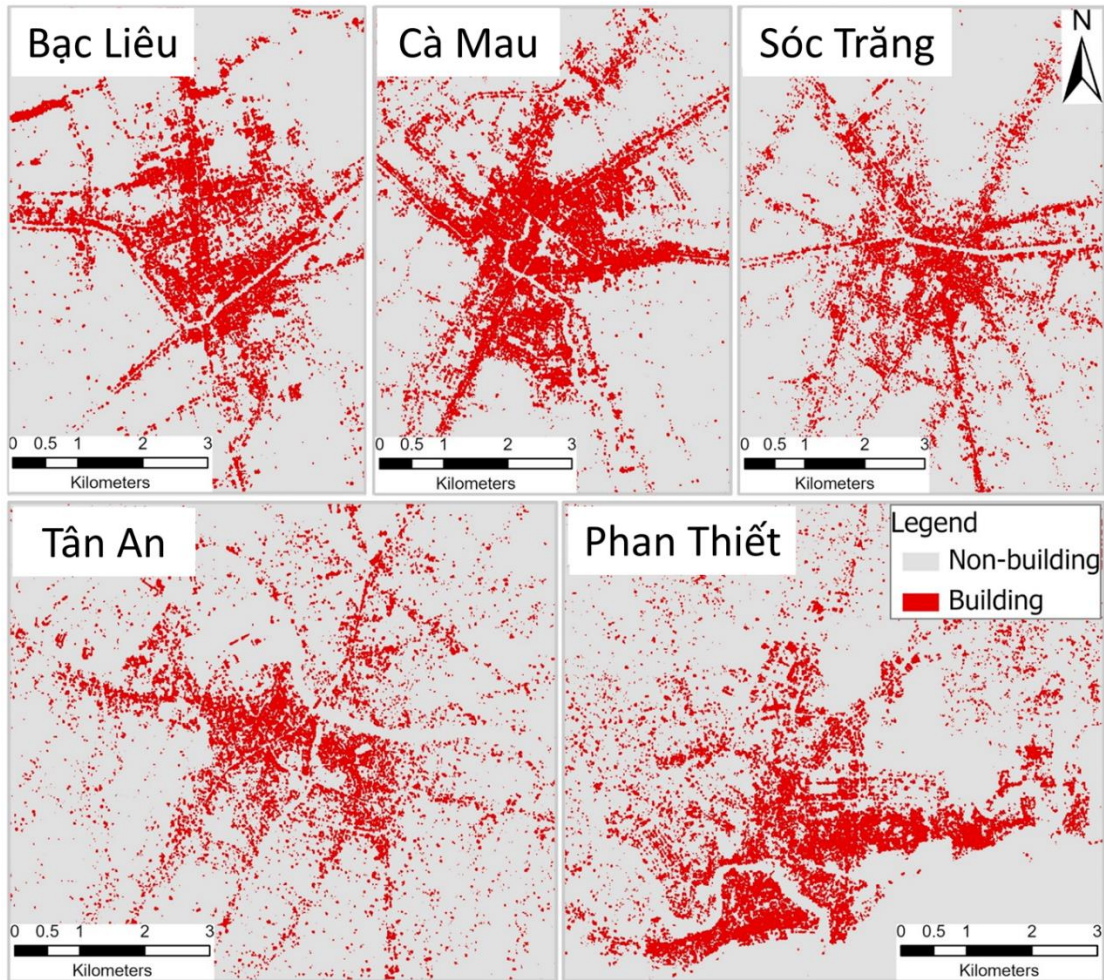
Figure 3.6 Classification map of five cities: Bạc Liêu, Cà Mau, Sóc Trăng, Tân An, and Phan Thiết.

For Cà Mau, Tỉnh Ủy Cà Mau (Cà Mau Party Committee) and Ủy ban nhân dân tỉnh Cà Mau (Cà Mau Province's People Committee) in Ward 2 are at the center of Cà Mau. Cà Mau is expected to be Class I city in 2025 (see Table 4.1 for Class I population and Table 4.2 for Class I infrastructure), so many streets have been built and upgraded. The city has expanded in all directions with many houses along main roads and rivers in the directions

of Bạc Liêu (the east of Cà Mau), Thới Bình District (the north and north-east of Cà Mau), U Minh District (the west of Cà Mau), and Đầm Dơi and Cái Nước District (the south of Cà Mau). One of the well-known residential areas in Cà Mau is the Gas-Power-Fertilizer Complex housing area near the Cà Mau River. West, north, and east of Cà Mau are surrounded by extensive shrimp aquaculture where guard shacks can also be identified.
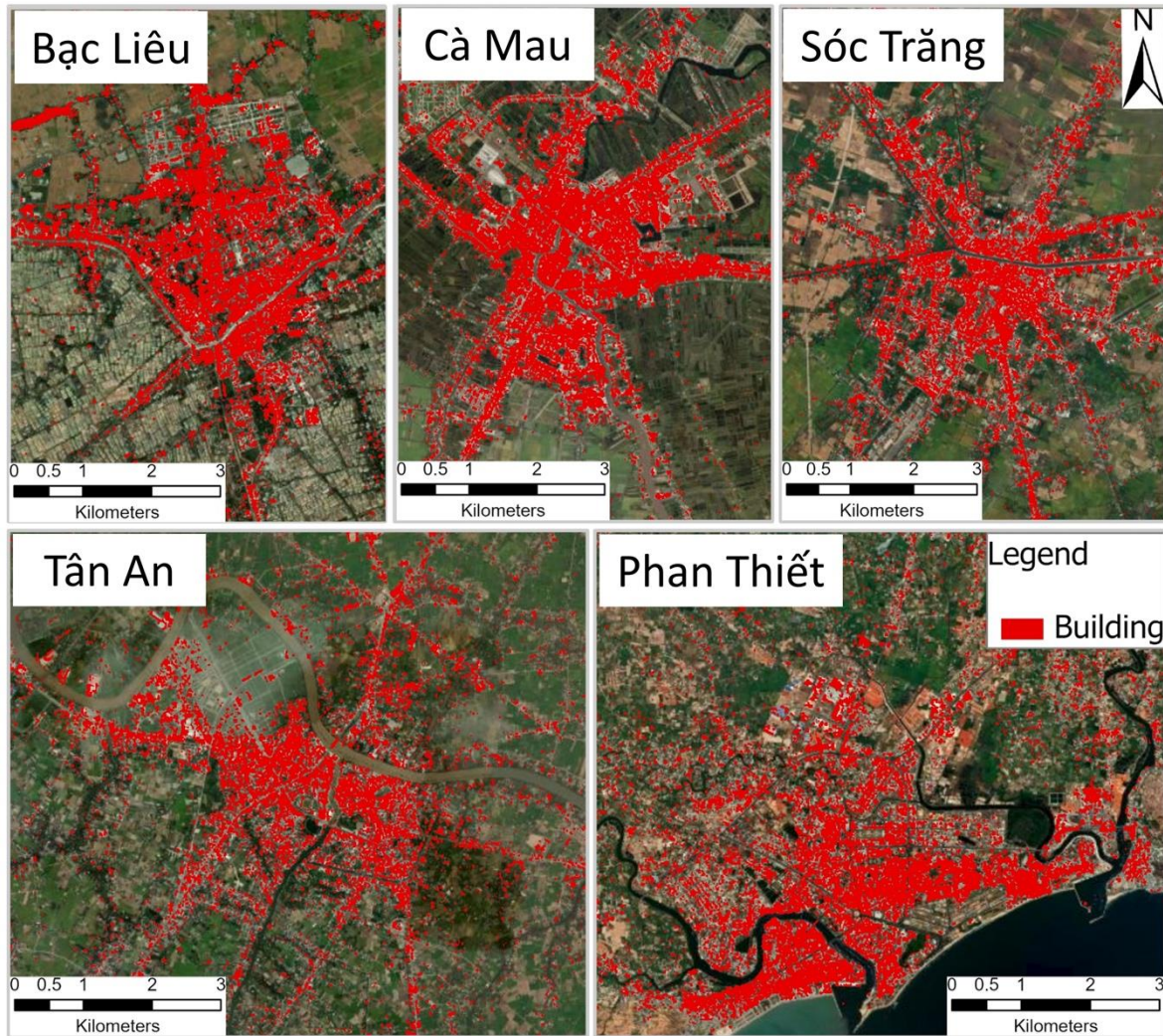
Figure 3.7 Classification map of five cities overlaid on ArcGIS base map: Bạc Liêu, Cà Mau, Sóc Trăng, Tân An, and Phan Thiết.

For Sóc Trăng, Tỉnh Ủy Sóc Trăng (Sóc Trăng Party Committee) and Ủy ban nhân dân tỉnh Sóc Trăng (Sóc Trăng Province's People Committee) in Ward 1 are located at the center of the city. Urban development in Sóc Trăng is primarily along main roads to the city and along the Maspero river. New residential and commercial areas (Trần Quang Diệu, Hạnh Phúc, Lê Duẩn) have been built in Ward 2, Ward 3, and Ward 4 to meet the city's population growth. The city has also expanded toward the south of the Maspero river along Trần Hưng Đạo and Lê Hồng Phong street and toward the north of Maspero river along

51

Hùng Vương and Tôn Đức Thắng street. Sóc Trăng city is surrounded by paddy fields, so there are houses in small villages along irrigation canals.

Tân An, Ward 1, is at the center, where Tỉnh Ủy Long An (Long An Party Committee) and Ủy ban nhân dân tỉnh Long An (Long An Province's People Committee) were built. From the center, the city has sprawled toward the south of the Vàm Cỏ Tây river. Many buildings and houses have been constructed in Ward 1 and Ward 2 along Bảo Định canal. As part of its progress toward a Class I city in 2025, the authorities of Tân An are constructing a wide range of residential areas (Vàm Cỏ riverside urban area; Tân An, Đồng Tâm residential area) along the Vàm Cỏ Tây river in Ward 6. The mapping also shows houses along Quốc Lộ 1A street and Đường tỉnh 827 and 828 roads (connecting Tân An with other districts in the region). Tân An is surrounded by paddy fields and dragon fruit plantations. Unlike Bạc Liêu city, Tân An has more houses in rural areas, but these houses are scattered across the landscape and not found in parallel along main roads or rivers.

For Phan Thiết, Bình Thuận Province Public Administration Centre is at the center of the city. From the center, the residential areas have expanded to the north and north-east of the city center, such as the An Phú and Phú Tài-Phú Trinh residential areas. Commercial and medical service buildings (Coopmart supermarket, An Phước General Hospital) built to meet the social and health care demands are also visible in the map of building structures. Toward the south of the city center, more houses have been constructed along the Cà Ty River since this river is the main waterway connecting the sea and the fishing port at the Cà Ty River mouth. In response to the tourism boom in the city, a variety of policies for tourism development have been issued. Moreover, many large hotels and resorts have been built along the shore toward Mũi Né tourist site. Due to hilly terrain in the rural areas, houses are found scattered across the landscape and not along main roads like in Bạc Liêu, Cà Mau, and Sóc Trăng.

Evaluated with in-situ data and field observations, Table 3.3 shows the accuracy of building mapping in Bạc Liêu, Cà Mau, Sóc Trăng, Tân An, and Phan Thiết. Within these five cities, Bạc Liêu had the highest accuracy with false negative rate = 8.6% and false positive rate = 5.2%. Phan Thiết had the lowest mapping accuracy with false negative rate = 13.3% and false positive rate = 8.2%. Cà Mau, Sóc Trăng, and Tân An had similar mapping accuracies, with the false negative rate ranging from 9.5% to 11.9% and the false positive rate from 5.5% to 7.0%. For all cities, the average false negative rate was 10.9%, and the average false positive rate was 6.4% after the corrections for water-tree interactions and mountain topography effects.

Table 3.3 Accuracy assessment.

Cities	N_building (pixels)	N_others (pixels)	False Negative Rate (FNR) (%)	False Positive Rate (FPR) (%)
Bạc Liêu	320	330	8.6	5.2
Cà Mau	306	344	9.5	5.5
Sóc Trăng	310	340	11.4	6.1
Tân An	318	332	11.9	7.0
Phan Thiết	338	312	13.3	8.2
All cities	1592	1658	Average FNR = 10.9%	Average FPR = 6.4%

To illustrate the major difference in the ability of the SAR data product of persistent building structures to represent true settlements versus the excessive appearance of NTL extent, the case of Phan Thiết city (capital of Bình Thuận Province), surrounded by vast dragon fruit plantations in the "Dragon Kingdom" of Vietnam, was examined. For NTL, the satellite Visible Infrared Imaging Radiometer Suite (VIIRS) Day and Night Band (DNB) data product (in units of $nW/cm^2/sr$) with stray light correction was used (Group, 2021) for February 2018 when the cloud cover was minimal to allow a good unobstructed observation of NTL. Figure 3.8 presents a map of persistent building structures detected by Sentinel-1 SAR around the area of Phan Thiết together with VIIRS NTL in Bình Thuận Province.

As shown in Figure 3.8, the extent of building structures around Phan Thiết is only a small fraction of what is shown with the NTL over the dragon fruit plantations surrounding Phan Thiết. Moreover, the NTL in the city was distinctively dimmer than the NTL from the dragon fruit plantation regions. This is because farmers use high-intensity artificial lights shining up toward the cactus canopy at night (Figure 3.8) to drive the photoconversion process of phytochromes (Group, 2021)and increase the yield of dragon fruit production to multiple times per year (Rockwell and Lagarias, 2006). The innovative use of night lighting has transformed the agriculture in this arid rural region of Bình Thuận Province, from rags to riches, with a dramatic expansion of dragon fruit plantations where earnings from this high-value cash crop approach a billion USD (Paull and Chen, 2019). This example demonstrates that the vast extent of NTL over the rural regions of Bình Thuận exceeds by far the true urban areas and will thereby lead to an excessive overestimation of FFCO2 emission using NTL as a proxy indicator of human settlements.
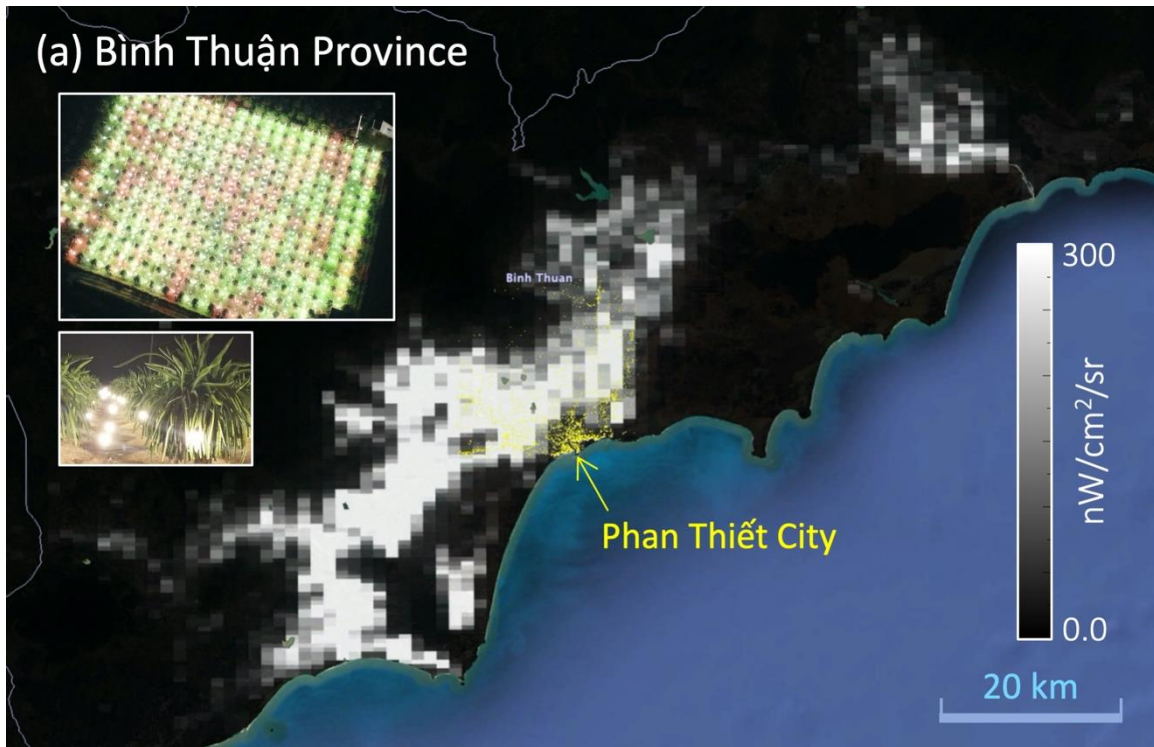
Figure 3.8 VIIRS NTL observations for Bình Thuận Province together with building structures detected by Sentinel-1 SAR represented by the yellow color in the area of Phan Thiết City. The insets are aerial (upper inset) and surface (lower inset) photographs of the dragon fruit lighting at night. The land-water mask used in this figure was obtained from the SRTM Water Body Data (JPL, 2020).

3.3.2 Results for Building Structures on the Sea Surface

This section presents the results of building structure mapping on the sea surface from huge oil platforms in major oil fields to tiny guard shacks in marine clam farms. The Bạch Hổ (White Tiger) oil field and Sư Tử Đen (Black Lion) oil field are two major offshore oil production areas in the Cửu Long basin due east of the Mekong Delta of Vietnam. The joint Vietnamese–Russian Vietsopetro operates at Bạch Hổ, while PetroVietnam with partners from ConocoPhillips, Korean National Oil, and others operates at Sư Tử Đen. Figure 3.9 reveals multiple persistent structures including oil platforms or oil rigs detected by the method in the period of March 2017 to May 2018 in the areas around Bạch Hổ (7 structures, within the frame in Figure 3.9a) and Sư Tử Đen (5 structures, within the frame in Figure 3.9b). A very rare image from Maxar acquired in 2006 captured an oil rig right at the location of Structure 710 in Sư Tử Đen and independently confirmed the SAR detection of this oil rig. In the Bạch Hổ and Sư Tử Đen areas, the centroid for each oil field structure is listed in Table 3.4.

54
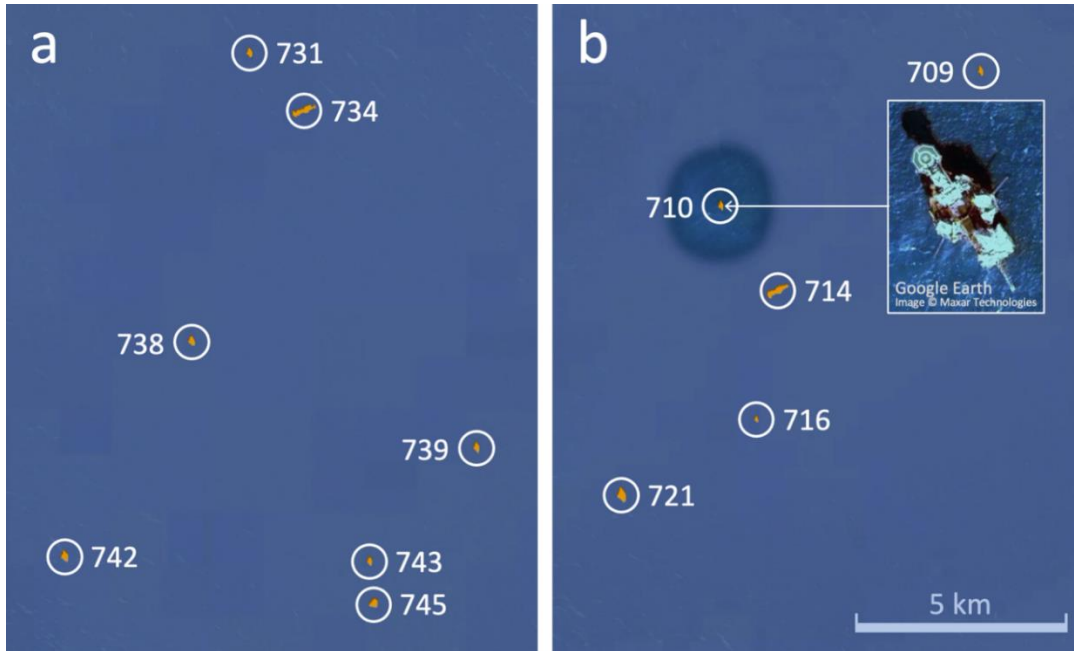
Figure 3.9 Detection of offshore structures (orange pixels inside circles) on the sea surface around (a) Bạch Hổ and (b) Sư Tử Đen oil fields. Each structure is assigned a unique identification (ID) number.

Table 3.4 Centroid locations of structures including oil platforms or oil rigs around Bạch Hổ and Sư Tử Đen oil fields. The ID of the structures detected in the oil fields correspond to those in Figure 3.9.

Oil Field	Structure ID	Longitude (º)	Latitude (º)
Sư Tử Đen	709	108.4377899	10.46973133
	710	108.3818665	10.44124126
	714	108.3938675	10.42325497
	716	108.3894806	10.39616489
	721	108.3605118	10.38012123
Bạch Hổ	731	107.9596634	9.984884262
	734	107.9711685	9.972677231
	738	107.947319	9.923978806
	739	108.0084839	9.901568413
	742	107.9201202	9.878500938
	743	107.9855728	9.877530098
	745	107.9864731	9.86863327

55

In the littoral zone off the shore of Bạc Liêu, the first wind energy farm in southeast Asia was developed in an area of 540 ha producing 99.2 MW of electricity. Figure 3.10 shows each individual wind tower detected on the sea surface. The towers are aligned in parallel rows with a spacing of approximately 800 m as found in the building detection map. Each row has a maximum of eight towers with equal spacing between these towers (~250 m). The wind tower closest to the sea dike on the shoreline was detected about 600 m away.
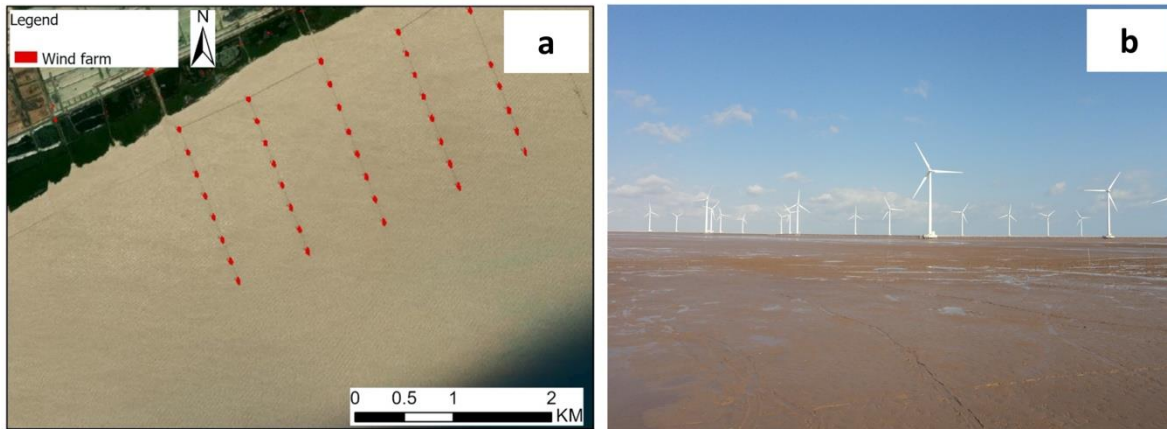
Figure 3.10 Wind energy farm off the shore of Bạc Liêu (a) wind-energy tower map detected from Sentinel-1 SAR and (b) ground-truth field photograph on 26 February 2019 at 9°13′49.76″ N and 105°48′12.12″ E.

For the case of the Hòn Tre and Hòn Sơn islands, interestingly, not only houses in a small village could be captured on the shore land, but also the lines of power poles on the sea surface connecting the two islands to the mainland can be detected, as illustrated in Figure 3.11. The entire length of power lines connecting Hòn Tre to the mainland is 13 km including 27 poles, while the entire length for Hòn Sơn is 24.5 km with 49 poles. Since the two islands are close to the mainland, Southern Power Corporation (Tổng Công ty Điện lực miền Nam) built the electric power lines above sea surface rather than running power cables underwater, which is costly and commonly performed for islands far away from the mainland such as Phú Quốc island. The first power cables underwater in Vietnam connecting Phú Quốc to the mainland in Hà Tiên is 56 km long and cost approximately USD 100 million.
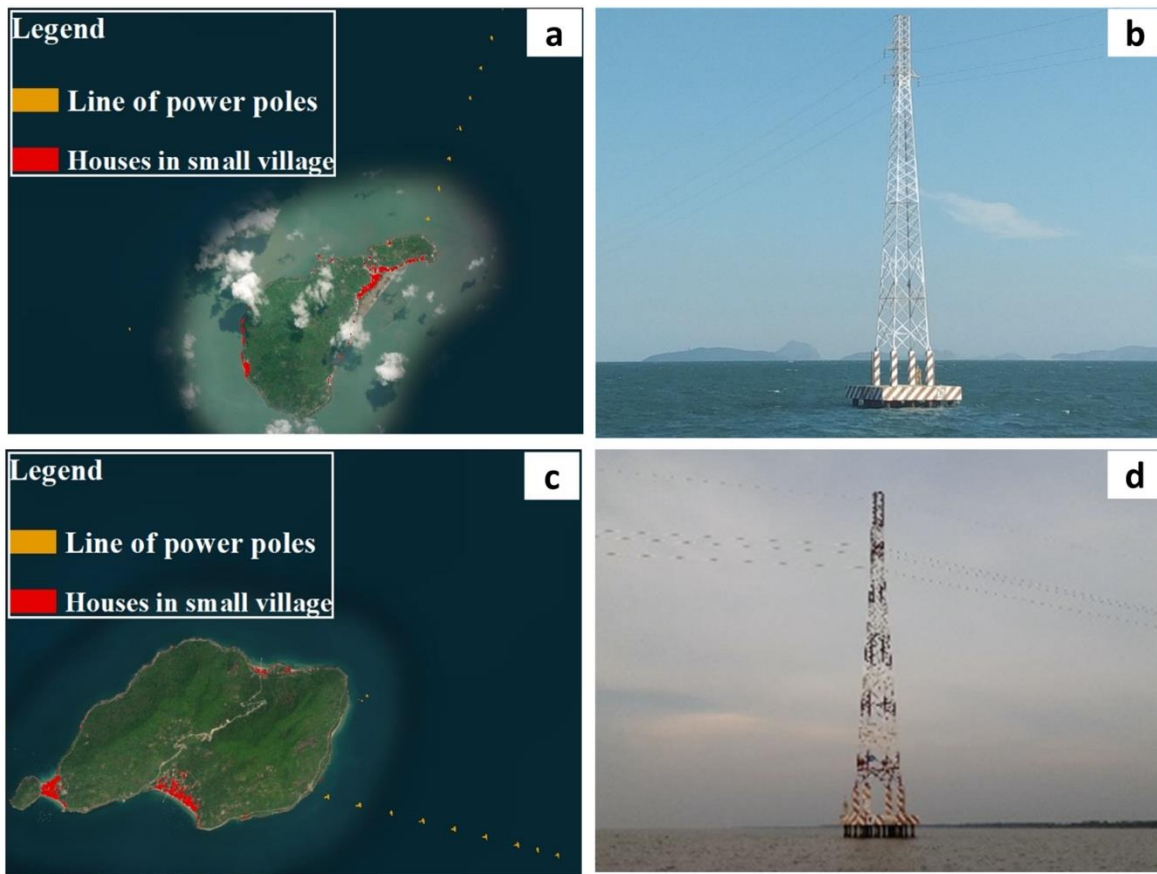
Figure 3.11 Detection of building structures on sea surfaces in Kiên Giang: (a) electric power line connecting Hòn Tre island to mainland in Kiên Giang, (b) ground-truth photograph on 4 January 2021 at 9°59′55.05″ N and 104°51′32.20″ E, (c) electric power line connecting Hòn Sơn island to mainland in Kiên Giang, (d) ground-truth photograph on 14 January 2021 at 9°44′48.99″ N and 104°51′42.47″ E.

The marine aquaculture in Kiên Giang province (in the Mekong Delta, southern Vietnam) includes farming of blood clams in shallow areas near the shore as a part of the regional development of sustainable fisheries. In 2008, the People Committee of An Biên District issued a policy on an economic development plan for shallow areas along the shore by leasing land, giving loans, and supporting culture techniques to locals. Thanks to this policy, farmers have rented mudflat areas from the local government, and built long wood fences and guard shacks on their farm (Figure 3.12). They usually live in guard shack month by month to protect their blood clam farm from other fishermen who illegally exploit the blood clams. Gradually, the guard shacks become fishing sites, seafood trading sites, and aqua-tourism sites.
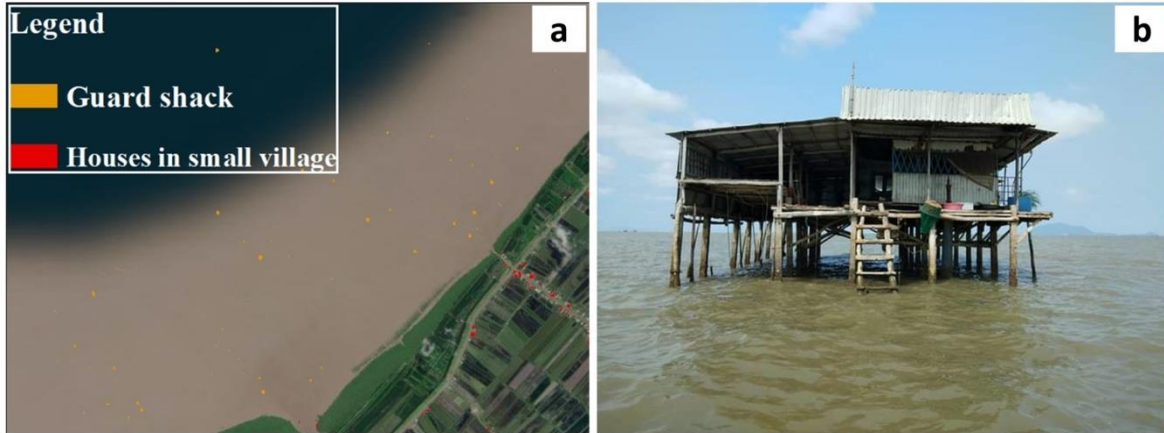
Figure 3.12 Detection of building structures on shallow areas near the shore in Kiên Giang: (a) guard shacks in blood clam farms in An Biên, (b) ground-truth photograph on 20 February 2021 at 9°53′32.81″ N and 104°59′1.24″ E.

3.4 Discussion

For the discussion here, the findings presented in this study are related to highlight the advances in the innovative SAR methods. First, the use of the 2-D dual-polarization VV-VH space (Figure 3.3) enabled a robust algorithm to be developed to overcome the confounding effects of complex variations in incidence and azimuth angles of satellite SAR data. This algorithm is important as it allows the use of SAR modes with wide swaths, and therefore more frequent observations with large coverages in comparison with data acquired with narrow swaths. The issue with wide-swath modes is that the range of incidence angles is large (29.1° to 46.0° for the Sentinel-1 SAR wide swath mode used in this study) and changes in backscatter signatures need to be corrected based on the backscatter slope as a function of incidence angles for different land cover classes (Phung *et al.*, 2020). Such incidence angle corrections demand a priori knowledge of surface types, which may not be available to start with.

For structures aligned preferentially in a specific direction on land (e.g., houses built along roads, trees grown along riverbanks, plowed fields in agricultural areas, etc.) and on the sea surface (e.g., waves along shores, roughness on sea surface directionally driven by wind directions, etc.), backscatter signatures can be strongly dependent on the azimuth angles of SAR data acquired in ascending and descending orbit tracks with different azimuth looks. The new approach for building structure detection using the 2-D VV-VH space is independent of incidence angles and azimuth direction, and thereby resolves the problem due to variations in incidence and azimuth angles.

The 2-D VV-VH space (Figure 3.3) revealed a distinctive domain for SAR backscatter signatures of building structures explicitly from the domains of multiple land cover types (e.g., trees, paddy fields, aquaculture areas) across the landscape over different regions in southern Vietnam, except for some minor overlap in the VV-VH domain for trees that may

58

have high backscatter. This finding demonstrates the ability of SAR to successfully identify building structures across urban-suburban to rural-natural landscapes with different background environments in wet and dry areas from inland to coastal regions. Furthermore, the identification of the overlap between the domains of buildings and trees in the 2-D VV-VH space led to the recognition that water-tree interactions in reflection and scattering processes of transmitted and received SAR signals (Figure 3.4) would cause high backscatter from trees. This prompted the development of the approach using NDVI from Sentinel 2 as an effective method to correct for the misclassification between buildings and trees.

In mountainous regions, land surfaces vary from steep to flat terrains; however, building structures are typically built-in areas that are level. The innovative use of the geomorphon concept in the method recognizes this issue, and therefore accounts for the misclassification of building structures caused by topographic effects on SAR signatures (Figure 3.5). Alternative algorithms that only use land surface height from DEM data would not be sufficient, as flat land may be located at different altitudes from coastal areas to foothill vicinities, and up on high plateaus. Therefore, the implementation of the full landform characterization with geomorphons is necessary in this method.

On the sea surface, backscatter values in upwind, downwind, and crosswind directions can strongly affect backscatter by an order of magnitude, with low and high wind speeds creating very different wave conditions (Carswell *et al.*, 1994; Nghiem *et al.*, 1995). These wind effects confound the detection of man-made structures with different sizes having different backscatter magnitudes. Rather than relying on complicated algorithms such as multi-modal signature decompositions or convolution neural networks that may introduce non-linearity, non-uniqueness, and/or extraneous outcomes, the method overcomes the effects of wind and waves to robustly detect persistent structures on the sea surface, ranging from very large oil platforms to small individual guard shacks in blood clam farms (Figure 3.9, Figure 3.10, Figure 3.11, and Figure 3.12).

The study has further demonstrated the utility of SAR to map building structures in various cities and regions with different environmental and socioeconomic conditions. More specifically, it has shown the ability of Sentinel-1 C-band SAR to make building maps with a high spatial resolution (10 m) from the SAR data archive since 2014 (Sentinel-1A and 1B) and potentially from future missions (Sentinel-1C and 1D) (ESA, 2021). Such long-term SAR records are crucial to monitor urban expansion that is continuing in most cities in Vietnam and other countries from the local and provincial to the state and national levels. Moreover, the robust ability to identify structures on the sea surface is important for

monitoring coastal developments such as aquacultural farms and both fossil and renewable energy industries in the marine environment.

3.5 Conclusions

This study has presented an innovative method to detect and map building structures on land and sea using times-series records of satellite Sentinel-1 SAR data. The results were validated with in-situ and field truth observations obtained in southern and central regions of Vietnam. The conclusion from this study includes the following key points:

- The novel use of satellite Sentinel-1 SAR data in the two-dimensional polarization domain enables the method to be robust against confounding factors such as variations due to different incidence and azimuth angles, due to water-tree radar signal interactions (with synergistic Sentinel-2 MSI data), and due to different landforms on complex typography (with the geomorphon concept), without having to rely on more complicated methods such as neural networks that may introduce non-linearity, non-uniqueness, or extraneous outcomes.

- A demonstration of the ability of radar backscatter signatures to detect building structures is founded on radar responses to true physical structures of buildings (Nghiem *et al.*, 2009; Sorichetta *et al.*, 2020), rather than optical colors or spectral appearances of land cover types. As this method is based on radar signatures of physical building structures, it can successfully capture the characteristics of urban building patterns corresponding to different urban development classes and socioeconomic status (see Table 3.1 and Table 3.2), and in different rural-urban landscapes in both inland and coastal regions with wet and arid environmental conditions, or over sea surfaces under different wind and wave effects.

- Founded on time-series satellite SAR data records consistently tracked at each pixel location, the method successfully detects and maps persistent (rather than temporary) building structures, which truly represent sustained human settlements in order to circumvent the shortfalls of the proxy indicator derived from NTL data (Gaughan *et al.*, 2019), as illustrated in the case of Phan Thiết city versus the dragon fruit plantations in Bình Thuận (Figure 3.8). Such spatial data products of physical building structures are crucial for urban mapping applications, in particular for accurate estimations of FFCO2 emission required for the successful implementation of the UNFCCC Paris Agreement. In fact, the U.S. National Academies of Sciences, Engineering, and Medicine recognizes that the improvement in greenhouse gas (GHG, including FFCO2) measurement and monitoring is foundational to the control of global GHG emissions (National Academies of Sciences, Engineering, 2021).

Regarding future research extension, the algorithm in this study can be modified or adapted for use with SAR data at other frequencies such as X band (the current TerraSAR-X/TanDEM-X and COSMO-SkyMed satellite SAR Missions and the future LOTUSat 1 and 2 satellite SAR Missions in the 2020s), L band (the current ALOS-2 PALSAR-2 Mission and the future Copernicus ROSE-L Mission), and combined L band and S band

(the NASA-ISRO SAR Mission to be launched in 2022). A synergistic combination of satellite SAR datasets offers a great potential to derive global building structure data products over a wide range of temporal and spatial scales, not only for two-dimensional building footprint, but also potentially for three-dimensional building volume (Mathews and Nghiem, 2021).

This chapter developed the novel method to detect persistent building structures on land and sea surface and successfully minimize the misclassification between building structure vs trees that are still problems when using supervised classification algorithm in Chapter 2. The following chapter (Chapter 4) will develop the novel method to identify and map seasonal inundated LCLU (e.g rice paddy) and persistent surface water (e.g aquaculture). This novel method will minimize the misclassified pixels between rice paddy and aquaculture when running supervised classification algorithm in Chapter 2.

Chapter 4 Surface Cover Classification

In previous chapter (Chapter 3), the novel use of satellite Sentinel-1 SAR data in the two-dimensional polarization to identify building structures on land and sea surface is discussed. This chapter will develop a novel method to identify and map persistent surface water and seasonal inundated land cover and land use (LCLU).

4.1 Introduction

As a region affected by marine interactions together with an extensive coastal wetland, Bạc Liêu province has founded shrimp production to be the leading sector in local economic development. In the late 1990s, Bạc Liêu started brackish water shrimp farming. In recent years, the high-tech shrimp farming or super-intensive shrimp farming was developed and expanded in Bạc Liêu due to high profits (Duc, 2021). The high-tech shrimp farming system utilizes shrimp breeding ponds in combination with the installation of aeration facilities, anti-sunlight nets on the top of pond, and plastic sheets on the soil bed (Trong, 2021).

In 2020, the Bạc Liêu province had more than 25,800 ha of super-intensive and intensive shrimp farming areas (VietnamPlus, 2021). This new system aims at offering high production values, sustainable to environment, and quality control and food safety to meet international export demands. However, the abuse of antibiotics and chemicals in intensive shrimp farming is destroying aquatic ecosystems (Binh, 2019), and wastewater from the super-intensive shrimp aquaculture poses major challenges to soil and surface water in wetland areas in Bạc Liêu province. It is crucial to monitor aquaculture areas by remotely sensed data. Nevertheless, the use of geospatial data in monitoring the aquaculture areas, particularly Sentinel-1 SAR satellite data, has been inadequate in Bạc Liêu as well as other aquaculture areas in the Mekong Delta.

SAR backscatter is sensitive to soil moisture and surface roughness (Son *et al.*, 2017). This SAR backscatter property can advance LCLU classification including water areas such as shrimp farms, rice paddies, and persistent surface water (such as lakes, rivers, persistently inundated unproductive land). Shrimp ponds, persistent surface water, and rice paddies

have similar backscatter at some specific time. Between sowing and the beginning of tillering (0-20 days), the rice paddy is mostly wet bare soil and the backscatter has low values (Phan *et al.*, 2018). Similarly, shrimp ponds contain water during cultivation period and also have low backscatter. This leads to LCLU misclassification in areas such as in Bạc Liêu province where rice paddies and shrimp aquaculture are widely cultivated.

To address the above challenges, the objective is to develop a new innovative algorithm for detection of water areas that change seasonally in different environmental conditions. The algorithm robustness must be tested across urban, suburban, rural, and natural areas on land in Bạc Liêu province using Sentinel-1 SAR time series data. First, a novel method is introduced to identify water in various LCLU mixtures using a three-dimensional (3-D) composite consisting of VV-VH polarization of the SAR backscatter data (2-D in the dual-polarization plane) and their seasonal change (1-D in time). This 3-D composite is hence denoted as VV-VH-DS, where VV is the vertical co-polarization backscatter, VH is the cross-polarization backscatter, and DS is the seasonal change of the backscatter data. Next, how to assess the accuracy of the water classification results is described. Finally, maps of persistent surface water, aquaculture field, map of rice paddy together with other LCLU (buildings, man-made structures, trees, and forests) in Bạc Liêu province are presented.

Regarding the advances of the new method, (1) the advantage of using the three-dimension (3-D) composite for land cover mapping is highlighted to robustly resolve the issue of incidence and azimuth angle dependence, (2) the ability of consistent time-series Sentinel-1 SAR to detect persistent surface water, and (3) the utilization of time dimension to map rice paddies versus shrimp farms. Finally, in the discussion and conclusion, future research extension with multi-temporal Sentinel-1 SAR to detect water areas together with LCLU classes in other coastal and marine regions in Vietnam in particular and elsewhere in general is noted.

4.2 Methods
An innovative approach is presented to map LCLU in Bạc Liêu province. The analysis, consisting of image processing, mapping, and accuracy assessment, was carried out using

the Google Earth Engine (GEE) platform and ArcGIS software. The flow chart in Figure 4.1 summarizes the overall methods in which each component is depicted in further detail below.

Original data

REMOTE SENSING IMAGERY
• Sentinel-1A SAR: 35 time series images, VV-VH polarization, 10 m resolution.
• Sentinel-2 MSI: 20-27 images (cloudiness < 20%), 10 m resolution.

Processing in GEE

IMAGE CALIBRATION
•   Apply orbit file.
•   Radiometric calibration.
•   Terrain correction.
•   Speckle filtering (using a multi-temporal 3-point mean filter).
•   Cloud masking (Sentinel-2 MSI).

Mapping

CLASSIFICATION
•   Extract pixel values for all land cover types (both VV and VH polarization, all incidence angle bins and azimuth looks).
•   Plot VV and VH in the 2D-polarization plane.
•   Determine threshold to classify each domain: urban, forest, shrimp, and bare domain.
•   Calculate the seasonal maximum backscatter, the seasonal minimum backscatter, and the seasonal backscatter difference for both aquaculture and rice paddy in the shrimp domain.
•   Determine threshold to classify rice paddy, count the numbers of times that each pixels identified as rice paddy, and determine the optimal rice paddy count threshold.
•   Determine threshold to classify aquaculture, count the numbers of times that each pixels identified as aquaculture, and determine the optimal aquaculture count threshold.
•   Determine threshold to classify persistent surface water, count the numbers of times that each pixels identified as persistent surface water, and determine the optimal persistent surface water count threshold.
•   Calculate NDVI to identify tree cover class.

Accuracy assessment

ACCURACY CALCULATION
•   Collect in-situ ground truth data.
•   Calculate mapping accuracy based on ground truth data, Google Earth Image, ArcGIS base map.

Figure 4.1 Processing and mapping workflow

4.2.1 Image Processing

Time series Sentinel-1 SAR images were pre-processed to derive the backscatter coefficient in decibel (dB) for each pixel. The pre-processed steps included applying orbit file, thermal noise removal, radiometric calibration and terrain correction using the Shuttle Radar Topography Mission (SRTM) 30-m topographic data. Then spatial co-registration of temporal data based on a referenced image was conducted to obtain the time series data in the same coordinate system. All these steps were carried out in the GEE platform.

To reduce speckle noise in SAR images, a multi-temporal 3-point mean filter (a moving average over a given time window) that would be computationally effective for noise elimination (Ngo *et al.*, 2021) was utilised. The calculation was implemented as follows:

$$p_{mean(ij\ at\ t)} = average(p_{ij\ at\ t-1} : p_{ij\ at\ t+1}) \tag{1}$$

Equation 4.1 Calculation of multi-temporal 3-point mean

In (1), $p_{mean(ij\ at\ t)}$ is the output pixel value at location i,j (i: numbers of image rows, j: numbers of image columns) at time t; $p_{ij\ at\ t-1}$ is the input pixel value at location i,j at time t-1; and $p_{ij\ at\ t+1}$ is the input pixel value at location i,j at time t+1.

In this case study, t has a value in the range of 1 to 35 (35 being the total number of SAR images in the period under consideration). After the mean calculation, the first and the last images in the time series were removed and only 33 images were used for further analysis. As an example, Figure 4.2 shows the raw backscatters, geometric mean, and arithmetic mean of Sentinel-1A SAR time series for VH and VV polarizations over shrimp farm in Bạc Liêu province.
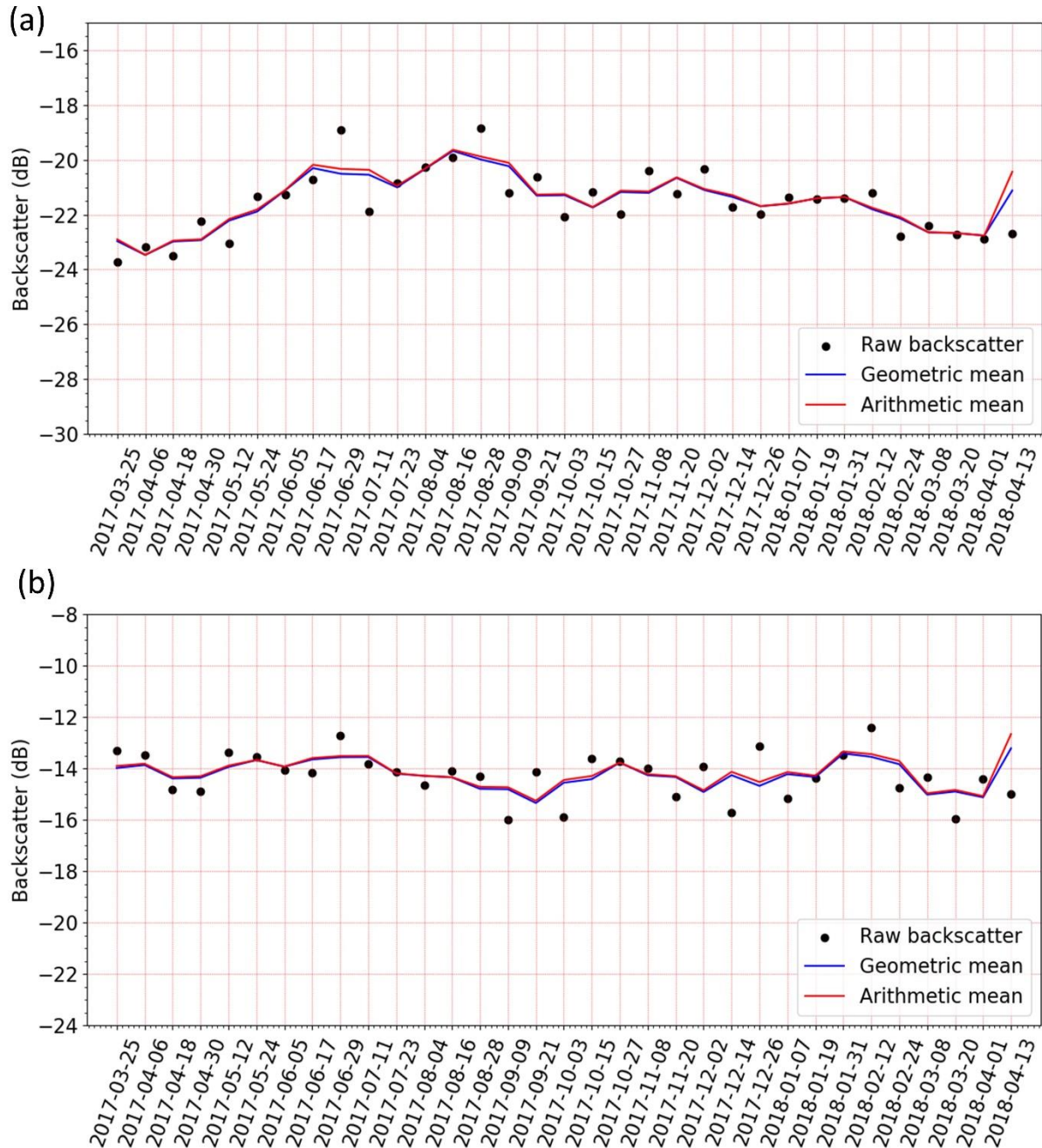
**Figure 4.2 Example of filtering of raw Sentinel-1A SAR time series for (a) VH and,
(b) VV polarizations over shrimp farm in Bạc Liêu province.**

4.2.2 Mapping

The 3-D VV-VH-DS composite is used to identify four domains with each domain primarily dominated by one of the four classes (urban, forest, shrimp farm, and bare surface) independent of incidence and azimuth angles. The incidence angle in SAR images

may influence backscatter values across the radar swath (Ngo *et al.*, 2021). To determine how backscatter changes as a function of incidence angle, a scatter plot with VV polarization for the x-axis and VH polarization for the y-axis was made. The 3-point mean backscatter values of all types of land cover including buildings, trees, paddy fields (such as rice paddies), and aquaculture (such as shrimp farms) at each incidence angle bin at 35, 38, and 42 degrees and azimuth direction (ascending versus descending) are shown in Figure 4.3. The thresholds in the 2-D VV-VH plane were determined to identify four domains as follows:

- Urban domain: a pixel was assigned to an urban class containing building structures on land if it satisfied the following conditions: VV backscatter greater than −5dB (VV > −5dB) or VH backscatter greater than −12 dB (VH > −12 dB). This domain almost totally contains the urban class. Thus, it can be used directly to identify and map urban areas.

- Forest domain: a pixel was assigned to a forest class if it satisfied the following conditions determined by the condition: VV backscatter smaller than −5dB (VV < −5dB) and VH backscatter smaller than or equal to −12 dB and VH backscatter greater than −17 dB (−17 dB < VH ≤ −12 dB). This domain primarily contains all forest class with a mixture of rice fields.

- Shrimp domain: a pixel was assigned to a shrimp class if it satisfied the following conditions determined by the condition: VV backscatter smaller than −5dB (VV < −5dB) and VH backscatter smaller than or equal to −17 dB and VH backscatter greater than −25 dB (−25 dB < VH ≤ −17 dB). This domain primarily contains all shrimp class with a mixture of rice fields.

- Bare domain: a pixel was assigned to a bare class if it satisfied the following conditions: VV backscatter smaller than −5dB (VV < −5 dB) or VH backscatter smaller than or equal to −25 dB (VH < −25 dB). This domain mainly contains the rice-field class where both VV and VH are very low due to little or no vegetation

cover. Thus, it can be used to identify bare rice fields or bare soil that can be inundated or non-inundated.
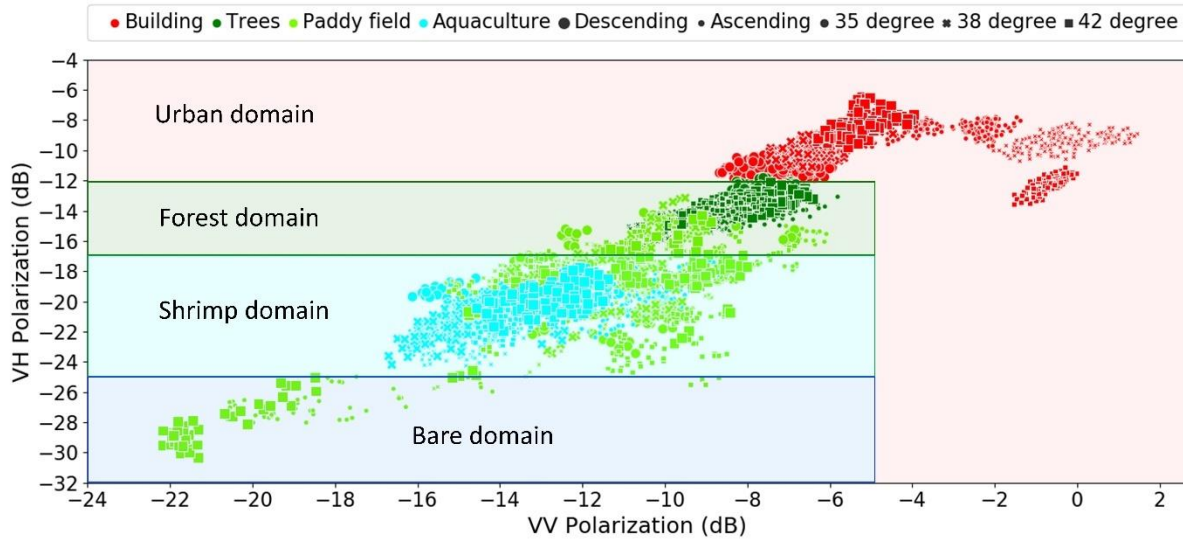
Figure 4.3 Dual-polarization backscatter plane of land cover classes, and four-domain classification in the 2-D space for VV on the horizontal axis and VH on the vertical axis in dB.

Figure 4.3 shows that urban domain and bare domain can be identified and mapped independent of incidence and azimuth angles. The issue remains with the forest domain and the shrimp domain, where each domain has a mixture with paddy fields. To resolve the mixing problem in the forest and shrimp domain, a third dimension is necessary. The third dimension can come from the time dimension, in which the seasonal variability of rice field can be different from the host domain (either the forest domain or the shrimp domain).

4.2.2.1 Urban mapping

The result of building structure mapping in previous chapter (Chapter 3) was used as urban class. In addition, the mapping result of building structure can be used as a mask for other land cover classes.

4.2.2.2 Rice mapping

To distinguish aquaculture (mostly shrimp farm) from rice paddy in shrimp domain the temporal variation of backscatter in time series was used. In fact, shrimp farm did not have

vegetation cover over the year, so the backscatter in time series did not have much change. While rice could have a significant seasonal change depending on seasonal rice growth cycles (Nguyen, Gruber and Wagner, 2016b). The backscattering coefficients (both polarizations) gradually increased during the growing period until they approached their maximum at the end of the reproductive state where rice had a dense canopy at the peak growth (Nguyen, Gruber and Wagner, 2016a). Thus, to identify shrimp from rice, the seasonal maximum backscatter (σ_{max}), the seasonal minimum backscatter (σ_{min}), and the seasonal backscatter difference (Δ_{VH}) were used in the following steps:

- Step 1: Each time series at pixel_ij consisted of about 33 data points in time. Each point in shrimp domain in the scatter plot (Figure 4.3) was associated with one corresponding series from March 2007 to April 2018. The maximum (σ_{max}) and the minimum backscatter (σ_{min}) in each time series of 33 data points were determined.

- Step 2: The maximum backscatter (σ_{max}) was assigned to each of the 33 data backscatter points to have 33 pairs of (σ_i, σ_{max}) where σ_i was the backscatter value at time i (i= 1, 2, 3… 33). The maximum backscatter (σ_{max}) was calculated for VH polarization at each incidence angle bin at 35, 38, and 42 degrees and azimuth direction (ascending versus descending) (Figure 4.3).

- Step 3: The backscatter difference (Δ_{VH}) was calculated in dB as:

$$\Delta_{VH} = \sigma_{max\_VH} - \sigma_{min\_VH}$$

Equation 4.2 Calculation of the backscatter difference

- Step 4: The seasonal maximum backscatter (σ_{max}), the seasonal minimum backscatter (σ_{min}), and the seasonal backscatter difference (Δ_{VH}) was calculated for both shrimp farm and rice paddy in the shrimp domain.

The threshold in the 3-D VV-VH-DS composite was determined to identify rice paddy. A pixel was assigned to a rice paddy class if it satisfied the following conditions: VV

backscatter smaller than −5dB (VV < −5dB) and VH backscatter smaller than or equal to −17 dB and VH backscatter greater than −25 dB (−25 dB < VH ≤ −17 dB) and the seasonal maximum backscatter greater than −16.5 dB ($\sigma_{max} > -16.5$ dB) (Figure 4.4) and the seasonal backscatter difference greater than 7.5 ($\Delta_{VH} > 7.5$) (Figure 4.5).

To capture the rice paddy pixels, the condition above was applied to all Sentinel-1A images in the time series (33 images). All output images (with value 1 for rice paddy pixels, and with value 0 for non-rice paddy pixels) were combined to count the number of times that each pixel was identified as rice paddy class. If pixel_ij was identified as a rice paddy T times out of the 33 images, then the count of pixel_ij was set to T. Each pixel in the combined output image could have a value of T in the range of 0 (for pixels in which rice paddies were never detected) to 33 (for pixels detected as rice paddies at all the times). To minimize misclassifying rice paddy pixels from real non-rice paddy pixels, the optimal rice paddy count threshold (rice_count_threshold) with the discrete derivative of rice paddy pixels ($\Delta_{m\_n\_rice}$) were determined depending on where the $\Delta_{m\_n\_rice}$ curve became invariant of flattened. Pixel_ij was detected as a rice paddy if rice_count_ij > rice_count_threshold where the rice_count_threshold could be from 1 to 33. The discrete derivative of rice paddy pixels was calculated as follows:

$$\Delta_{m\_n\_rice} = N_{threshold\_m\_rice} - N_{threshold\_n\_rice}$$

Equation 4.3 Calculation of discrete derivative of rice paddy pixels

where the terms $\Delta_{m\_n\_rice}$ is for the derivative between thresholds m and n, $N_{threshold\_m}$ is for number of rice paddy pixels at threshold m ($1 \leq m \leq 33$), and $N_{threshold\_n}$ is for number of rice paddy pixels at threshold n ($1 \leq m \leq 33$). Based on the formulation given by Equation 4.3, discrete derivative curves were utilised to determine the optimal rice paddy count threshold. This method required a rice paddy to exist persistently for a minimum period of about 1.5 months (see Appendix A).

4.2.2.3 Shrimp mapping

Similarly, the threshold to map shrimp aquaculture areas was determined. A pixel was assigned to an aquaculture class if it satisfied the following conditions: VV backscatter smaller than −5dB (VV < −5dB) and VH backscatter smaller than or equal to −17 dB and VH backscatter greater than −25 dB (−25 dB < VH ≤ −17 dB) and the seasonal maximum backscatter (σ_{max}) smaller than or equal to -16.5 dB (σ_{max} ≤ -16.5 dB) (Figure 4.4) and the seasonal backscatter difference greater than 7.5 (Δ_{VH} ≤ 7.5) (Figure 4.5).

To capture the aquaculture pixels, the condition above was applied to all Sentinel-1A images in the time series (33 images). Like rice paddy identification step above, all output images (with value 1 for aquaculture pixels, and with value 0 for non-aquaculture pixels) were combined to count the number of times that each pixel was identified as aquaculture. If pixel_ij was identified as aquaculture T times out of the 33 images, then the count of pixel_ij was set to T. Each pixel in the combined output image could have a value of T in the range of 0 (for pixels in which aquaculture were never detected) to 33 (for pixels detected as aquaculture at all the times). To minimize misclassifying aquaculture pixels from real non-aquaculture pixels, the optimal aquaculture count threshold (aquaculture_count_threshold) with the discrete derivative of aquaculture pixels ($\Delta_{m\_n\_aquaculture}$) was determined depending on where the $\Delta_{m\_n\_aquaculture}$ curve became invariant of flattened. Pixel_ij was detected as an aquaculture if aquaculture_count_ij > aquaculture_count_threshold where the aquaculture_count_threshold could be from 1 to 33. The discrete derivative of aquaculture pixels was calculated by the following equation:

$$\Delta_{m\_n\_aquaculture} = N_{threshold\_m\_aquaculture} - N_{threshold\_n\_aquaculture} \qquad (3)$$

Equation 4.4 Calculation of discrete derivative of aquaculture pixels

where the terms $\Delta_{m\_n\_aquaculture}$ is for the derivative between thresholds m and n, $N_{threshold\_m\_aquaculture}$ is for number of aquaculture pixels at threshold m ($1 \leq m \leq 33$), and $N_{threshold\_n\_aquaculture}$ is for number of aquaculture pixels at threshold n ($1 \leq m \leq 33$). Based on the formulation given by Equation 4.4, discrete derivative curves were utilised to

determine the optimal aquaculture count threshold. This method requires an aquaculture to exist persistently for a minimum period of about 1.5 months (see Appendix A).
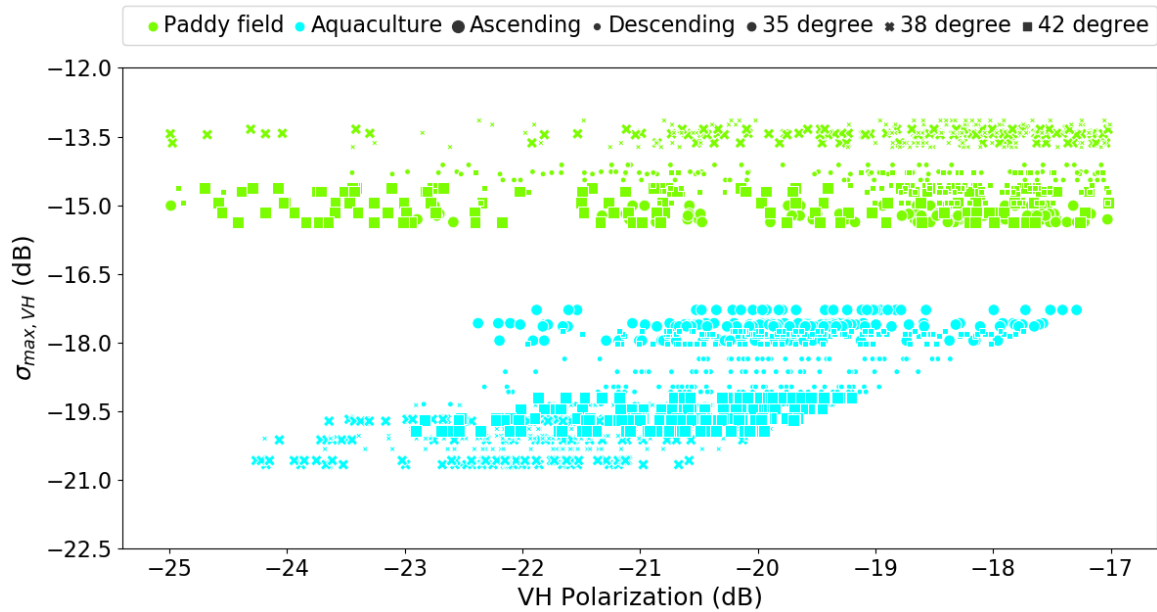
Figure 4.4 Multi-temporal backscatter of paddy field and aquaculture in time dimensional space for VH on the horizontal axis and Sigma_max ($\sigma_{max,VH}$) on the vertical axis in dB.
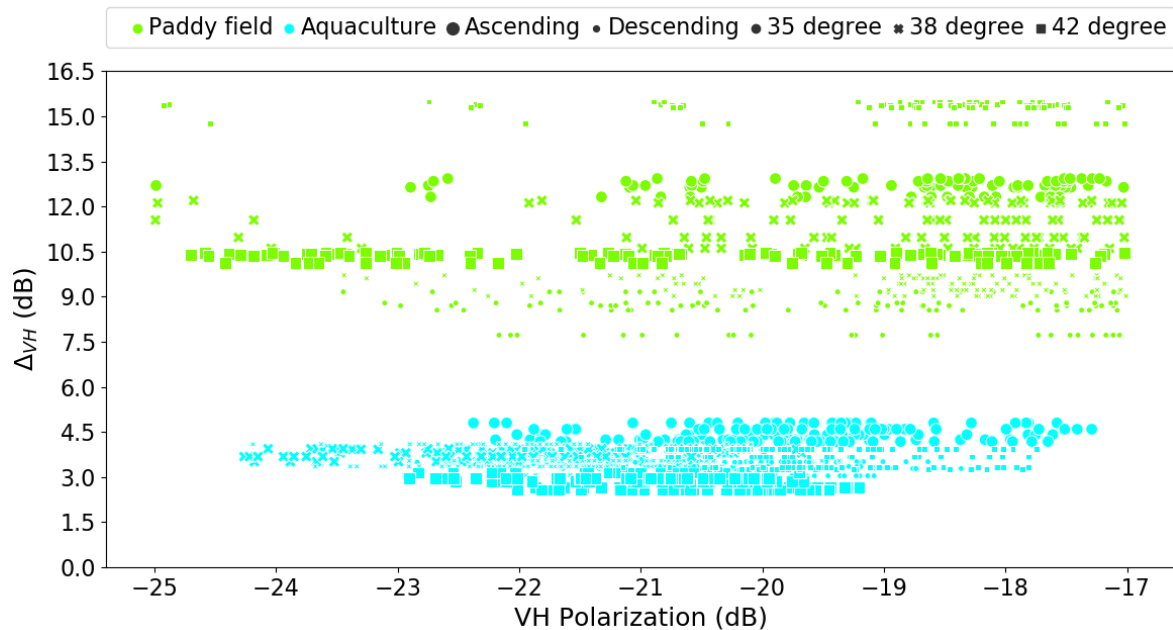
Figure 4.5 Multi-temporal backscatter of paddy field and aquaculture in time dimensional space for VH on the horizontal axis and Delta_VH (Δ_{VH}) on the vertical axis in dB.

4.2.2.4 Persistent surface water mapping

To detect persistent surface water in bare domain, the condition VH backscatter smaller than or equal to −25 dB (VH ≤ −25 dB) was used (Figure 4.3). To capture the persistent surface water pixels, the condition above was applied to all Sentinel-1A images in the time series (33 images). Like rice paddy and aquaculture identification step above, all output images (with value 1 for persistent water pixels, and with value 0 otherwise) were combined to count the number of times that each pixel was identified as persistent surface water class. If pixel_ij was identified as a persistent surface water T times out of the 33 images, then the count of pixel_ij was set to T. Each pixel in the combined output image could have a value of T in the range of 0 (for pixels in which persistent surface water were never detected) to 33 (for pixels detected as persistent surface water at all the times). To minimize misclassifying persistent surface water pixels from real non-persistent surface water pixels, the optimal persistent surface water count threshold (persistent_water_count_threshold) with the discrete derivative of persistent surface water pixels ($\Delta_{m\_n\_persistent\_water}$) was determined depending on where the $\Delta_{m\_n\_persistent\_water}$ curve became invariant of flattened. Pixel_ij was detected as a persistent surface water if persistent_water_count_ij > persistent_water_count_threshold where the persistent_water_count_threshold could be from 1 to 33. The discrete derivative of persistent surface water pixels was calculated as follows:

$$\Delta_{m\_n\_ persistent\_water} = N_{threshold\_m\_persistent\_water} - N_{threshold\_n\_ persistent\_water}$$

Equation 4.5 Calculation of discrete derivative of persistent surface water pixels

where the terms $\Delta_{m\_n\_ persistent\_water}$ is for the derivative between thresholds m and n, $N_{threshold\_m\_persistent\_water}$ is for number of persistent surface water pixels at threshold m (1 ≤ m ≤ 33), and $N_{threshold\_n\_persistent\_water}$ is for number of persistent surface water pixels at threshold n (1 ≤ m ≤ 33). Based on the formulation given by Equation 4.5, discrete derivative curves were utilised to determine the optimal persistent surface water count threshold. This method requires a persistent surface water to exist persistently for a minimum period of a year (see Appendix A).

4.2.2.5 Forest mapping

Together with the forest domain defined earlier from the SAR backscatter data, the Normalized Different Vegetation Index (NDVI) (Haas and Ban, 2017; Ngo *et al.*, 2021) derived from the Multi-Spectral Instrument (MSI) aboard Sentinel-2 satellite was used to map tree cover. GEE was utilised to select Sentinel-2 MSI data on mostly-clear-sky days (cloudiness < 20%) to compute NDVI from March 2017 to April 2018. NDVI in each 10-m pixel was then calculated and the average of N largest values of NDVI (NDVI_avg_Nmax) in each pixel obtained over the period under consideration was computed. A pixel was classified as tree cover class if NDVI_avg_Nmax > NDVI_threshold. Multiple cases for N = 3, 5, 10, and 15 were tested and NDVI_threshold was found to range from 0.25 to 0.5 in each case. Based on this examination, the parameters to N = 3 and NDVI_threshold = 0.4 were set to identify tree cover class as these values yielded optimal results.

4.2.3 Post classification

A 3x3 window filter was used to clean isolated pixel due to spurious noise in SAR data in each binary rice paddy, aquaculture, and persistent surface water classification map. For instance, in the 3x3 window if the centre pixel (2,2) was non-rice and the total rice pixel count (N_rice_count) in the 3x3 window was greater than or equal to X (X = 5, 6, 7, 8), then all non-rice pixels in the 3x3 window were reclassified to be rice pixels. After each land cover class was applied isolated pixel filtering, all of them were then mosaicked to make final land cover map.

4.2.4 Ground truth data collection and accuracy assessment

In-situ ground truth data were collected across the Bạc Liêu province. Fieldwork included taking field observation with geotagged photographs of different LCLU types such as building structures (school, commercial centres, resident houses, etc.), trees (coastal forest, perennial trees, plantation), paddy fields (rice paddies), aquaculture areas (shrimp farms), persistent surface water (water treatment and solids settling ponds in shrimp farming zone). In addition, geotagged photographs were taken at different locations from rural to urban

areas of the Bạc Liêu province (Figure 4.6). The photographs were imported into ArcGIS Pro software to get the locations of ground truth points. These points were utilised as validation points in the accuracy assessment.

Based on in-situ ground truth data and field photographs together with high-resolution true colour images in Google Earth[TM] and the ArcGIS Pro base map, the quality of the mapping results was assessed. A stratified (by land cover) randomly spatial distributed set of 900 validations points were used to test accuracy. These points were positioned at the central of 3x3 homogeneous pixels. A confusion matrix, Kappa, and producer and user accuracy were used to measure the accuracy of mapping results. The error matrices and overall accuracy reports were calculated from ArcGIS Pro.
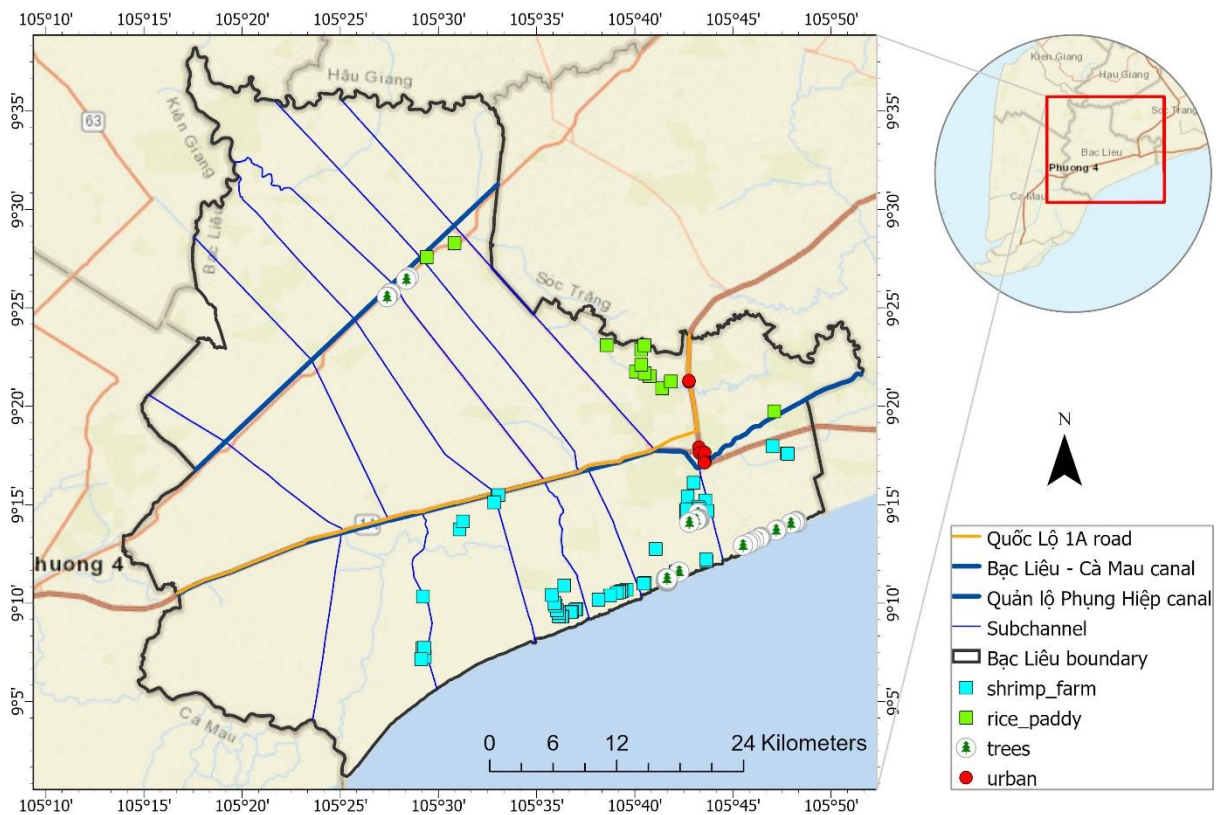
Figure 4.6 Locations of field photographs over Bạc Liêu province surveyed from 01 Oct 2019 to 05 May 2020.

4.3 Results

4.3.1 Classification results

Figure 4.7 shows an example of the classification result of persistent surface water for Bạc Liêu province. The map shows that persistent surface water pixels are in the aquaculture cultivation areas. Most of persistent surface water pixels are water treatment ponds and solids settling ponds in the intensive or super-intensive shrimp farms. In other cases, persistent surface water pixels can be abandoned shrimp ponds in which farmers no longer cultivate their shrimp farm due to shortage of financial investment or soil pollution.
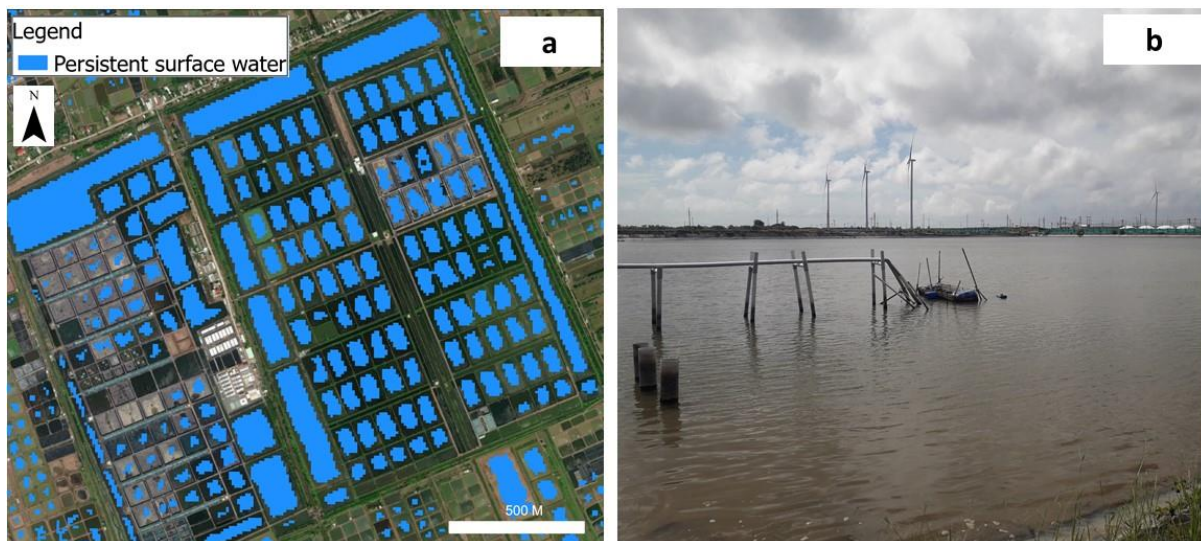
Figure 4.7 Detection of persistent surface water in Bạc Liêu: (a) water treatment and solids settling ponds at CP Bạc Liêu shrimp farm, (b) ground-truth photograph on 05 Sept 2021 at 9° 11' 25'' N and 105° 38' 15'' E.

Figure 4.8 shows the result of aquaculture farm detection for Bạc Liêu province. Aquaculture farm pixels detected in Bạc Liêu are intensive shrimp ponds where water is pumped in and discharged at harvest and between crops.

Figure 4.8 Detection of aquaculture farm in Bạc Liêu: (a) shrimp farm at Vĩnh Hậu village, Bạc Liêu, (b) ground-truth photograph on 05 Sept 2021 at 9° 12' 01'' N and 105° 43' 13'' E.

Figure 4.9 shows an example of the rice paddy detection result for Bạc Liêu province. The map shows that rice paddy pixels are surrounded by roads or canals.
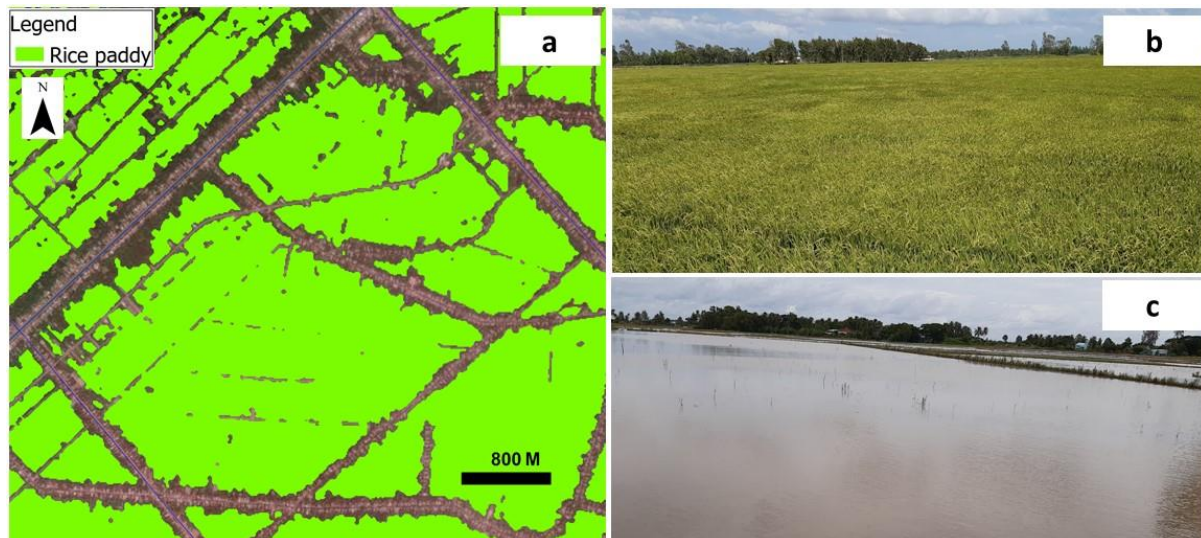
Figure 4.9 Detection of rice paddy in Bạc Liêu: (a) rice paddy map detected from Sentinel-1 SAR at Vĩnh Phú Đông village, (b) ground-truth photograph on 29 Nov 2021 at 9° 28' 05'' N and 105° 30' 15'' E, (c) ground-truth photograph on 23 Sept 2021 at 9° 21' 35'' N and 105° 40' 40'' E.

Figure 4.10 shows the results of the land cover classification for Bạc Liêu province. The map shows that building pixels emanating outward from urban to rural areas. Most building

pixels cluster around Bạc Liêu city and disperse along main roads and waterways. Tree pixels concentrate in inundated areas by tides along coastline. Most rice paddy pixels are identified in North of Quốc Lộ 1A road while aquaculture farms and persistent surface water are detected in South of Quốc Lộ 1A road, east of Bạc Liêu city, and west of Bạc Liêu province adjacent to Cà Mau province. The classification results reveal the distinctive spatial patterns of different LCLU associated with their unique characteristics of fresh versus marine water, population distribution drivers, and infrastructure development standard.
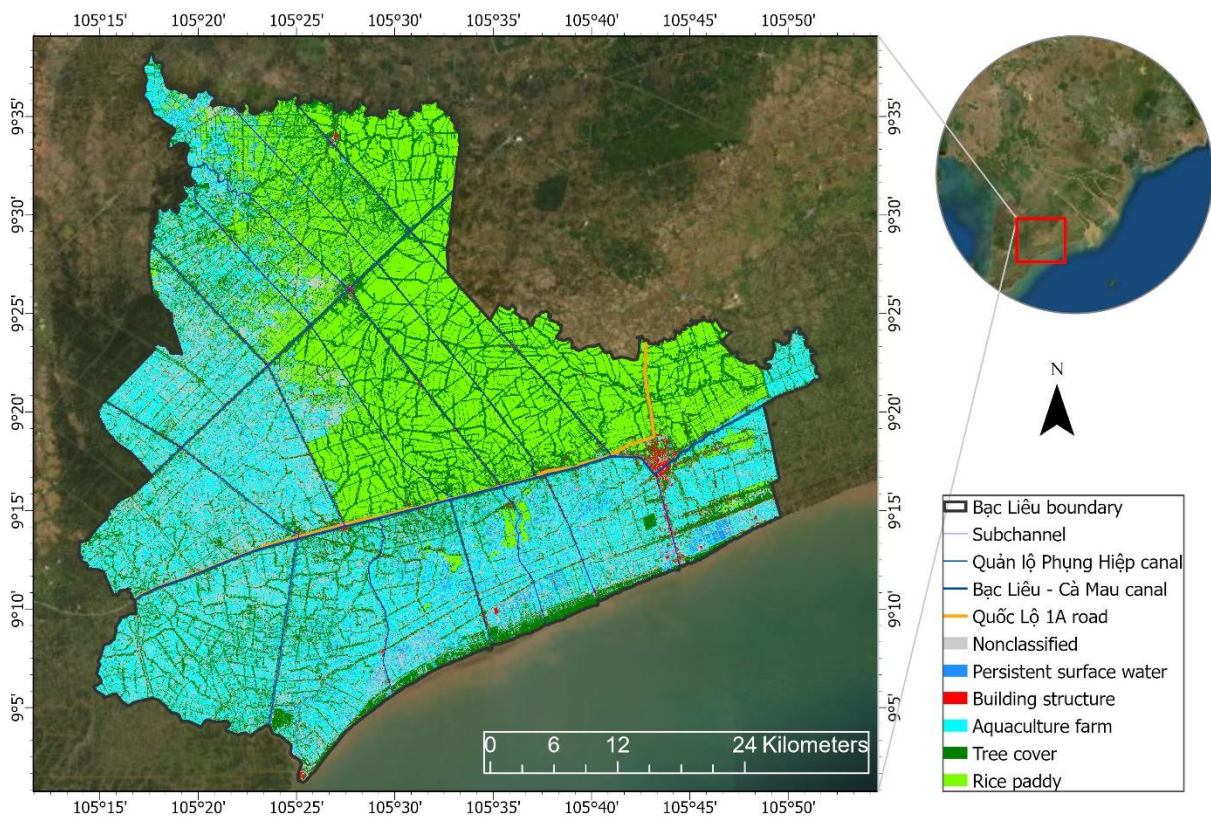
Figure 4.10 Classification map of all land cover/land use classes in Bạc Liêu.

4.3.2 Validation

Assessed with in-situ data and field observation, Table 4.1 summarizes the accuracy of land cover mapping in Bạc Liêu province. Generally, the mapping results achieves high accuracy with overall accuracy of 91.2% and Kappa coefficient of 0.89. Within five land cover classes, building structure had the highest accuracy with producer accuracy of 99.3% and user accuracy of 98.6% respectively as the backscatter intensity values were unique

compared to the other land cover classes. In contrast, shrimp farming has lowest accuracy with producer accuracy of 87.9% and user accuracy of 89.0% as aquaculture cultivation activities including water exchange, drainage, and soil conditioning during crops influence backscatter values.

Table 4.1 Accuracy assessment results for error matrices using 900 validations points.

Ground truth data (points)	Classification results (pixels)						
	Shrimp farming	Tree	Paddy	Built-up	Persistent surface water	Non-classified	Total
Shrimp farming	145	1	1	0	4	12	163
Tree	3	120	12	1	2	1	139
Paddy	10	2	140	0	3	2	157
Built-up	0	2	0	144	0	0	146
Persistent surface water	4	0	1	0	132	3	140
Non-classified	3	6	2	0	4	140	155
Total	165	131	156	145	145	158	900
Producer accuracy (%)	87.9	91.6	89.7	99.3	91.0	88.6	
User accuracy (%)	89.0	86.3	89.2	98.6	94.3	90.3	
Overall accuracy (%)	91.2						
Kappa coefficient	0.89						

4.4 Discussion

The findings presented in this chapter is related to highlight the advances in the novel SAR methods. First, the use of the 3-D VV-VH-DS composite allows a robust algorithm to be developed to overcome the confounding effects of variations in incidence and azimuth angles of SAR data. This algorithm is crucial because it enables the use of wide swath modes of SAR with large coverages compared to data acquired with narrow swath. In wide-swath modes of Sentinel-1 SAR, the range of incidence angles is between 29.1º to 46.0º, so the change in backscatter signature need to be corrected based on the backscatter slope as a function of incidence angles for different land cover classes (Phung *et al.*, 2020; Ngo *et al.*, 2021). To correct the incidence angle, a priori knowledge of all different surface types is required, which may not be available to start with (Ngo *et al.*, 2021).

The inclusion of time dimension in 3-D VV-VH-DS composite can help resolve the mixing issue in forest domain and shrimp domain. The 2-D VV-VH space (Figure 3) reveals that the mixing issue remains with the forest domain and the shrimp domain, each has a mixture

with rice field. Rice can have a dense canopy at the peak growth in some crops during the year. Depending on seasonal rice growth cycles, the seasonal variability of rice field can be large and different from the host domain (either the forest domain or shrimp domain). In contrast, the seasonal variability of established forest is small and shrimp farms have no vegetation cover over the year. Therefore, seasonal backscatter difference and the seasonal maximum backscatter can be used to distinguish rice paddy field from aquaculture (shrimp farm).

The mapping method can be applied for detecting persistent surface water, which can be used to monitor unproductive lands, which can be considered as fallow wet land. High-tech shrimp farming is currently expanded in Bạc Liêu province since this farming model enables high productive (40-50 tonnes/ha/crop) and success rate above 90% (Duc, 2021). However, environment issues are a major challenge because raising shrimp in this farming type has high density of shrimp per square meter (250-300 shrimp/m^2). This means a large amount of untreated waste and wastewater from shrimp ponds is discharged to canals, and may have negative impacts on the nearby canals and rivers (Chi, 2020). SAR backscatter will vary depending on farming activities at shrimp ponds such as aeration activities, water supplies between crops or drainage at harvest. Therefore, if the land is polluted, unproductive and not suitable for shrimp farming, farmers will leave the pond inundated (persistent surface water). With 12 days revisits of a single Sentinel-1 SAR satellite, the mapping method will annually help the relevant authorities monitor productive land and unproductive lands.

4.5 Conclusions

This chapter has presented a novel method to map persistent surface water and seasonal inundated land cover and land use using time-series records of satellite Sentinel-1 SAR data. The accuracy of mapping results was accessed with in-situ and field truth observations obtained in the Bạc Liêu province. The conclusion from this chapter consists of the following key points:

- The innovative use of satellite Sentinel-1 SAR data in the three-dimensional polarization and seasonal change composite allows the method to be robust and to circumvent confounding effects of different incidence and azimuth angles.

- The use of the three-dimensional composite is successfully in detecting rice paddy, aquaculture, and persistent surface water. This novel method can be utilized to monitor aquaculture that has contributed to the transformation of the overall agriculture and economics in the Bạc Liêu province.

In terms of future research extension, the algorithm in this chapter can be customized or adapted for use with SAR data at other frequencies such as X band, S band, and L band for applications not only in Vietnam but also in other countries. A synergistic combination of satellite SAR datasets will provide a great potential to derive agriculture and aquaculture data product across a wide range of temporal and spatial scales.

Chapter 5 Synthesis

5.1 Summary

This thesis investigates the utility of satellite Sentinel-1A SAR data to map land cover in various cities and regions with different environmental and socioeconomic conditions in Vietnam. The importance of SAR data as an up-to-date additional data source of land cover information for local authorities is not widely appreciated and rarely addressed, but this thesis demonstrates important implications for supporting land use master plan and monitoring illegal land use changes (Chapter 2). This thesis demonstrates the novel use of satellite Sentinel-1 SAR data in the two-dimensional polarization domain to detect building structures that represent sustained human settlements (Chapter 3). This thesis illustrates the innovative use of satellite Sentinel-1 SAR data in the three-dimensional polarization and seasonal change composite to map persistent surface water and seasonal inundated land cover and land use (Chapter 4). Potential future directions for research in the disciplines of remote sensing are provided in this synthesis chapter.

5.2 Research questions

5.2.1 How can SAR imagery support in LCLU mapping for natural resource management in the Mekong Delta?

Chapter 2 demonstrates the utility of SAR imagery for characterizing LCLU in Bạc Liêu, a coastal and rapidly developing province in the Mekong Delta. This chapter examines different LCLU classification algorithms and compares single date versus multi-temporal SAR image datasets in terms of classification accuracy. The results indicated the potential use of multi-temporal SAR imagery as an up-to-date complementary data source of LCLU information for local authorities, to support their natural resource management for land use planning and illegal land use changes monitoring.

5.2.2 How can persistent building structures on land and on sea surfaces be detected using SAR data?

Chapter 3 develops a novel method to identify and map persistent building structures on land and sea surface using time-series records of satellite Sentinel-1 SAR data. This chapter used the two-dimensional (2-D) space of VV-VH polarization to determine the VV-VH

domain for detecting building structures from the annual composites of SAR data. The persistence of building structures was defined based on the number of times that a pixel was identified as a building in time-series data. Moreover, the algorithm accounted for misclassified buildings due to water-tree interactions in radar signatures and due to topography effects in complex mountainous landforms. The method was tested in five cities across urban-suburban to rural-natural landscapes with different back- ground environments in wet and dry areas from inland to coastal regions. Using in-situ data and field observations, the methods were validated, and the results were found to be accurate. The algorithm could also detect small houses in rural settlements and in small islands such as in Hòn Sơn and Hòn Tre. Over sea surfaces, the algorithm effectively identified lines of power poles connecting islands to the mainland, guard shacks in marine blood clam farms in Kiên Giang, individual wind towers in the offshore wind farm in Bạc Liêu, and oilrigs in the Vũng Tàu oil fields. The new approach was developed to be robust against variations in SAR incidence and azimuth angles. This chapter demonstrates the potential use of satellite dual-polarization SAR to identify persistent building structures annually across rural–urban landscapes and on sea surfaces with different environmental conditions.

5.2.3 How can persistent surface water and seasonal inundated land cover be identified with the use of the 3-D dual-polarization VV-VH-Season space?

Chapter 4 proposes a novel and robust method to map LCLU that includes persistent surface water and seasonal inundated land cover. This chapter used the three-dimensional (3-D) space of VV-VH polarization of the SAR data and Season space to identify four domains (urban, forest, shrimp farm, and bare surface). The method was tested in Bạc Liêu province where aquaculture areas are expanding. Using in-situ data and field observations, the mapping results were validated, and the mapping results achieves high accuracy. The results demonstrates that the use of the 3-D dual-polarization VV-VH-Season space enabled a robust algorithm to be developed to overcome the issue of incidence and azimuth angle dependence of SAR data. The mapping method can be utilized for identifying persistent surface water, which can be used to monitor aquaculture areas in wetland regions.

5.3 Significance, limitations and future research extension

This thesis demonstrates the potential use of multi-temporal Sentinel-1 SAR land cover mapping. The SAR images can be used as a reliable reference source to assess the accuracy of existing cadastral maps and to assist land use master plan. The revisit of 12 days of Sentinel-1 SAR satellite help track land use activities and monitor illegal land use changes. Long-term monitoring of land use will be crucial for decision makers, to ensure sustainability and food security in the Mekong Delta region. The study contributed to a better understanding of spatial-temporal changes in the coastal landscapes, especially in tropical countries where frequent cloud cover obstructs optical remote sensing. The application of SAR in mapping LCLU can be applied to other regions having similar socioeconomic conditions and background environments as in the Mekong Delta.

Accurate mapping and monitoring of greenhouse gases is crucial to the successful implementation of the Paris Agreement within the United Nations Framework Convention on Climate Change (Gaughan *et al.*, 2019). The estimation of fossil fuel CO_2 (FFCO2) emission is currently based on night-time light (NTL) data as a proxy for human settlements (Sorichetta *et al.*, 2020). This thesis produced the maps of physically defined building structures derived by the two-dimensional polarization domain, which can improve the shortfalls of the proxy indicator derived from NTL data as indicated in the case of Phan Thiết city versus the dragon fruit plantations in Bình Thuận.

One of the limitations of this thesis is the availability of Sentinel-1 satellite data. In fact, Sentinel-1 mission originally composed of a constellation of two satellites, Sentinel-1A (launched on 3 April 2014) and Sentinel-1B (launched on 25 April 2016). However, due to an equipment failure on Sentinel-1B in December 2021, the Sentinel-1B satellite has been retired, leaving Sentinel-1A the only satellite of the constellation. European Space Agency planned to launch Sentinel-1C into orbit and operational in March 2024 to complement the data shortage.

The second limitation is the accuracy assessment of mapping results. Most in-situ ground truth data in this thesis were collected in Bạc Liêu and Sóc Trăng in the Vietnamese

Mekong Delta and Phan Thiết in the central in Vietnam. Further in-situ ground truth data for accuracy assessment needs to be collected to replicate the approach to other applications or elsewhere. However, acquiring ground truth data can be time consuming and labor intensive.

The third limitation is that the algorithm in this thesis determining LCLU classification thresholds was dedicated to the Sentinel-1 SAR C-band data. In the future, the approach can be adapted to LOTUSat-1 data (Vietnamese satellite) and COSMO-SkyMed data (Italian satellite) at other frequencies such as X-band. This will provide greater coverage and more data. Although we used a range of remote sensing information from SAR imagery to classify LCLU including magnitude, polarization, and seasonal change, there were still misclassified pixels, particularly, between rice paddy and aquaculture. Those misclassifications can be minimized through a combination of different SAR frequency, for example, C-band and X-band. The combinations of different SAR frequencies on different platforms may provide much more information for rice paddy and aquaculture and minimize the possibility for such misclassifications.

The thesis demonstrates the utility of SAR for identifying and mapping permanent building structures that truly represent sustained human settlements. The novel algorithm effectively detected manmade structures on sea surfaces such as lines of power poles, guard shacks in marine blood clam farms, wind towers in the offshore wind farm, oilrigs in the oil fields. This new approach may be also helpful for those countries having large areas of sea surface such as Malaysia and Japan. This method can be applicable to the countries with borders on the South China Sea (Biển Đông) to detect whether persistent targets are under construction such as military installations (someone is building something on islands).

The algorithms in this thesis describe the range of SAR applications for describing land use change from buildings, agriculture, and windfarms. These approaches can be used for mapping key socio-ecological challenges in the region. For example, detecting the environmental impacts of Indonesia's new capital relocation. Indonesia has made ambitious plans to relocate its capital to Nusantara - the island of Borneo, expected to take

place by 2045. However, environmentalists concerned about the environmental impacts of building a sprawling 256,000-hectare city down in Borneo's East Kalimantan province, which is home to orangutans, leopards and a wide range of other wildlife. The method in this thesis may support the mapping of the remaining natural forest and building structure construction. SARs cloud penetrating ability has great utility and is critical for mapping locations, such as tropical Borneo, due to the high frequency of cloud cover.

5.4 Conclusion

This thesis has highlighted the ability of radar backscatter signatures and the utility Google Earth Engine in mapping LCLU. It demonstrated that the results were validated with in-situ and field truth data obtained in Vietnam. Several key findings arose from this research.

Firstly, the novel utility of satellite Sentinel-1 SAR data in the two-dimensional polarization domain enables the method to be robust against confounding factors such as variations due to different incidence and azimuth angles, due to water-tree radar signal interactions (with synergistic Sentinel-2 MSI data), and due to different landforms on complex typography (with the geomorphon concept).

A demonstration of the ability of radar backscatter signatures to detect building structures is founded on radar responses to true physical structures of buildings, rather than optical colors or spectral appearances of land cover types. As the method is based on radar signatures of physical building structures, it can successfully capture the characteristics of urban building patterns corresponding to different urban development classes and socioeconomic status, and in different rural-urban landscapes in both inland and coastal regions with wet and arid environmental conditions, or over sea surfaces under different wind and wave effects.

The innovative use of satellite Sentinel-1 SAR data in the three-dimensional polarization and seasonal change composite is successfully in detecting rice paddy, aquaculture, and persistent surface water. This novel method can be utilized to monitor shrimp aquaculture and support the environmental footprint assessment of shrimp pond in the Bạc Liêu province.

BIBLIOGRAPHY

Aschbacher, J. and Milagro-Pérez, M. P. (2012) 'The European Earth monitoring (GMES) programme: Status and perspectives', *Remote Sensing of Environment*, 120(2012), pp. 3–8. doi: 10.1016/j.rse.2011.08.028.

Bac Lieu People Committee (2017) *The synthesis explanatory report: Adjustment of land use master plan up to 2020 and land use plan for the last period (2016-2020) in Bac Lieu province*. Bac Lieu.

Bac Lieu People Committee (2018) *Action Plan on Prawn Sector Development in Bac Lieu toward 2025 (Phát triển ngành tôm tỉnh Bạc Liêu đến năm 2025)*. Bac Lieu.

Ban, Y. *et al.* (2017) 'EO4Urban: Sentinel-1A SAR and Sentinel-2A MSI data for global urban services', *2017 Joint Urban Remote Sensing Event (JURSE)*, pp. 1–4. doi: 10.1109/JURSE.2017.7924550.

Barber, D. G. and LeDrew, E. F. (1991) 'SAR Sea Ice Discrimination Using Texture Statistics: A Multivariate Approach Photogrammetric Engineering and Remote Sensing', *Photogrammetric Engineering and Remote Sensing*, 57 (4), pp. 385–395.

Barsi, A. *et al.* (2018) 'Accuracy dimensions in remote sensing', *International Archives of the Photogrammetry, Remote Sensing and Spatial Information Sciences - ISPRS Archives*, 42(3), pp. 61–67. doi: 10.5194/isprs-archives-XLII-3-61-2018.

Belgiu, M. and Dragut, L. (2016) 'Random forest in remote sensing : A review of applications and future directions', *ISPRS Journal of Photogrammetry and Remote Sensing*, 114, pp. 24–31. doi: 10.1016/j.isprsjprs.2016.01.011.

Binh, T. (2019) *Application of biotechnology in shrimp farming*, *Directorate of Fisheries*. Available at: https://tongcucthuysan.gov.vn/en-us/aquaculture/aquaculture/doc-tin/012187/2019-01-28/application-of-biotechnology-in-shrimp-farming.

Bouvet, A. and Le Toan, T. (2011) 'Use of ENVISAT/ASAR wide-swath data for timely rice fields mapping in the Mekong River Delta', *Remote Sensing of Environment*, 115(4), pp.

1090–1101. doi: 10.1016/j.rse.2010.12.014.

Breiman, L. (2001) 'Random forests', *Machine Learning*, 45(1), pp. 5–32. doi: 10.1023/A:1010933404324.

Burges, C. J. C. (1998) 'A Tutorial on Support Vector Machines for Pattern Recognition', *Data mining and knowledge discovery*, 2(2), pp. 121–167. doi: 10.1023/A:1009715923555.

Campbell, I. C. (2012) 'Biodiversity of the Mekong Delta - The Mekong Delta System: Interdisciplinary Analyses of a River Delta', in Renaud, F. G. and Kuenzer, C. (eds). Dordrecht: Springer Netherlands, pp. 293–313. doi: 10.1007/978-94-007-3962-8_11.

Cantho University (2017) 'Land Use Map of The Mekong Delta in 2014 (Ban do su dung dat vung dong bang song cuu long nam 2014)'. Can Tho City, Vietnam: Cantho University.

Carswell, J. R. *et al.* (1994) 'Airborne Scatterometers: Investigating Ocean Backscatter Under Low- and High-Wind Conditions', *Proceedings of the IEEE*, 82(12), pp. 1835–1860. doi: 10.1109/5.338074.

Chan, K. M. and Vu, T. T. (2017) 'A landscape ecological perspective of the impacts of urbanization on urban green spaces in the Klang Valley', *Applied Geography*, 85, pp. 89–100. doi: 10.1016/j.apgeog.2017.06.002.

Chapman, A. and Darby, S. (2016) 'Evaluating sustainable adaptation strategies for vulnerable mega-deltas using system dynamics modelling: Rice agriculture in the Mekong Delta's An Giang Province, Vietnam', *Science of the Total Environment*, 559, pp. 326–338. doi: 10.1016/j.scitotenv.2016.02.162.

Chi, L. (2018) 'Challenges caused by high tide and inundation (Khổ vì nước ngập và triều u cường dâng)', *Bac Lieu Online*. Available at: http://www.baobaclieu.vn/doi-song-xa-hoi/kho-vi-nuoc-ngap-va-trieu-cuong-dang-54206.html.

Chi, L. (2020) *Bảo vệ môi trường trong nuôi tôm: Vẫn còn nhiều bất cập*, *Bac Lieu Online*. Available at: https://www.baobaclieu.vn/nong-nghiep-nong-dan-nong-thon/bao-ve-moi-

truong-trong-nuoi-tom-van-con-nhieu-bat-cap-63013.html.

Clausi, D. A. (2002) 'An analysis of co-occurrence texture statistics as a function of grey level quantization', *Canadian Journal of Remote Sensing*, 28(1), pp. 45–62. doi: 10.5589/m02-004.

Congalton, R. G. and Green, K. (2009) *Assessing the Accuracy of Remotely Sensed Data: Principles and Practices*, *The Photogrammetric Record*. doi: 10.1111/j.1477-9730.2010.00574_2.x.

Corbane, C. *et al.* (2018) 'Enhanced automatic detection of human settlements using Sentinel-1 interferometric coherence', *International Journal of Remote Sensing*, 39(3), pp. 842–853. doi: 10.1080/01431161.2017.1392642.

Dang, T. D. *et al.* (2018) 'Future hydrological alterations in the Mekong Delta under the impact of water resources development, land subsidence and sea level rise', *Journal of Hydrology: Regional Studies*, 15(May 2017), pp. 119–133. doi: 10.1016/j.ejrh.2017.12.002.

Do, T. N. and Bennett, J. (2009) 'Estimating wetland biodiversity values: A choice modelling application in Vietnam's Mekong River Delta', *Environment and Development Economics*, 14(2), pp. 163–186. doi: 10.1017/S1355770X08004841.

Duc, H. (2021) *Thời của nuôi tôm công nghệ cao*, *Nông Nghiệp Việt Nam*. Available at: https://nongnghiep.vn/thoi-cua-nuoi-tom-cong-nghe-cao-d274567.html.

Eisavi, V. *et al.* (2015) 'Land cover mapping based on random forest classification of multitemporal spectral and thermal images', *Environmental Monitoring and Assessment*, 187(5), pp. 1–14. doi: 10.1007/s10661-015-4489-3.

ESA (2021) *Sentinel-1*.

Esch, T. *et al.* (2013) 'Urban Footprint Processor—Fully Automated Processing Chain Generating Settlement Masks From Global Data of the TanDEM-X Mission', *IEEE Geoscience and Remote Sensing Letters*, 10(6), pp. 1617–1621. doi:

10.1109/LGRS.2013.2272953.

Esch, T. *et al.* (2018) 'Where we live-A summary of the achievements and planned evolution of the global urban footprint', *Remote Sensing*, 10(6). doi: 10.3390/rs10060895.

Fukuda, S., Katagiri, R. and Hirosawa, H. (2002) 'Unsupervised approach for polarimetric SAR image classification using support vector machines', in *IEEE International Geoscience and Remote Sensing Symposium*, pp. 2599–2601 vol.5. doi: 10.1109/IGARSS.2002.1026713.

Gamba, P. and Lisini, G. (2013) 'Fast and Efficient Urban Extent Extraction Using ASAR Wide Swath Mode Data', *IEEE Journal of Selected Topics in Applied Earth Observations and Remote Sensing*, 6(5), pp. 2184–2195. doi: 10.1109/JSTARS.2012.2235410.

Garschagen, M., Renaud, F. G. and Birkmann, J. (2011) 'Dynamic Resilience of Peri-Urban Agriculturalists in the Mekong Delta Under Pressures of Socio-Economic Transformation and Climate Change BT - Environmental Change and Agricultural Sustainability in the Mekong Delta', in Stewart, M. A. and Coclanis, P. A. (eds). Dordrecht: Springer Netherlands, pp. 141–163. doi: 10.1007/978-94-007-0934-8_9.

Gaughan, A. E. *et al.* (2019) ' Evaluating nighttime lights and population distribution as proxies for mapping anthropogenic CO 2 emission in Vietnam, Cambodia and Laos ', *Environmental Research Communications*, 1(9), p. 091006. doi: 10.1088/2515-7620/ab3d91.

Gawrysiak, L. and Kociuba, W. (2020) 'Application of geomorphons for analysing changes in the morphology of a proglacial valley (case study: The Scott River, SW Svalbard)', *Geomorphology*, 371, p. 107449. doi: https://doi.org/10.1016/j.geomorph.2020.107449.

Giri, C., Defourny, P. and Shrestha, S. (2003) 'Land cover characterization and mapping of continental Southeast Asia using multi-resolution satellite sensor data', *International Journal of Remote Sensing*, 24(21), pp. 4181–4196. doi: 10.1080/0143116031000139827.

GIZ (2020) *No Title*, *Vietnam*. Available at: https://www.giz.de/en/worldwide/357.html (Accessed: 25 September 2019).

Gómez, C., White, J. C. and Wulder, M. A. (2016) 'Optical remotely sensed time series data for land cover classification: A review', *ISPRS Journal of Photogrammetry and Remote Sensing*, 116, pp. 55–72. doi: https://doi.org/10.1016/j.isprsjprs.2016.03.008.

Google Earth Pro (2017) 'Bac Lieu 9018'07.20"N 105043' 01.51" E, Elevation 18KM'. Google. Available at: https://www.google.com/earth/desktop/ (Accessed: 29 January 2018).

Group, E. O. (2021) *See the World at Night, VIIRS Nighttime Light*, *Earth Observation Group*. Available at: https://eogdata.mines.edu/products/vnl/ (Accessed: 29 April 2021).

Ha, T. P. *et al.* (2018) 'Governance conditions for adaptive freshwater management in the Vietnamese Mekong Delta', *Journal of Hydrology*, 557, pp. 116–127. doi: 10.1016/j.jhydrol.2017.12.024.

Haas, J. and Ban, Y. (2017) 'Sentinel-1A SAR and sentinel-2A MSI data fusion for urban ecosystem service mapping', *Remote Sensing Applications: Society and Environment*, 8(January), pp. 41–53. doi: 10.1016/j.rsase.2017.07.006.

Hai, N. (2019) *Xây dựng đô thị phan thiết phát triển bền vững và thân thiện với môi trường.*, *Phan Thiet Online*. Available at: http://phanthiet.gov.vn/bai-viet/xay-dung-do-thi-phan-thiet-phat-trien-ben-vung-va-than-thien-voi-moi-truong-3626.html (Accessed: 13 November 2020).

Hall-Beyer, M. (2017) 'GLCM Texture: a Tutorial'. doi: 10.13140/RG.2.2.12424.21767.

Haralick, R. M., Shanmugam, K. and Dinstein, I. (1973) 'Textural Features for Image Classification', *IEEE Transactions on Systems, Man, and Cybernetics*, SMC-3(6), pp. 610–621. doi: 10.1109/TSMC.1973.4309314.

Hoanh, C. T. *et al.* (2012) 'Modelling to support land and water management: experiences from the Mekong River Delta, Vietnam', *Water International*, 37(4), pp. 408–426. doi: 10.1080/02508060.2012.706797.

Holobâcă, I.-H., Ivan, K. and Alexe, M. (2019) 'Extracting built-up areas from Sentinel-1

imagery using land-cover classification and texture analysis', *International Journal of Remote Sensing*, 40(20), pp. 8054–8069. doi: 10.1080/01431161.2019.1608391.

Huu Nguyen, H. *et al.* (2016) 'A review of the drivers of 200 years of wetland degradation in the Mekong Delta of Vietnam', *Regional Environmental Change*, 16(8), pp. 2303–2315. doi: 10.1007/s10113-016-0941-3.

Jasiewicz, J. and Stepinski, T. F. (2013) 'Geomorphons — a pattern recognition approach to classification and mapping of landforms', *Geomorphology*, 182, pp. 147–156. doi: https://doi.org/10.1016/j.geomorph.2012.11.005.

JPL (2020) *Shuttle Radar Topography Mission, The Mission to Map the World*, *JPL, NASA*. Available at: https://www2.jpl.nasa.gov/srtm/ (Accessed: 11 November 2020).

Käkönen, M. (2008) 'Mekong Delta at the crossroads: more control or adaptation?', *Ambio*, 37(3), pp. 205–212. doi: 10.1579/0044-7447(2008)37[205:MDATCM]2.0.CO;2.

Karila, K. *et al.* (2014) 'Monitoring changes in rice cultivated area from SAR and optical satellite images in ben tre and tra vinh provinces in mekong delta, vietnam', *Remote Sensing*, 6(5), pp. 4090–4108. doi: 10.3390/rs6054090.

Kong, J. A. (1990) *Electromagnetic Wave Theory*. Second. Wiley-Interscience.

Kontgis, C. *et al.* (2017) 'Leveraging Sentinel-1 time-series data for mapping agricultural land cover and land use in the tropics', in *2017 9th International Workshop on the Analysis of Multitemporal Remote Sensing Images (MultiTemp)*, pp. 1–4. doi: 10.1109/Multi-Temp.2017.8035199.

Kontgis, C., Schneider, A. and Ozdogan, M. (2015) 'Mapping rice paddy extent and intensification in the Vietnamese Mekong River Delta with dense time stacks of Landsat data', *Remote Sensing of Environment*, 169, pp. 255–269. doi: 10.1016/j.rse.2015.08.004.

Kramm, T. *et al.* (2017) 'Accuracy Assessment of Landform Classification Approaches on Different Spatial Scales for the Iranian Loess Plateau', *ISPRS International Journal of Geo-Information*, 6(11). doi: 10.3390/ijgi6110366.

Lan, N. T. P. (2011) 'From Rice to Shrimp: Ecological Change and Human Adaptation in the Mekong Delta of Vietnam BT - Environmental Change and Agricultural Sustainability in the Mekong Delta', in Stewart, M. A. and Coclanis, P. A. (eds). Dordrecht: Springer Netherlands, pp. 271–285. doi: 10.1007/978-94-007-0934-8_16.

Lan, N. T. P. (2013) 'Social and ecological challenges of market-oriented shrimp farming in Vietnam', *SpringerPlus*, 2(1), p. 675. doi: 10.1186/2193-1801-2-675.

Lardeux, C. *et al.* (2009) 'Support vector machine for multifrequency SAR polarimetric data classification', *IEEE Transactions on Geoscience and Remote Sensing*, 47(12), pp. 4143–4152. doi: 10.1109/TGRS.2009.2023908.

Lee, J. *et al.* (1999) 'Polarimetric SAR Speckle Filtering and Its Implication for Classification', 37(5), pp. 2363–2373.

Leinenkugel, P., Esch, T. and Kuenzer, C. (2011) 'Settlement detection and impervious surface estimation in the Mekong Delta using optical and SAR remote sensing data', *Remote Sensing of Environment*, 115(12), pp. 3007–3019. doi: 10.1016/j.rse.2011.06.004.

Leinenkugel, P., Oppelt, N. and Kuenzer, C. (2014) 'A new land cover map for the Mekong : Southeast Asia ' s largest transboundary river basin', *Pacific Geographies*, 41(February), pp. 10–14.

Li, X. *et al.* (2017) 'Recent evolution of the Mekong Delta and the impacts of dams', *Earth-Science Reviews*, 175(October), pp. 1–17. doi: 10.1016/j.earscirev.2017.10.008.

Liew, S. C. *et al.* (1998) 'Application of multitemporal ERS-2 synthetic aperture radar in delineating rice cropping systems in the Mekong River Delta, Vietnam', *IEEE Transactions on Geoscience and Remote Sensing*, 36(5), pp. 1412–1420. doi: 10.1109/36.718845.

van der Linden, S. *et al.* (2015) 'The EnMAP-Box—A Toolbox and Application Programming Interface for EnMAP Data Processing', *Remote Sensing*, 7(9), pp. 11249–11266. doi: 10.3390/rs70911249.

Linh, P. (2020) *Công bố chương trình phát triển đô thị TP. Sóc Trăng đến năm 2030.*, *Soc Trang Online*. Available at: http://baosoctrang.org.vn/thanh-pho-soc-trang-tren-duong-phat-trien/cong-bo-chuong-trinh-phat-trien-do-thi-tp-soc-trang-den-nam-2030-40825.html (Accessed: 13 November 2020).

Linh, T. (2020) *Xây dựng TP Bạc Liêu trở thành đô thị loại I vào năm 2025.*, *Nong Nghiep Viet Nam*. Available at: https://nongnghiep.vn/xay-dung-tp-bac-lieu-tro-thanh-do-thi-loai-i-vao-nam-2025-d272784.html (Accessed: 10 September 2020).

Lisini, G. *et al.* (2018) 'SAR-Based Urban Extents Extraction: From ENVISAT to Sentinel-1', *IEEE Journal of Selected Topics in Applied Earth Observations and Remote Sensing*, 11(8), pp. 2683–2691. doi: 10.1109/JSTARS.2017.2782180.

Van Long, N. and Cheng, Y. (2018) 'Urban Landscape Design Adaption to Flood Risk: A Case Study in Can Tho City, Vietnam', *Environment and Urbanization ASIA*, 9(2), pp. 138–157. doi: 10.1177/0975425318783587.

Lunetta, R. S. *et al.* (1991) 'Remote Sensing and Geographic Information System Data Integration: Error Sources and Research Issues', *Photogrammetric Engineering and Remote Sensing*, 57(6), pp. 677–687.

Lwin, K. and Murayama, Y. (2009) 'A GIS Approach to Estimation of Building Population for Micro-spatial Analysis', *Transactions in GIS*, 13(4), pp. 401–414. doi: 10.1111/j.1467-9671.2009.01171.x.

Manzoni, M., Monti-Guarnieri, A. and Molinari, M. E. (2021) 'Joint exploitation of spaceborne SAR images and GIS techniques for urban coherent change detection', *Remote Sensing of Environment*, 253, p. 112152. doi: https://doi.org/10.1016/j.rse.2020.112152.

Mathews, A. J. *et al.* (2019) 'Satellite scatterometer estimation of urban built-up volume: Validation with airborne lidar data', *International Journal of Applied Earth Observation and Geoinformation*, 77, pp. 100–107. doi: https://doi.org/10.1016/j.jag.2019.01.004.

Mathews, A. and Nghiem, S. (2021) 'Examining Urban Built-up Volume: three-dimensional analyses with lidar and radar data', in, pp. 17–45. doi: 10.1002/9781119625865.ch2.

Minderhoud, P. S. J. *et al.* (2018) 'The relation between land use and subsidence in the Vietnamese Mekong delta', *Science of The Total Environment*, 634, pp. 715–726. doi: 10.1016/J.SCITOTENV.2018.03.372.

Mishra, V. N. *et al.* (2017) 'Dual-polarimetric C-band SAR data for land use/land cover classification by incorporating textural information', *Environmental Earth Sciences*, 76(1), pp. 1–16. doi: 10.1007/s12665-016-6341-7.

MoC (2020a) *Cà Mau: Thành phố trẻ hội nhập, phát triển.*, *Ministry of Construction*. Available at: http://moc.gov.vn/vn/tin-tuc/1184/63988/ca-mau--thanh-pho-tre-hoi-nhap--phat-trien.aspx (Accessed: 13 November 2020).

MoC (2020b) *Long An: Phát triển đô thị, tạo động lực thúc đẩy kinh tế.*, *Ministry of Construction*. Available at: http://moc.gov.vn/vn/tin-tuc/1184/64077/long-an--phat-trien-do-thi--tao-dong-luc-thuc-day-kinh-te.aspx (Accessed: 13 November 2020).

National Academies of Sciences, Engineering, and M. (2021) 'Research on Approaches Critical to Managing Climate Risk', in *Global Change Research Needs and Opportunities for 2022-2031*. Washington, DC: The National Academies Press. doi: 10.17226/26055.

Nghiem, S.V.; Borgeaud, M.; Kong, J.A.; Shin, R. . (1990) 'Polarimetric Remote Sensing of Geophysical Media with Layer Random Medium Model', in Kong, J. A. (ed.) *Progress in Electromagnetics Research*. Amsterdam, The Netherlands: Elsevier, pp. 1–73.

Nghiem, S. V. *et al.* (1995) 'Observations of Radar Backscatter at Ku and C Bands in the Presence of Large Waves during the Surface Wave Dynamics Experiment', *IEEE Transactions on Geoscience and Remote Sensing*, 33(3), pp. 708–721. doi: 10.1109/36.387586.

Nghiem, S. V *et al.* (2009) 'Observations of urban and suburban environments with global satellite scatterometer data', *ISPRS Journal of Photogrammetry and Remote Sensing*, 64(4), pp. 367–380. doi: https://doi.org/10.1016/j.isprsjprs.2009.01.004.

Ngo, K. D. *et al.* (2021) 'Building structure mapping on level terrains and sea surfaces in vietnam', *Remote Sensing*, 13(13). doi: 10.3390/rs13132439.

Ngo, K. D., Lechner, A. M. and Vu, T. T. (2020) 'Land cover mapping of the Mekong Delta to support natural resource management with multi-temporal Sentinel-1A synthetic aperture radar imagery', *Remote Sensing Applications: Society and Environment*, 17. doi: 10.1016/j.rsase.2019.100272.

Nguyen, C. H. (2013) 'Vietnamese international student mobility: past and current trends', *Asian Education and Development Studies*, 2(2), pp. 127–148. doi: 10.1108/20463161311321411.

Nguyen, D. *et al.* (2015) 'Mapping Rice Seasonality in the Mekong Delta with Multi-Year Envisat ASAR WSM Data', *Remote Sensing*, 7(12), pp. 15868–15893. doi: 10.3390/rs71215808.

Nguyen, D. B., Gruber, A. and Wagner, W. (2016a) 'Mapping rice extent and cropping scheme in the Mekong Delta using Sentinel-1A data', *Remote Sensing Letters*, 7(12), pp. 1209–1218. doi: 10.1080/2150704X.2016.1225172.

Nguyen, D. B., Gruber, A. and Wagner, W. (2016b) 'Mapping rice extent and cropping scheme in the Mekong Delta using Sentinel-1A data', *Remote Sensing Letters*, 7(12), pp. 1209–1218. doi: 10.1080/2150704X.2016.1225172.

Nguyen, H. H. *et al.* (2013) 'The relationship of spatial-temporal changes in fringe mangrove extent and adjacent land-use: Case study of Kien Giang coast, Vietnam', *Ocean and Coastal Management*, 76, pp. 12–22. doi: 10.1016/j.ocecoaman.2013.01.003.

NISAR (2018) *NASA-ISRO SAR (NISAR) Mission Science Users' Handbook*, *NASAR-ISRO SAR (NISAR) Mission Science User's Handbook*. Available at: https://nisar.jpl.nasa.gov/system/documents/files/26_NISAR_FINAL_9-6-19.pdf.

Oon, A. *et al.* (2019) 'Assessment of ALOS-2 PALSAR-2L-band and Sentinel-1 C-band SAR backscatter for discriminating between large-scale oil palm plantations and smallholdings on tropical peatlands', *Remote Sensing Applications: Society and Environment*, 13. doi: 10.1016/j.rsase.2018.11.002.

Paull, R. E. and Chen, N. . (2019) *Overall Dragon Fruit Production and Global Marketing,*

FTTC Agricultural Marketing Policy, FTTC Agricultural Marketing Policy. Taipei, Taiwan.

Pelletier, C. *et al.* (2016) 'Remote Sensing of Environment Assessing the robustness of Random Forests to map land cover with high resolution satellite image time series over large areas', *Remote Sensing of Environment*, 187, pp. 156–168. doi: 10.1016/j.rse.2016.10.010.

Phan, H. *et al.* (2018) 'Mapping of rice varieties and sowing date using X-band SAR data', *Sensors (Switzerland)*, 18(1). doi: 10.3390/s18010316.

Phung, H.-P. *et al.* (2020) 'Monitoring rice growth status in the Mekong Delta, Vietnam using multitemporal Sentinel-1 data', *Journal of Applied Remote Sensing*, 14(01), p. 1. doi: 10.1117/1.jrs.14.014518.

Planet Labs Inc (2017) *Bac Lieu 9.250 N 105.730 E, Elevation 14 KM*. Available at: https://www.planet.com/explorer/#/mosaic/global_monthly_2016_03_mosaic/center/105.724,9.291/zoom/14 (Accessed: 29 January 2018).

Renaud, F. G. *et al.* (2015) 'Resilience and shifts in agro-ecosystems facing increasing sea-level rise and salinity intrusion in Ben Tre Province, Mekong Delta', *Climatic Change*, 133(1), pp. 69–84. doi: 10.1007/s10584-014-1113-4.

Rizk, I. and Rashed, M. (2015) 'Monitoring urban growth and land use change detection with GIS and remote sensing techniques in Daqahlia governorate Egypt', *International Journal of Sustainable Built Environment*, 4(1), pp. 117–124. doi: 10.1016/j.ijsbe.2015.02.005.

Rockwell, N. C. and Lagarias, J. C. (2006) 'The Structure of Phytochrome: A Picture Is Worth a Thousand Spectra', *The Plant Cell*, 18(1), pp. 4–14. doi: 10.1105/tpc.105.038513.

Rodriguez-Galiano, V. F. *et al.* (2012) 'Random Forest classification of Mediterranean land cover using multi-seasonal imagery and multi-seasonal texture', *Remote Sensing of Environment*, 121, pp. 93–107. doi: 10.1016/j.rse.2011.12.003.

Rutten, M. *et al.* (2014) 'Land use dynamics, climate change, and food security in Vietnam:

A global-to-local modeling approach', *World Development*, 59, pp. 29–46. doi: 10.1016/j.worlddev.2014.01.020.

Sakamoto, T. *et al.* (2006) 'Spatio–temporal distribution of rice phenology and cropping systems in the Mekong Delta with special reference to the seasonal water flow of the Mekong and Bassac rivers', *Remote Sensing of Environment*, 100(1), pp. 1–16. doi: https://doi.org/10.1016/j.rse.2005.09.007.

Sakamoto, T. *et al.* (2009) 'Analysis of rapid expansion of inland aquaculture and triple rice-cropping areas in a coastal area of the Vietnamese Mekong Delta using MODIS time-series imagery', *Landscape and Urban Planning*, 92(1), pp. 34–46. doi: 10.1016/j.landurbplan.2009.02.002.

Sawaya, K. E. *et al.* (2003) 'Extending satellite remote sensing to local scales: land and water resource monitoring using high-resolution imagery', *Remote Sensing of Environment*, 88(1), pp. 144–156. doi: https://doi.org/10.1016/j.rse.2003.04.006.

Shumway, R. H. and Stoffer, D. S. (2017) 'Spectral Analysis and Filtering', in Shumway, R. H. and Stoffer, D. S. (eds) *Time Series Analysis and Its Applications: With R Examples*. Cham: Springer International Publishing, pp. 165–239. doi: 10.1007/978-3-319-52452-8_4.

Silveira, C. T. da *et al.* (2018) 'Automated Classification of Landform Elements in the State Of Parana (Brazil) Applying the Proposal of the Geomorphons', *Rev. Brasi. Geomorf*, 19(1), pp. 33–57. doi: 10.20502/rbg.v19i1.1263.

Son, N.-T. and Thanh, B.-X. (2018) 'Decadal assessment of urban sprawl and its effects on local temperature using Landsat data in Cantho city, Vietnam', *Sustainable Cities and Society*, 36(September 2017), pp. 81–91. doi: 10.1016/j.scs.2017.10.010.

Son, N. T. *et al.* (2013) 'A phenology-based classification of time-series MODIS data for rice crop monitoring in Mekong Delta, Vietnam', *Remote Sensing*, 6(1), pp. 135–156. doi: 10.3390/rs6010135.

Son, N. T. *et al.* (2017) 'Assessment of Sentinel-1A data for rice crop classification using

random forests and support vector machines', *Geocarto International*, 6049(June), pp. 1–15. doi: 10.1080/10106049.2017.1289555.

Sorichetta, A. *et al.* (2020) 'Transformative Urban changes of Beijing in the decade of the 2000s', *Remote Sensing*, 12(4). doi: 10.3390/rs12040652.

Su, W. *et al.* (2008) 'Textural and local spatial statistics for the object-oriented classification of urban areas using high resolution imagery', *International Journal of Remote Sensing*, 29(11), pp. 3105–3117. doi: 10.1080/01431160701469016.

Thu, K. (2018) 'Shrimp Export in Vietnam: 20 years Summary (Xuat khau tom Viet Nam: 20 nam nhin lai)', *Vietnam Association of Seafood Exporters and Producers*. Available at: http://vasep.com.vn/Tin-Tuc/1203_52000/Xuat-khau-tom-Viet-Nam-20-nam-nhin-lai.htm.

Thu, T. *et al.* (2012) 'Mapping the irrigated rice cropping patterns of the Mekong delta , Vietnam , through hyper-temporal SPOT NDVI image analysis', *International Journal of Remote Sensing*, 1161(June 2017). doi: 10.1080/01431161.2010.532826.

Tong, P. H. S. *et al.* (2004) 'Assessment from space of mangroves evolution in the Mekong Delta, in relation to extensive shrimp farming', *International Journal of Remote Sensing*, 25(21), pp. 4795–4812. doi: 10.1080/01431160412331270858.

Torres, R. *et al.* (2012) 'GMES Sentinel-1 mission', *Remote Sensing of Environment*, 120, pp. 9–24. doi: 10.1016/j.rse.2011.05.028.

Tran, H., Tran, T. and Kervyn, M. (2015) 'Dynamics of land cover/land use changes in the Mekong Delta, 1973-2011: A Remote sensing analysis of the Tran Van Thoi District, Ca Mau Province, Vietnam', *Remote Sensing*, 7(3), pp. 2899–2925. doi: 10.3390/rs70302899.

Trisasongko, B. H. *et al.* (2017) 'Comparing six pixel-wise classifiers for tropical rural land cover mapping using four forms of fully polarimetric sar data', *International Journal of Remote Sensing*, 38(11), pp. 3274–3293. doi: 10.1080/01431161.2017.1292072.

Trong, D. (2021) *Bạc Liêu chú trọng nuôi tôm công nghệ cao*, *Nhân Dân Online*. Available

at: https://nhandan.vn/tin-tuc-kinh-te/bac-lieu-chu-trong-nuoi-tom-cong-nghe-cao-629241/.

Tue, N. T. *et al.* (2014) 'Carbon storage of a tropical mangrove forest in Mui Ca Mau National Park, Vietnam', *Catena*, 121(October), pp. 119–126. doi: 10.1016/j.catena.2014.05.008.

Van, T. T. *et al.* (2015) 'Changes in mangrove vegetation area and character in a war and land use change affected region of Vietnam (Mui Ca Mau) over six decades', *Acta Oecologica*, 63, pp. 71–81. doi: 10.1016/j.actao.2014.11.007.

Vapnik, V. N. (1998) *Statistical Learning Theory*. New York: Wiley.

Veselský, M. *et al.* (2015) 'Semi-automated recognition of planation surfacesand other flat landforms: a case study from theAggtelek Karst, Hungary', *Open Geosciences*, 7(1). doi: doi:10.1515/geo-2015-0063.

Vietnam National Space Center, V. (2019) *Signing Ceremony of the Package "LOTUSat-1 Satellite, Equipment and Capacity Development" in Project For Disaster And Climate Change Countermeasure Using Earth Observation Satellite (Vietnam Space Center Project)*, *VNSC*. Available at: https://vnsc.org.vn/en/news-events/signing-ceremony-of-the-package-lotusat-1-satellite-equipment-and-capacity-development-in-project-for-disaster-and-climate-change-countermeasure-using-earth-observation-satellite-v/.

Vietnamese National Assembly (2013) *Land Law (Luật Đất Đai)*. Ha Noi, Vietnam.

Vietnamese State Government (2018) *Decision 101/NQ-CP dated August 3rd 2018 on Adjustment of land use master plan up to 2020 and land use plan the last period (2016-2020) in Bac Lieu*. Ha Noi, Vietnam.

VietnamPlus (2021) *High-tech shrimp farming brings high profits in Bac Lieu province*, *Vietnam News Agency*. Available at: https://en.vietnamplus.vn/hightech-shrimp-farming-brings-high-profits-in-bac-lieu-province/200274.vnp.

Vo, Q. T. *et al.* (2013) 'Remote sensing in mapping mangrove ecosystems - an object-based approach', *Remote Sensing*, 5(1), pp. 183–201. doi: 10.3390/rs5010183.

Wang *et al.* (2017) 'Remote sensing image classification based on the optimal support vector machine and modified binary coded ant colony optimization algorithm', *Information Sciences*, 402, pp. 50–68. doi: 10.1016/j.ins.2017.03.027.

Wang, G. and Gertner, G. Z. (2013) 'Spatial Uncertainty Analysis When Mapping Natural Resources Using Remotely Sensed Data', in Weng, Q. and Wang, G. (eds) *Remote Sensing of Natural Resources*. Boca Raton: CRC Press, pp. 87–107.

Wang, Z., Lechner, M. A. and Baumgartl, T. (2018) 'Ecosystem Services Mapping Uncertainty Assessment: A Case Study in the Fitzroy Basin Mining Region', *Water* . doi: 10.3390/w10010088.

Wölcke, T. *et al.* (2016) *Integrated Coastal Protection and Mangrove Belt Rehabilitation in the Mekong Delta*, *Deutsche Gesellschaft für Internationale Zusammenarbeit (GIZ) GmbH*. Available at: https://www.unique-landuse.de/images/publications/vereinheitlicht/Pre-feasibility-study-for-investment_coastal_EN.pdf.

Xiao, Y. and Zhan, Q. (2009) 'A review of remote sensing applications in urban planning and management in China', *2009 Joint Urban Remote Sensing Event*, pp. 1–5. doi: 10.1109/URS.2009.5137653.

Yang, C. *et al.* (2017) 'Improving Land Use/Land Cover Classification by Integrating Pixel Unmixing and Decision Tree Methods', *Remote Sensing*, 9(12), p. 1222. doi: 10.3390/rs9121222.

Zakeri, H., Yamazaki, F. and Liu, W. (2017) 'Texture Analysis and Land Cover Classification of Tehran Using Polarimetric Synthetic Aperture Radar Imagery', *Applied sciences*, 7. doi: 10.3390/app7050452.

Zhang, K. *et al.* (2021) 'Unsupervised Multitemporal Building Change Detection Framework Based on Cosegmentation Using Time-Series SAR', *Remote Sensing* . doi: 10.3390/rs13030471.

Zhang, L. and Milanova, M. (2013) 'An Effective Multi-feature Fusion Object-based

Classification Method on ArcGIS Platform Using Very High-resolution Remote Sensing Image', *International Journal of Advanced Research in Computer Science and Software Engineering*, 3(11), pp. 10–23. Available at: http://ijarcsse.com/Before_August_2017/docs/papers/Volume_3/11_November2013/V3I 11-0138.pdf.

Appendix A

Data import into Google Earth Engine script

In terms of developing a remote sensing application, the first step is to import satellite images into Earth Engine script. There are two ways to add satellite images into Earth Engine script: users may search the dataset in a searching box on the top or write codes into script. Figure A1 shows an example how to import Sentinel-1 SAR into Earth Engine script. Users may then filter image collections to meet application criteria such as a certain study area at a specific time. The following example codes (Figure A2) illustrate how to filter image collection according to area of interest, the acquisition time, orbit, and space resolution.

(a)

(b)
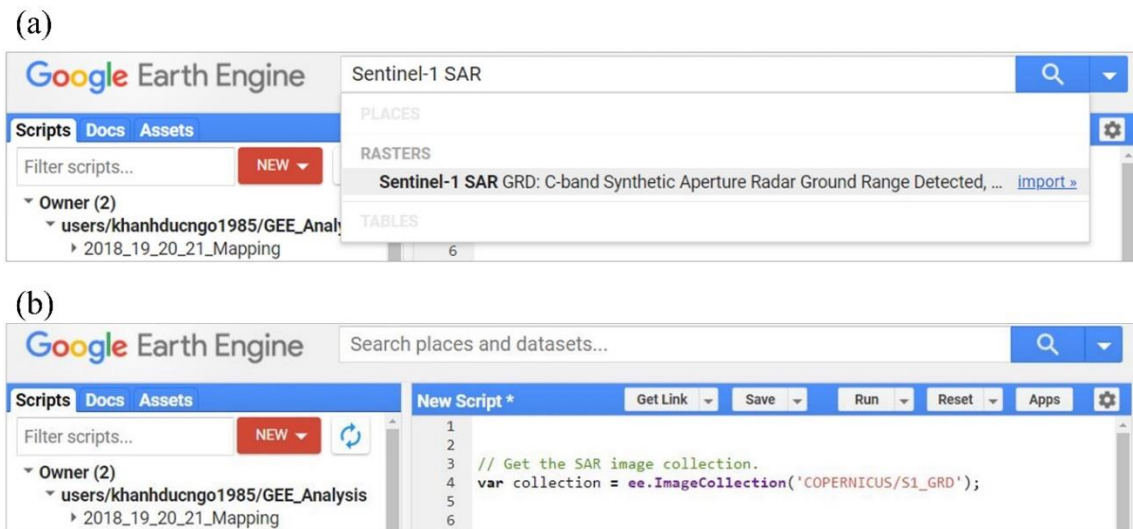
Figure A1 Import remote sensing data into Earth Engine script: (a) search dataset in searching box, (b) writing codes into script.

```
2D_Urban_Map_BacLieu_3PW_Mean          Get Link    Save    Run    Reset    Apps

13
14  var collection = ee.ImageCollection('COPERNICUS/S1_GRD')
15      .filterMetadata('platform_number', 'equals', 'A')
16      .filterMetadata('resolution_meters', 'equals' , 10)
17      .filter(ee.Filter.eq('instrumentMode', 'IW'))
18      .filter(ee.Filter.eq('orbitProperties_pass', 'ASCENDING'))
19      .filterBounds(boundary)
20      .filterDate('2017-03-13', '2018-05-01');
21      |
22  print('Collection SAR', collection);
23
```

Figure A2 Filtering the image collection

Incidence angle normalization

Since the scene of Sentinel-1 SAR image has a 250 km swath, the incidence angle has an effect the radar scattering results. The study area is on incidence angle bin from 35.5 to 40.5 degree. To reduce the influence of incidence angle on radar scattering, it is necessary to normalize to a reference local incidence angle $\theta_{ref} = 35.5^0$ using linear relationship:

$$\sigma^0_{nor} = \sigma^0(\theta) - \beta.[\theta - \theta_{ref}]$$

Equation A1 Incidence angle normalization

where σ^0_{nor} is the normalized backscatter coefficient, $\sigma^0(\theta)$ is the unnormalized backscatter coefficient at incidence angle θ, β is the slope parameter of the linear regression between $\sigma^0(\theta)$ and θ, and θ_{ref} is the reference incidence angle.
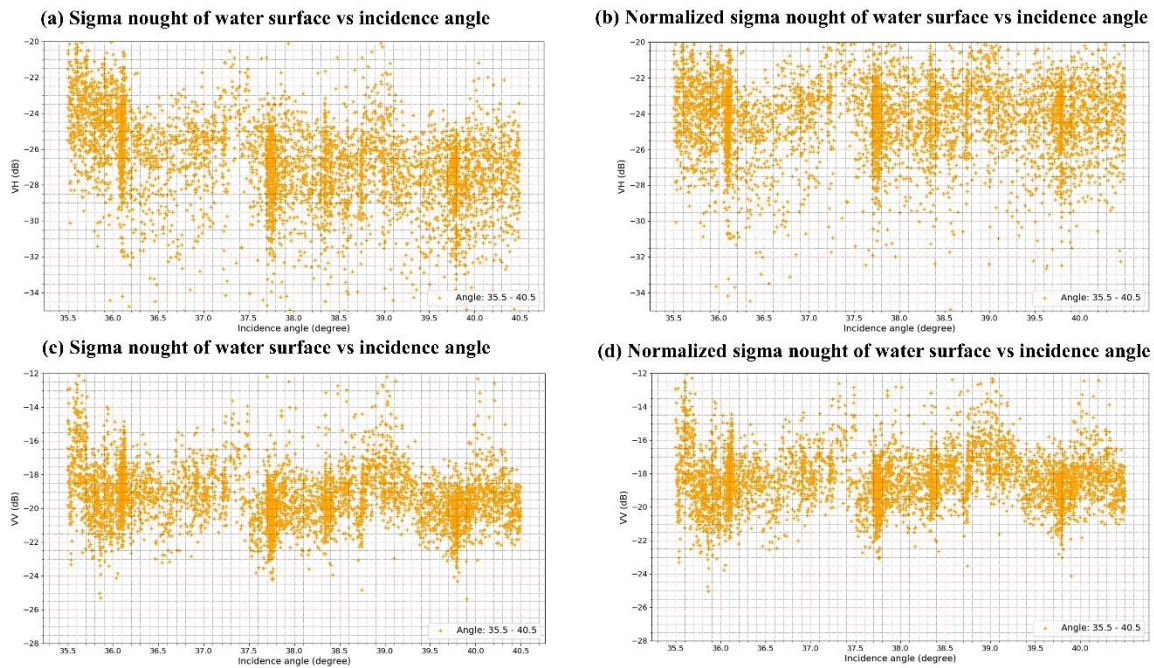
Figure A3 The backscatter values of the (a) VH and (c) VV polarization of water surface influenced by incidence angle; and the backscatter values of the (b) VH and (d) VV polarization of water surface after incidence angle normalization.

A total of 5,000-pixel values at each VH and VV polarization band and linear regression are used to find the slope parameter β. The results of incidence angle normalization of the VH and VV polarization are illustrated in Figure A3. It shows that after normalization the backscatters of water surface have stable values corresponding to the incidence angle.

Harmonic analysis

The use of time series SAR data helps reduce the amount of speckle noise, but there are still significant variations in the time series of scattering values due to morphology or land cover changes. Therefore, interpolation of data gaps and smoothing to minimize noise are often used when processing time series data.

The phenomenon of noise due to abnormal changes to each pixel is identified by applying harmonic analysis. To build the harmonic model (or Fast Fourier transformation) a frequency domain approach described in Shumway and Stoffer (2017) is applied. A cycle is defined as a complete period of a sine or cosine function over a unit time interval as

$$x_t = A\cos(2\pi\omega t - \phi)$$

Equation A2 A simple trigonometric function

For $t = 0, \pm1, \pm2$, etc…, where ω is a frequency index defined in cycles per unit time, A determining amplitude of the function, ϕ called the phase specifying the beginning point of the cosine function.

To simplify data analysis, using a trigonometric identity the time series x_t in the equation above can be written as:

$$x_t = \beta_0 + \beta_1 t + \beta_2 \cos(2\pi\omega t) + \beta_3 \sin(2\pi\omega t)$$

Equation A3 An extended trigonometric function

where β_0 is a constant, β_1 is coefficient for the overall trend in t, β_2 is a coefficient for the sine function at frequency ω of time t, β_3 is a coefficient for the cosine function at the frequency ω of time t. A total of 33 SAR images at VH polarization was used to apply harmonic analysis. The values of time t were estimated by image's acquisition time. The coefficients were derived by linear regression model in Google Earth Engine. The harmonic frequency was set to 2 *(ω=2)*. Figure A4 shows the result of harmonic analysis on 33 SAR images. The result show that Fast Fourier transform (FFT) has significant effect on the backscatter curve of four land cover classes. The result can be used as input data for further land cover classification.
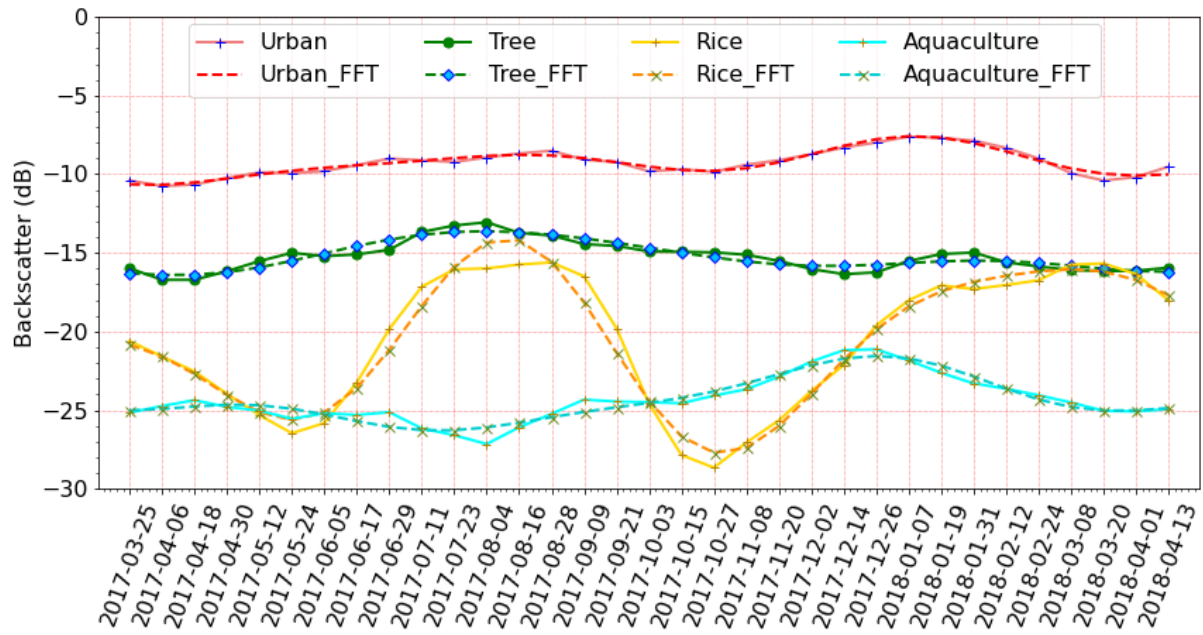
Figure A4 Harmonic analysis on four LCLU in Bạc Liêu province

Appendix B

Figure B1 shows the plot of number of pixels versus threshold, and the plot of the discrete derivative of building pixels versus threshold for Bạc Liêu, Cà Mau, Sóc Trăng, Tân An, and Phan Thiết. The plots show that threshold = 9 (i.e., building count = 10 or more) is optimal as the derivative curves are flattened for larger threshold values. This means that the building detection results converge and become stable so that the inclusion of an excessively large threshold count is ineffective and unnecessary. It is noted that threshold = 9 is found valid for all cities in various environments from wet to dry regions and from in-land areas to coastal zones, across the landscape from natural and rural to urban conditions. The building count of at least 10 signifies that the building structure must persistently exist for a minimum period consisting of 9 two-week intervals (Sentinel-1 SAR revisit time is two weeks), which is equivalent to 18 weeks or 4.15 months.

Figure B2 shows the plot of number of pixels versus threshold, and the plot of the discrete derivative of pixels versus threshold for buildings, paddy fields, aquaculture, and persistent surface water in Bạc Liêu city.
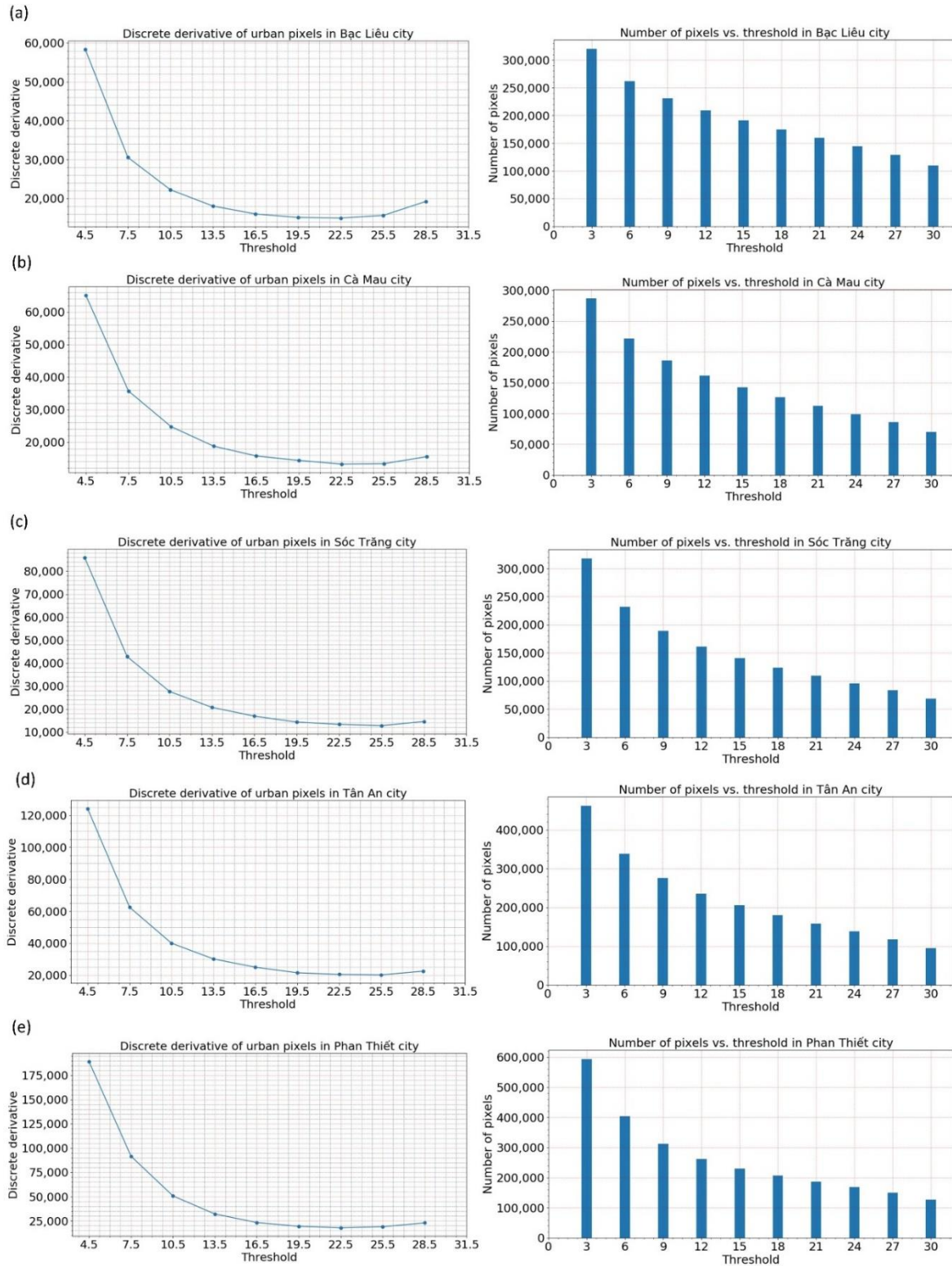
Figure B1. Discrete derivative of building pixel vs. threshold in (a) Bạc Liêu, (b) Cà Mau, (c) Sóc Trăng, (d) Tân An, and (e) Phan Thiết
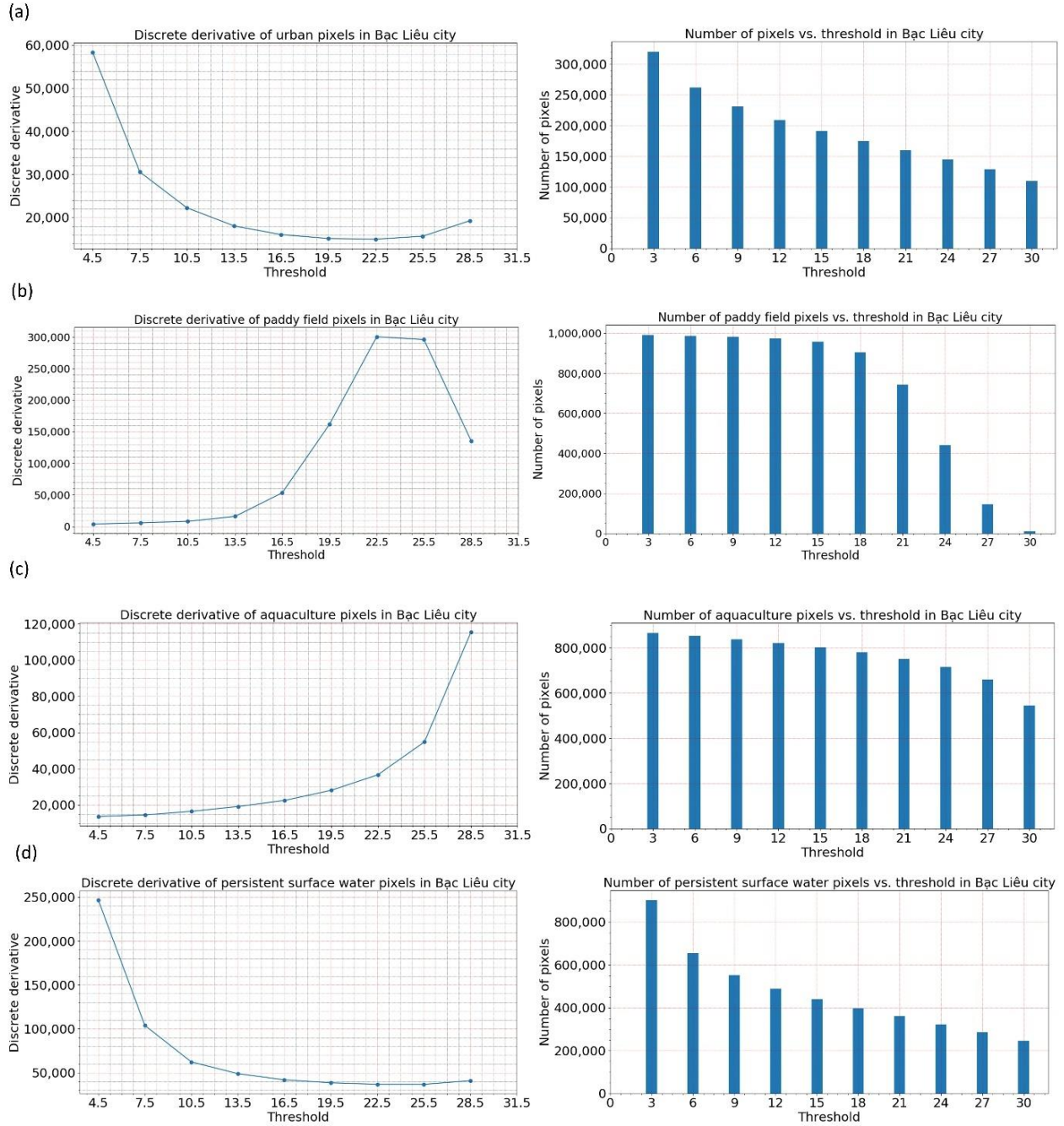
Figure B2. Discrete derivative of pixels vs. threshold of (a) building, (b) rice paddy field, (c) aquaculture, and (d) persistent surface water in Bạc Liêu city.

Appendix C

The following geotagged photos were taken at different locations from wetland to urban areas of Bạc Liêu province. The photographs were imported into ArcMap software and converted into points. These points were used to validate the mapping results.

Figure C1. An intensive shrimp pond (photo taken on 15 Feb 2019 at Vinh My A villages, Hoa Binh district, Bạc Liêu province)

Figure C2. A patch of coastal forest (photo taken on 15 Feb 2019 at Vinh Hau A village, Hoa Binh district, Bạc Liêu province)

Figure C3. A rice field (photo taken on 15 Feb 2019 at Hung Hoi Village, Vinh Loi district, Bạc Liêu province)

Figure C4. A built-up area (photo taken on 15 Feb 2019 at Hung Vuong Square, Nguyen Tat Thanh street, Bạc Liêu city, Bạc Liêu province).

Figure C5. A shrimp-rice rotation crop land lot next to extensive shrimp pond (photo taken on 18 Feb 2019 near Cau 3000 bridge, Ninh Thanh Loi village, Hong Dan district, Bạc Liêu province).